2015

Mechanism of Hip Dysplasia and Identification of the Least Energy Path for its Treatment by using the Principle of Stationary Potential Energy

Mohammed Abdulwahab M. Zwawi
University of Central Florida

MECHANISM OF HIP DYSPLASIA AND IDENTIFICATION OF THE LEAST ENERGY PATH FOR ITS TREATMENT BY USING THE PRINCIPLE OF STATIONARY POTENTIAL ENERGY

by

MOHAMMED A. ZWAWI
B.S. King Abdulaziz University, 2005
M.S. University of Central Florida, 2012

A dissertation submitted in partial fulfillment of the requirements
for the degree of Doctor of Philosophy
in the Department of Mechanical and Aerospace Engineering
in the College of Engineering and Computer Science
at the University of Central Florida
Orlando, Florida

Fall Term
2015

Major Professor: Faissal Moslehy

ABSTRACT

Developmental dysplasia of the hip (DDH) is a common newborn condition where the femoral head is not located in its natural position in the acetabulum (hip socket). Several treatment methods are being implemented worldwide to treat this abnormal condition. One of the most effective methods of treatment is the use of Pavlik Harness, which directs the femoral head toward the natural position inside the acetabulum.

This dissertation presents a developed method for identifying the least energy path that the femoral head would follow during reduction. This is achieved by utilizing a validated computational biomechanical model that allows the determination of the potential energy, and then implementing the principle of stationary potential energy. The potential energy stems from strain energy stored in the muscles and gravitational potential energy of four rigid-body components of lower limb bones. Five muscles are identified and modeled because of their effect on DDH reduction. Clinical observations indicate that reduction with the Pavlik Harness occurs passively in deep sleep under the combined effects of gravity and the constraints of the Pavlik Harness.

A non-linear constitutive equation, describing the passive muscle response, is used in the potential energy computation. Different DDH abnormalities with various flexion, abduction, and hip rotation angles are considered, and least energy paths are identified. Several constraints, such as geometry and harness configuration, are considered to closely simulate real cases of DDH.

Results confirm the clinical observations of two different pathways for closed reduction. The path of least energy closely approximated the modified Hoffman-Daimler method. Release of the pectineus muscle favored a more direct pathway over the posterior rim of the acetabulum. The direct path over the posterior rim of the acetabulum requires more energy. This model supports the observation that Grade IV dislocations may require manual reduction by the direct path. However, the indirect path requires less energy and may be an alternative to direct manual reduction of Grade IV infantile hip dislocations. Of great importance, as a result of this work, identifying the minimum energy path that the femoral head would travel would provide a non-surgical tool that effectively aids the surgeon in treating DDH.

To my parents (Abdulwahab and Noor), my wife (Lujain), my big boy (Abdulelah), and my little daughter (Aseel), I am presenting this work on behalf of your support and your patience during the past three years. You always encourage me, pray for me, push me to do something that can help mankind, and I succeeded. I wish from my deep heart with my results the physicians can improve the treatment of the babies with hip dysplasia.

ACKNOWLEDGMENT

First of all, I am grateful to the Almighty Allah for establishing me to complete and succeed in this research.

I would like to thank King Abdulaziz University for giving me the opportunity to study and live in the United States during my research. Also, I would like to express my sincere gratitude to the Department of Mechanical and Aerospace Engineering for letting me fulfill my dream of getting my doctoral degree. This study was supported in part by the National Science Foundation under Grant number CBET-1160179, and the International Hip Dysplasia Institute.

To my committee, Professor Alain Kassab, Professor Hansen Mansy, and Professor Eduardo Divo, I am extremely grateful for your assistance and suggestions throughout my research. To Dr. Charles Price, I am glad that I worked with you during this research, and I wish to continue our work on this manner to support humanity for a better life. To my colleague, Christopher Rose, I am thankful for your help and support.

Most of all, I am fully thankful to my advisor Professor Faissal A. Moslehy for his full support, understanding, patience, and encouragement during my research. I progressed quickly with high performance and quality due to his inspiration. It was a journey that had many difficulties and limits, but with these types of professors, I was guided to pass through all these challenges and merge the mechanical science with the medical one to help the affected babies.

TABLE OF CONTENTS

LIST OF FIGURES

LIST OF TABLES

CHAPTER 1: INTRODUCTION

1.1 Background

When the femoral head is dislocated and placed somewhere outside of its natural position in the acetabulum (hip socket), the femur with lower limb bones will be in a non-equilibrium condition due to muscle forces acting on these bones. This non-equilibrium condition is called hip dysplasia. Hip dysplasia is one of the most abnormal conditions in newborn babies. It is a common condition requiring treatment in approximately 1% to 3% of newborn infants. One in six may demonstrate neonatal instability while complete dislocation occurs in approximately 0.1% to 0.3% of live births. During the growth of the baby intrauterine, particularly at eleventh week, the hip joints will be fully formed where the hip dislocation may occur. In 1832-1834, Dupuytren was the first to establish the lack of development of the acetabulum, and later it was referred to by others as dysplasia [1].

The causes of hip dysplasia are unknown to researchers till now, but there are some factors that increase the probabilities, and it is widely believed that this condition is developmental. Some researchers have discussed the causes. According to Seringe, et al. [2], there are two categories of causes: constitutional factors and mechanical factors. One constitutional factor can be considered the insufficient depth of the acetabulum. Additionally, a shallow acetabulum could be regarded as a constitutional factor that increases the probability of dislocation. Furthermore, the mechanical factors can be attributed to several causes. The causes are when babies are born in the breech

presentation, born with high weight, or born with a mechanical deformation of the foot or knee. Traditional swaddling techniques could be considered as one of the mechanical factors that increases the possibility of hip dislocation.

The clinical sign of hip dysplasia is a clicking sound at birth for certain cases. This click is a clear evidence of slight or moderate dysplasia. However, the sign for severe dislocation (the femoral head is dislocated superiorly to the acetabulum) is the abnormal limitation of the abduction of the hip [1]. On the other hand, the Ortolani Sign can be an evidence of hip dysplasia. Originally, the link between the femoral head and the acetabulum is loosened, and the femoral head can be made to slide in and out of the acetabulum [3]. These factors contribute to the femoral head being dislocated from the acetabulum, or the one that is dislocated can be relocated back inside the acetabulum. The physicians usually do this kind of diagnosis at birth. If either diagnosis is missed at birth, the nature of the hip could follow one of the four scenarios as introduced by Weinstein. The hip can become normal, it can go on to subluxation or partial contact, it can go on to complete dislocation, or it can remain located but retain dysplastic features [4].

Developmental Dysplasia of the Hip develops after birth and affects 1 in 20 infants and should be treated within the first six months [5]. There are several hip dysplasia classifications that are defined by the International Hip Dysplasia Institute (IHDI) and are called grades. Hence, IHDI defined four grades of the hip dysplasia, as displayed in Figure 1, and the most common hip dysplasia grades are 3 and 4.

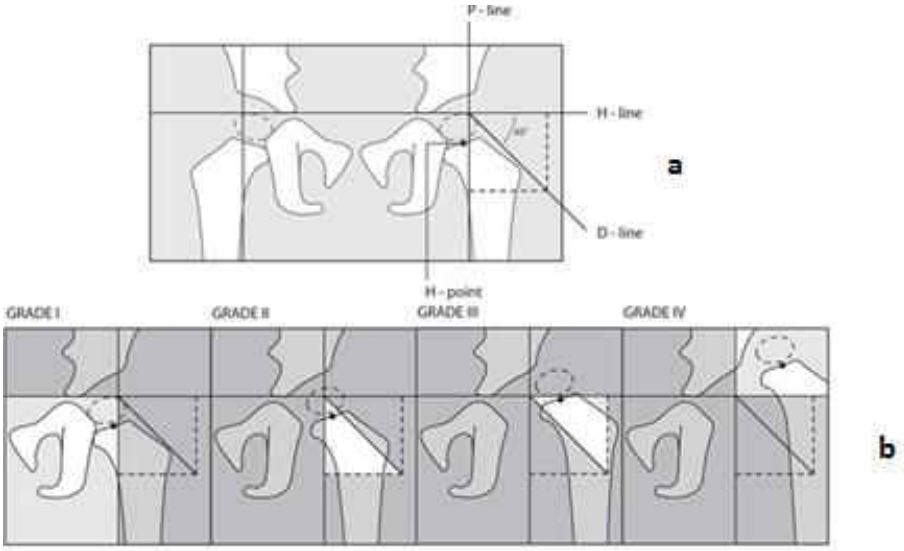

Figure 1 International Hip Dysplasia Institute grades, a) grading lines, b) four grades [6]

As shown in the above figure, the three lines that are introduced in the anteroposterior view of the hip are used to identify the classification of the hip dysplasia. The horizontal line, called the Hilgenreiner line (H-line), is between each triradiate cartilage (Y-shaped epiphyseal plate in the acetabulum). The line perpendicular to the H-line is the Perkin line (P-line) and is used to divide the hip into four quadrants through the supero-lateral edge of the acetabulum. The third line, which creates a 45-degree angle, is the Diagonal line (D-line). It has been shown that those lines are used to distinguish between the four grades defined by IHDI.

Several treatment methods are used to force the femoral head back into its natural position. Therefore, the purpose of the treatment is to relocate the femoral head into the acetabulum allowing the structures of the fast developing hip joint (femur, acetabulum, supporting ligaments, etc.) to regularly grow in their correct position.

Different treatment methods are considered for patients that have hip dysplasia. One of the most effective methods is the Pavlik Harness. Most of the newborn babies with dislocated hips can be treated magnificently when the harness is correctly used. It can be used for most of the hip dysplasia grades and has become an accepted worldwide treatment. The success rate with the Pavlik Harness and other methods depends on the severity of dislocation and initiation age of treatment. Early detection may improve the treatment, but severity remains an impediment to successful treatment with non-surgical methods [7].

The Pavlik Harness has different setups depending on the fixation and connection of the straps. Figure 2 shows the straps that are used to maintain the legs in different locations and orientations. Also, the straps are fixed for a particular time to assure the femoral head is in its natural position inside the acetabulum. The best results of using the Pavlik Harness are attained when it is used before three weeks of age. According to different studies, this treatment fails in about 15 percent of the cases [8].

Figure 2 Pavlik Harness as a treatment for the hip dysplasia [9].

In this dissertation, the principle of stationary potential energy is used to identify the optimal path for the surgeon during the hip dysplasia reduction. Thus, the femoral head will be successfully vectored into its correct physiological position in the acetabulum. The potential energy stems from strain energy stored in the considered muscles (Pectineus, Adductor Brevis, Adductor Longus, Adductor Magnus, and Gracilis) and gravitational potential energy of four rigid-body components of the lower limb. Hence, the potential energy will be introduced as a function of the pelvis surface, muscle forces as strain energy, and gravitational potential energy. This function will be used to find the optimal path to lead the surgeon to set up the harness and guide him/her to move the femoral head along the pelvic surface in a specific path at a specified femur orientation.

To identify the potential energy function with the least energy path with respect to all factors in the hip dysplasia problem, a computer program was developed to determine femoral head centers' coordinates while the head is in contact with the pelvic surface, as indicated in Figure 3.

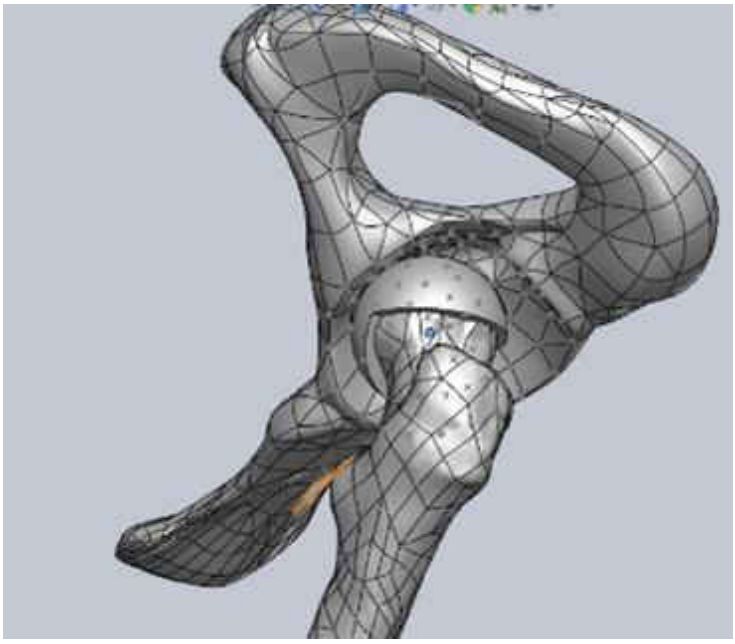

Figure 3 Femoral head in contact with the pelvis surface.

Then flexion, abduction, and hip rotation angles are independently varied for each location of the femoral head. After that, muscle lengths are determined and used to find the strain energy numerically from the muscle's strain. Lastly, the center of gravity heights of the lower extremity bones are determined, and the gravitational potential energy is thus calculated. Therefore, the potential energy (sum of strain energy and gravitational potential energy) as a function of femoral head position coordinates (X,Y,Z), flexion angle, abduction angle, hip rotation angle, and center of gravity height is computed. An optimization routine is developed to determine its extremum, and thus the least energy path is identified by the usage of Dijkstra’s algorithm to place the femoral head in its correct position from different hip dysplasia grades.

1.2 Motivation

This research defines the optimum strategy and procedure to guide the surgeon in moving and correctly placing the femoral head in its natural position inside the acetabulum for the four different grades with the required flexion, abduction, and hip rotation angles along the least energy path as dictated by the principle of stationary potential energy. The outcomes of this dissertation are the least energy paths for grades I, II, III, and IV as described by IHDI. These pathways contain the starting point (femoral head location during hip dislocation), the path that the femoral head should follow during the reduction process, the required orientation of the femur (flexion, abduction, and hip rotation angles), and the required energy for the reduction of the hip. These pathways are considered the ones that have the least energy and could potentially improve the treatment of the affected babies.

1.3 Thesis Overview

This dissertation has five chapters starting with the introduction chapter that has the background of developmental of hip dysplasia, the different causes of dysplasia, the clinical signs depending on the severity of the dysplasia, various types of treatment, and a brief introduction of the method that is used to determine the least energy path for the reduction process as shown previously.

The next chapter is the literature review, which contains a review of hip dysplasia and how they diagnose it, different treatment methods and how the mechanism of each

treatment works with the differences between them, the methods to find the potential energy map, and algorithms on how to find the optimal path between two points.

The following chapter explains the three-dimensional model that has the lower extremity bones and the corresponding muscles for the tension and movement of the bones, the assumed constraints for the model, and the energy method to identify the least energy path. Moreover, the muscle mechanics and introduction of the muscles are included in this chapter and muscle mechanics as described by Fung and Hill. Finally, the Dijkstra's algorithm is explained for the purpose of finding the least energy path.

The fourth chapter is to explain several outputs: the results of the potential energy method, different codes were used to support the proposed method, and the optimization method to find the pathways for all hip dysplasia grades. Lastly, the discussion and conclusion chapter is included.

CHAPTER 2: LITERATURE REVIEW

The literature review in this research encompasses several areas. The first area concerns the hip dysplasia and how it is diagnosed. The second area considers the different treatment methods and their mechanisms. Next, two primary methods for determining the potential energy map and algorithms for finding the optimal path between the starting point and the destination (target) point are presented.

Weinstein, et al. [4] introduced in their study that in case developmental hip dysplasia is not diagnosed directly after birth, the treatment will be painful, the risk will be greater, and the benefits of treatment will be less detectable. Indeed, if the diagnoses did not take place before six months old, the treatment and reduction will be more difficult, and the restoration of the normal hip and femoral head inside its natural position will be less likely. When the treatment fails, a surgical reduction operation is required for children between the ages of six to 18 months.

One of the most effective methods of treatment is the use of the Pavlik Harness. The word Pavlik was the family name of Professor Arnold Pavlik. In the 1950s, Professor Pavlik introduced this harness and called it the Pavlik Harness [10, 11, 7]. The inspiration and motivation to develop his harness were because of the high rate of avascular necrosis from conservative treatment methods and their lack of success. The harness uses the concept of manual reduction of the hip, then maintains the hip reduction by braces and corrects the acetabulum without the effect of avascular necrosis of the femoral head [12].

The functional method of the Pavlik Harness was described by Mubarak, et al. [12]. The seven principles that the Pavlik Harness was designed with are:

1- The reference for movement is the hip joint, and active movement should treat it.
2- Hip and knee flexion results in the hip abduction being nonviolent and unforced.
3- The stirrup configuration should assure hip flexion, gentle abduction, and redirection of the femoral head into the acetabulum socket.
4- The child will determine abduction range.
5- Hygiene of the child is easy to achieve even when in the orthosis.
6- The parents and caregiver can deal with the harness directly.
7- The harness should be simple and inexpensive.

By applying this treatment method to patients at that time with the previous principles, there were much fewer signs of avascular necrosis, and the success rate was higher especially 100 percent for dysplasia.

V. Bialik and N. D. Reis translated a paper for Arnold Pavlik in 1989 [13]. The topic for this translation was “Stirrups as an Aid in the Treatment of Congenital Dysplasias of the Hip in Children”. At the time the original article was published, the failure rate was 20 percent. The author reported that the high percentage of failures was due to the health condition of the patients, and the treatment methods applied to them. Pavlik defined two types of straps in his harness; the first one is stirrups for the lower

limb, which are tightened across the leg by two small straps, and the second strap crosses the shoulders and is then tightened. The author explained the configuration of the straps into four points: a) lower limb should be brought into flexion at the hip and knee joints, b) the lower limb should be moved free in the hip joint, c) give freedom to the flexion of the hip joints by the stirrups, d) the range of abduction should be determined by the patient as long as the adductor muscles provide, etc. Thus, by committing those requirements as described by the author the femoral head will be centered in the acetabulum socket with the help of unforced abduction and suitable flexion of the hip.

Another translation of Pavlik's work was done by Leonard F. Peltier in 1993 [11]. The paper introduced the method of the Pavlik Harness as a treatment for congenital hip dysplasia. Pavlik explained, that with the usage of the harness, the patients will be prevented from extending the hip joint and all other motions will be free. He introduced that the most important therapeutic factor in this kind of treatment was the active movements because it eliminates the effect of the passive mechanical method of treatment that causes femoral head necrosis. The arrangement of the harness as Pavlik explained is two shoulder straps crossed in the back and a strap in front to keep them in place, and the lower extremity is supported by the front strap just like a rider's position as shown in Figure 2. The flexion amount should be adjusted, and the foot should not be tightened. Another adjustment is that abduction motion should be relaxed by applying a diaper loosely. Pavlik wrote, "The relaxation of tension in the adductors through active motion, which is the first requirement for the spontaneous reduction, is

regulated by the child himself". During the abduction movement of the femoral head, the reduction will occur when the adductors are without tension and the acetabulum are empty.

Bin, et al. [14] wrote, "Very early Pavlik Harness therapy to ensure rapid hip reduction and stabilization optimize the potential of the acetabulum for spontaneous remodeling". The author explained in his article that the treatment protocol is for the hip to be flexed to 110 degrees and the knee to be at the level of the navel without abduction force.

According to Stuart L. Weinstein [7], at the hospital of children in San Diego, the treatment of newborns with hip dysplasia has a high success rate of 95%. Moreover, the use of the Pavlik Harness for older babies achieves an 85% success of reduction, while for children from six to nine months of age the rate of success drops. This device should be used for the newborn babies as soon as the diagnosis of dislocation has taken place, and for several weeks until the dislocated femoral head has localized and stabilized in its natural position in the acetabulum. This treatment may be used for an average of three months full-time and one more month part-time.

Another study that was conducted on the usage of the Pavlik Harness was done by Mubarak, et al. [15]. The work was to review the results of treating 18 patients with congenital dysplasia, subluxation, or dislocation of the hips. The most common problem was the failure of reduction. There were many reasons for failure as indicated in the article, and the most significant one was the improper use of the Pavlik Harness in the

treatment stage. However, the most important factor in the management of the hip dysplasia is that adduction and extension of the hip should be prevented while allowing flexion, abduction, and hip rotation. The author recommended a few points to achieve a high quality of treatment. First, the back straps should be crossed to prevent them from sliding over each other. The second recommendation is that the buckles for the anterior straps should be located at the child's anterior axillary line. Third, the buckles for the posterior straps should be located over the scapula. Fourth, the Velcro strap for the lower limb of the leg should be located just below the child's popliteal fossa. With this application, the results from the Pavlik Harness will be sufficient.

Kitoh, et al. [8] examined 221 hips of 210 patients. The results from his study were that 81.9% of the hips were reduced. In this study, they concluded that the best result of using the Pavlik Harness is when the abduction is more than 60 degrees. The harness was applied with hip flexed at 90 to 100 degrees. The posterior straps were laid-back enough for the knees to come to the midline in the position of the hip flexion.

According to Grill, et al. [16], the success of treatment of hip dysplasia with the Pavlik Harness is superior to others. The study was conducted for 3,611 hips, and the reduction rate was high. The author described the method behind the harness that two shoulder straps were crossed on the back and fixed by a front strap. Furthermore, there are two straps to hold the legs in slings, and the hip is flexed to more than 90 degrees with limited the extension, which will be kept by an anterior strap. The femur adduction should be prevented by the posterior strap, which will stop the crossing of the lower limb to the midline.

More studies of the hip dysplasia treatment were conducted by Guille, et al. [17]. They found that if the Pavlik Harness treatment were carried out at early ages for the babies, the reduction of the dysplasia is satisfactory. Moreover, Peled, et al. [18] studied the Pavlik Harness treatment and how the stirrups work. He considered in his study Graf III and IV, and the effect of the harness on the reduction of the hip with dysplasia.

Kalamchi, et al. [19], conducted the Pavlik Harness treatment for 122 patients over three months of age. Twenty-one patients had dislocated hips, and 101 patients were diagnosed with dysplasia, with an average age of five months old. The results were that 97% of patients successfully achieved reduction of the hip.

Another study that supports the usage of the Pavlik Harness at an early age was done by Atalar, et al. [20]. This study was conducted on 25 infants with a total of 31 patients with developmental dysplasia of the hip. They found that the success of the Pavlik treatment depended on Graf type, the age of treatment, and bilaterally.

Suzuki [21] studied the effect of the Pavlik Harness on hip dysplasia reduction. The study was recorded for nine infants with dislocation. There were two types of dislocation. For type A, the femoral head is displaced posteriorly and lies within the acetabulum with no contact with the anterior wall. For type B, the femoral head is in contact with the posterior side of the socket. The results of this study for type B were that reduction took place during deep sleep with no active movements. In type A, all six dislocations had the head settled slowly back to the bottom of the acetabulum. The author observed that in the manual reduction, the force to reposition the head is

needed, but with the usage of the Pavlik Harness, the force is generated from the weight of the legs, so it prevents the patients from extending the hip. He specified that this reduction was due to passive mechanical factors. Moreover, he described another type of dislocation called type C, where the femoral head dislocated out of the acetabulum. He concluded that in this case of dislocation, the head will not be reduced because of the posterior wall of the acetabulum blocks the movement, so manual reduction could force the head for reduction.

Also, Iwasaki [22] studied the mechanism of the Pavlik Harness and how the harness allowed reduction of the hip. The Pavlik Harness moves the femoral head to the posterior part of the acetabulum through flexion of the hip, and then moves it anteriorly into the socket through the abduction of the hip, as illustrated in Figure 4. Between 1966 and 1976, 240 dislocated hips of 204 patients were treated with the Pavlik Harness, and the ages were between one and seven months. During the treatment, the patients were frequently checked. When the neutral anteroposteriorly made in extension with the hip showed the femoral head at the center of the acetabulum, the hip was considered stable. After that, when the shallow acetabulum rim was improved, the harness was removed. The knee joint was to be at 90 degrees of flexion or more. Although, it is imperative to stretch the adductor muscles during the treatment where the weight of the lower extremity plays the role in stretching, which will allow the head to slide anteriorly over the acetabulum rim. The result was that 85 percent of the patients were successfully treated with the Pavlik Harness. The author

did a comparison with other treatment devices, and he found that the Pavlik Harness is simple and allows movements to the lower extremity other than an extension.

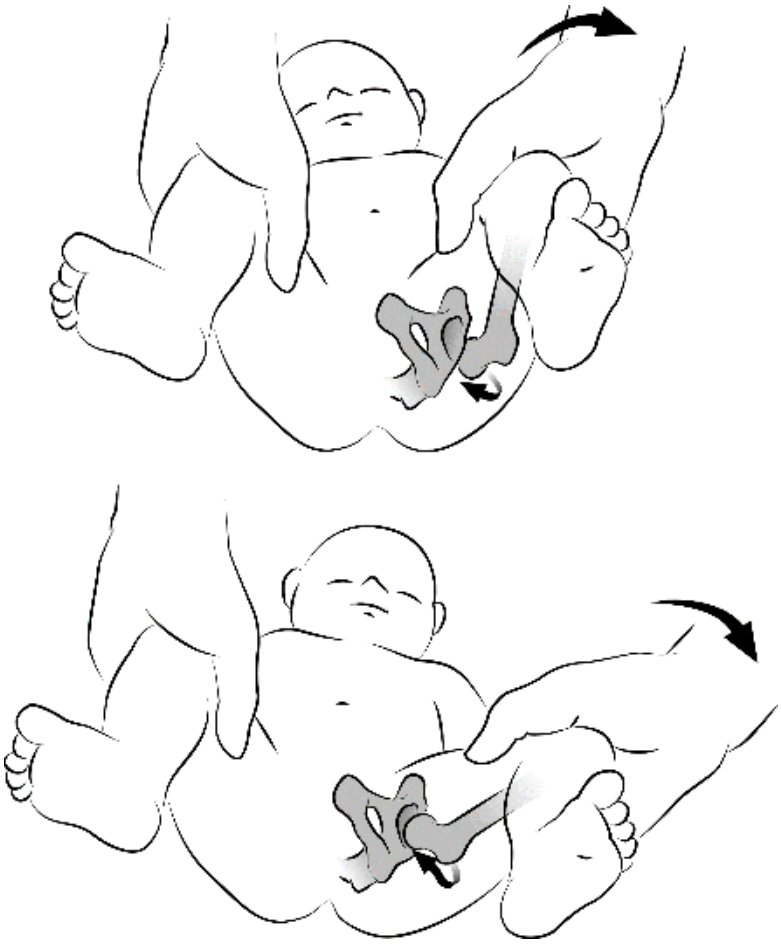

Figure 4 Direct reduction pathway identified by Iwasaki using the Pavlik harness, and for manual reduction.

Viere, et al. [23] explained in his study that the Pavlik Harness failed in some patients with dislocated hips. The author blamed the poor application of the harness for the cause of these failures. He agreed that it had gained widespread acceptance as a treatment for hip dysplasia, and it has limited complications if it is used in the proper way.

Abduction Orthosis is considered as an alternative method to the Pavlik Harness treatment [7, 24]. The orthosis is appropriated for infants of more than nine months old who require continued treatment of abduction positioning. This treatment method is applied to patients while walking. Moreover, it is sufficient for patients up to two and half years old. In this method of treatment, the abduction and flexion forces are transferred mainly to the pelvis by the straps.

Seidl, et al. [25], between November 2007 and December 2010, studied and evaluated the treatment consequences of the Tubingen hip flexion splint of newborn patients with unstable hips. The results from Seidl's study were a total of 50 dysplastic or dislocated hips in 42 patients who were treated magnificently with the Tubingen splint treatment.

Bernau [26] introduced a hip flexion splint that is used for reliable fixation of newborn patients with an unstable hip with a flexion angle of more than 90. One more study on the Tubingen splint was conducted by Atalar, et al. [27]. Their aim was to study the results of using the Tubingen splint for infants with hip dysplasia. Forty-nine patients were detected and studied. The upshots from their study were that 56 of 60 (93%) were successfully treated with no complications. Moreover, their conclusion is that the Tubingen provides abduction and offers advantages of preventing the hip adduction with no constraints for the knee and ankle joints to move.

One study was conducted by Wilkinson, et al. [28], which reviewed the results of 134 patients with hip dysplasia of Graf type-III and type-IV. They were treated with the

Craig splint, Pavlik Harness, and Von Rosen splint. The results of this study were that the patients treated with the Von Rosen splint are better compared to the other harnesses. The author said, “This may be because of the difficulty in maintaining the position of the femoral head in a very dysplastic acetabulum using the Pavlik Harness. It is probable that a more rigid splint would be more suitable”. He mentioned that the Pavlik Harness could be more efficient in cases of the lower dysplastic acetabulum.

Another study was by Tibrewal, et al. [10]. He studied the comparison between different hip dysplasia treatments. The first comparison was between the Frejka pillow and the Pavlik Harness. He found from the literature that the failure of reduction was 10% with a Frekja pillow and 12% in a Pavlik Harness. The usage of Pavlik Harness is better when applied to patients of an age less than 24 weeks. Another comparison was for the Craig splint, the Pavlik Harness, or the Von Rosen splint. He concluded that the Von Rosen splint gave the best results. The author said, “an acetabular angle of 36 degrees or greater was predictive of an unsuccessful outcome” with the use of the Pavlik Harness.

Papadimitriou, et al. [29] studied the Modified Hoffman-Daimler method for the treatment of late presenting Developmental Dysplasia of the Hip. This method involves guiding the femoral head to move gradually into the acetabulum by the muscle force of the adductor and flexor muscles of the hip. Figure 5 indicates the path of reduction as specified by Papadimitriou.

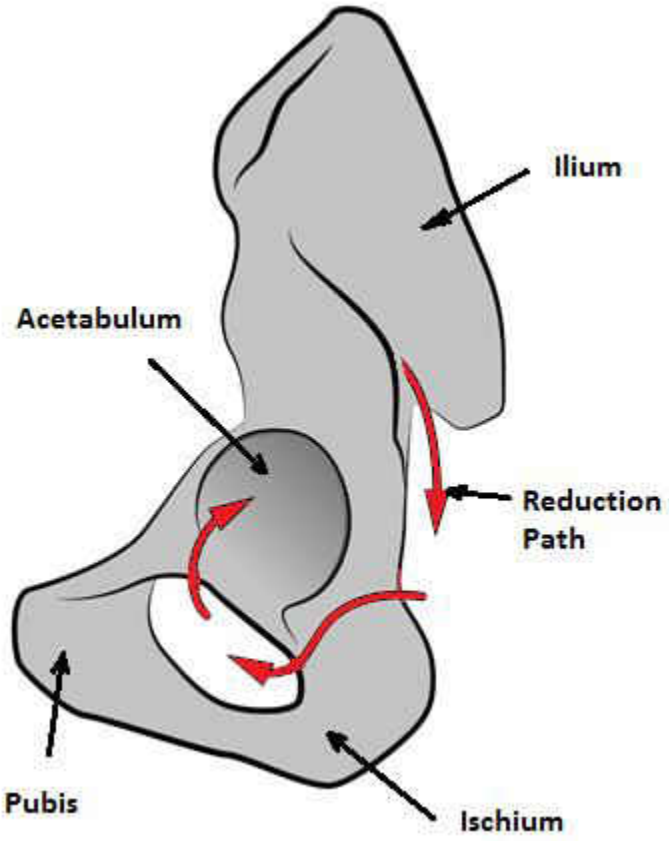

Figure 5 Reduction steps with using the Hoffman-Daimler method.

In the case of grade IV hip dysplasia, phase 1 of the reduction is when the child is placed in a harness with the hips in more than 90 degrees of flexion but less than 120 degrees. Phase 1 may last several weeks until the femoral head moves from the starting position to Obturator Foramen. When the femoral head has moved below the acetabulum, an abduction bar is placed between the legs. It keeps the hips in 90 degrees of flexion and each hip in 45 degrees of abduction for a total abduction of 90 degrees between the hips. In this position, the harness and abduction bar are worn at the same time for several more weeks. It allows the femoral head to travel medially and

then enter the acetabulum through the acetabular notch. After the hip is in the socket, the harness is removed, but the abduction bar is kept to prevent re-dislocation. As a conclusion, Papadimitriou said, “Late-presenting or neglected developmental dysplasia of the hip can be successfully treated with the use of a modified Hoffmann-Daimler method. The high rate of successful reduction, the low prevalence of osteonecrosis and residual dysplasia, and the limited complications may make this modified method a safe alternative to surgical treatment”.

Hip dysplasia can be studied by assuming the femur and the hip as rigid bodies connected by spring elements (the muscles). Each muscle is modeled as a spring having a constant “k”, initial length “L_o”, and a stretched length “L”. The corresponding potential energy “E” can be expressed as

$$E = \frac{1}{2}K(L_o - L)^2$$

This assumption is derived from the potential energy surface for a diatomic molecule [30]. However, the energy increases if the bond length “q” of the molecules is stretched. Hence, the potential energy at the original bond length will be zero, which is the bottom end of the parabola. Therefore, the first derivative of the energy function with respect to each generalized parameter is the stationary potential energy.

$$\frac{\partial E}{\partial q_i} = 0$$

According to Lewars [30], there will be a global minimum potential energy and local minima energy for the complex geometry. Figure 6 displays the global minimum

that has the lowest energy among the whole potential energy surface and the transition state where the molecule moves from one minimum to another.

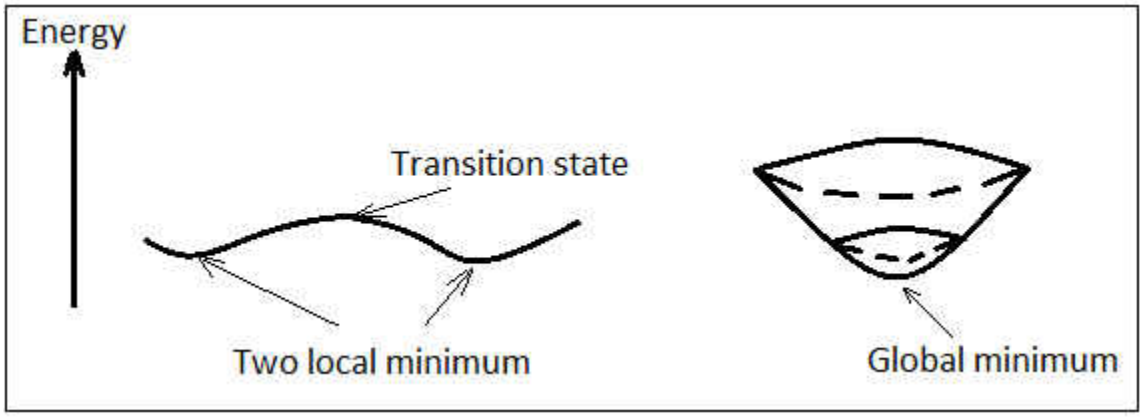

Figure 6 Local and global energy minima.

Huayamave [31] proposed a real-time response framework by using the Proper Orthogonal Decomposition (POD) method. His proposal was to provide a solution that calculates, in real-time, flow features and loads that result from wind-induced drag and lift forces on Photo-Voltaic (PV) systems. The solutions found are organized and stored to get the basis snapshots of POD decomposition matrix. A radial basis function (RBF) is used for interpolation network. Moreover, it will be employed to predict the solution from the POD decomposition, which will give a set of values of the design variables. Both the POD snapshot matrix and RBF interpolation network are stored. This stored data can be accessed anytime to predict the solutions.

Another study that used the POD is by Ostrowski, et al. [32]. Ostrowski was using it for an inverse method which was developed to estimate the unknown heat conductivity and the convective heat transfer coefficient. The POD was used here to

solve a sequence of direct problems within the body under consideration. Then each problem's solution is sampled at a matrix of a set of points. Moreover, each sampled field is known as POD snapshot. Furthermore, POD analysis is an efficient method to detect a correlation between the snapshots and yields a small set of orthogonal vectors (POD basis) constituting an optimal set of approximation functions. The result from this analysis is coefficients that are trained POD basis. Moreover, this basis is then used in the inverse analysis, which will be restored to a condition of minimization of the discrepancy between the measured temperatures and values calculated from the model.

Lewars developed an algorithm, which gives the path from the starting point to the global minimum through local minima and transition states, to optimize the geometry. For the purpose of finding a path, all points on the grid should be adjusted to give the lowest possible energy. Thus, for the chemical reaction, it is focused on the minima and the passage of the molecule from one minimum to another through a transition state. He described the potential energy surface as a plot of the energy that gives the energy as a function of coordinates, and it is called the Born-Oppenheimer surface. They used the first and second derivative of the energy function with respect to the generalized parameters "q_i".

$$E = \frac{1}{2}K(q - q_o)^2$$

$$E - E_o = K(q - q_o)^2$$

$$\frac{\partial E}{\partial q_i} = 2K(q - q_o)$$

$$\frac{\partial E^2}{\partial {q_i}^2} = 2K$$

Where ($\frac{\partial E}{\partial q_i}$), is the slope of the surface and ($\frac{\partial E^2}{\partial {q_i}^2}$), is the curvature, which is the force constant for motion along the geometrical coordinate.

Quapp, et al. [33] studied the properties of the potential energy surface by analyzing the concept of the minimum energy path with a choice of a coordinate system. They used the concept of potential energy surface for understanding the chemical reaction by using transition state theory. They used the term of path of least resistance to identify the continuous line connecting reactants and products in a chemical reaction. Quapp said, “This path is nothing else but a mathematically defined curve going from a higher to a lower potential”. He defined the potential energy function as “*U(x)”* and the gradient “$\frac{\partial U}{\partial X_i}$*=0”* is the description of stationary points.

According to Scharfenberg [34], the stationary points on the potential energy surface should be found by using geometry optimization methods instead of calculating the points on the surface. Initially, they have to find the first derivative of energy with respect to the coordinates “$\frac{\partial E}{\partial \xi_i} = 0$”, which are the stationary points, where ξ_i is the geometrical coordinates. He mentioned that to increase the efficiency of the derivatives, it is recommended to use analytical calculation rather than numerical methods. In

addition, to find the critical points on the surface that identify the minimum energy path, they have to calculate the eigenvalues and eigenvectors of the constant force matrix, which are the second derivatives of energy function with respect to geometrical coordinates "$\frac{\partial E^2}{\partial \xi_i{}^2}$", which is the transition states.

Smidstrup, et al. [35] proposed a method that generates an initial guess of a transition path without evaluation of the energy. The transition path is between initial and final states of the system. The author described the surface as a function that interpolated pairwise distances at each discretization point along the path, which was used to find the minimum energy path along the potential energy surface. The initial path guess is advanced from the nudged elastic band method, which represents the path as a discrete set of configurations for all the atoms in a chemical reaction system. The nudged elastic band method is constructed by a linear interpolation of the coordinate system between the initial and final states.

In chapter 8 of Schlegel [36], the author explained the potential energy surface and its components, i.e. global minima, transition states, saddle points, path, etc. The potential energy surface is defined as the energy surface of molecules that is a position function of atoms or nuclei. This function can be calculated from the electron energy and wave function for a series of fixed nuclear positions. Furthermore, when the gradient or the first derivatives of the potential energy surface are equal to zero, the local minima can be located. Schlegel used the concept of a matrix of second derivatives of the potential energy surface (Hessian matrix or force constant matrix) to

find the saddle points and transition states. All those factors are used in an algorithm to find the reaction path as an optimum path.

An algorithm was developed and analyzed for locating stationary points corresponding to local minima and transition states on the potential energy surface by Nichols, et al. [37]. The algorithm depends on the first derivative and second derivative of the energy function with respect to geometrical constants. The author identified the path between the minima through transition states. The method, which was proposed in this article, uses the local slope or gradient vector and Hessian matrix as the second derivative to find the step vector which was used to find the path on the three-dimensional potential energy surface.

A multidimensional potential energy surface has been studied with respect to finding transition states and the path by Basilevsky, et al. [38]. The authors used a concept of the reaction path on the potential energy surface, and gradients with second derivatives for local minima, saddle points, and transition states. They generated an algorithm called “the mountaineer’s algorithm”, which formulated a method of constructing a smooth curve linking the initial location to the destination with saddle points. The smooth curve was called the “optimum ascent path”.

Another method for the energy path was described by Kiryati, et al. [39]. He considered an estimation of the minimal distance and the shortest path between two points on a continuous three-dimensional surface. They used an algorithm to compute the shortest path with the shortest time. In a complex surface, it is better to start with an

initial guess to reduce the possibility of convergence to unimportant local minima. The three-dimensional surface is digitized and continuous. This surface is digitized as a set of voxels, which can be represented by a 6-directional chain code. By applying the method explained in their work, they found the minimum path for separate examples.

Stefanakis, et al. [40] examined the optimum path for travel problems. They implemented a movement algorithm on the plane surface, three-dimensional space, and movement on a spherical surface. It has been defined that the optimal path could be considered the shortest, least expensive, fastest, or least risky path. It was described in their approach that they have five steps to find the optimum path. First, determine a finite number of spots in space. Second, establish a network of those spots. Third, produce the travel cost. Fourth, assign an accumulated travel cost to the spots. Finally, determine the optimum path.

Another study continued and improved the method of Dijkstra's algorithm. This study was conducted in 1987 by Mitchell, et al. [41], and it determined the shortest path between a source and destination points in the polyhedral surface while the path stays on the surface. The idea was to locate the destination between the source and the destination in the subdivision that was created by the algorithm. They tested a 3-dimensional surface of a problem called Discrete Geodesic problem. In their theory, they divided the surface into triangles, and they found the optimal path between two points, not passing any point more than once. They called their algorithm the "continuous Dijkstra".

Aleksandrov, et al. [42] presented the first algorithm for computing the shortest paths in weighted three-dimensional domains by polynomial time approximation. They formulated their problem to calculate the path of the minimum cost from a fixed source to any destinations in the domain surface. The cost is defined as a weighted sum of lengths. The proposed shortest path algorithm was established by using the Voronoi Diagram.

Kimmel, et al. [43] tried to generate an algorithm to find the shortest path. They considered two stages in their study; the first phase is an algorithm that combines three-dimensional length estimators with the graph, and the second phase is developed to become a shortest geodesic curve. Those stages in this study were achieved by using an algorithm that deforms an arbitrary initial curve ending at two points on a given surface via geodesic curvature shortening flow. The authors mentioned in their study that to find the shortest path between two points on a continuous surface, a numerical solution of differential equations by numerical integration is involved. Moreover, an initial guess is needed to increase the convergence to the global optimum path.

CHAPTER 3: METHODOLOGY

3.1 Model

One of the difficulties encountered in this type of research is the lack of data for new-born babies. To implement the study, a group of researchers developed a rigid-body dynamic model [5]. It was generated by using SolidWorks® (Dassault Systems, Concord, MA) from CT scans of different models and scaling them to a particular baby model. Furthermore, a simulation software “OpenSim” (National Center for Simulation in Rehabilitation Research, Stanford, CA) of an adult model [44], which used cadavers with average height of 168.4 ± 9.3 cm and weight of 82.7 ± 15.2 kg [45], is used to study the muscle lengths and behaviors due to femur orientation and to verify the solid model from SolidWorks®. More importantly, the mechanics of several selected muscles is studied for potential energy calculation. A study is done to check all the constraints that affect the model.

3.1.1 SolidWorks Model

A group of researchers created a three-dimensional solid model that was constructed by using the solid model software. Initially, a simplified model was generated by the hip geometry with lower extremity bones and includes most of the anatomical properties to carry out the analysis [5]. Figure 7 shows the detailed model that was modified with SolidWorks®.

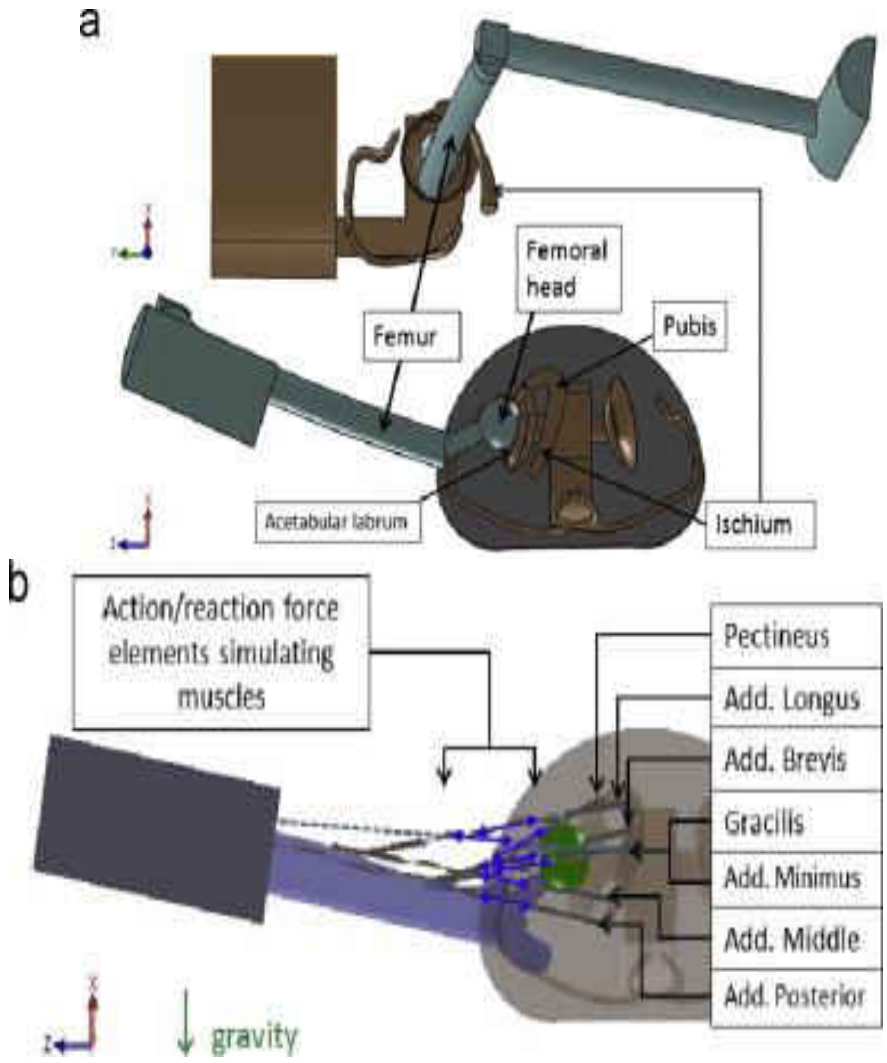

Figure 7 Initial 3D model, a) hip and bones, b) adductor muscles in the model [5].

This solid model was modified and constructed by using a CT-scan of a six-month-old female. The lower extremity was modeled in three segments: the femur, fibula, and foot.

Later research was implemented by Huayamave, et al. [9]. They reconstructed the lower limb bones model developed by SolidWorks® of the patient-specific infant geometry to represent the behavior and response of the femoral head using the Pavlik

Harness treatment [46, 9]. This model was generated and constructed with the use of different reference models and scaled to the size of a 10-week baby. The hip model was developed by using a 14-year-old female with an anisotropic scaling factor (X=0.35, Y=0.3, and Z=0.35) which matched an infant's orthopedic data found in Hensinger's Standards in Pediatric Orthopedics [16], as displayed in Figure 8.

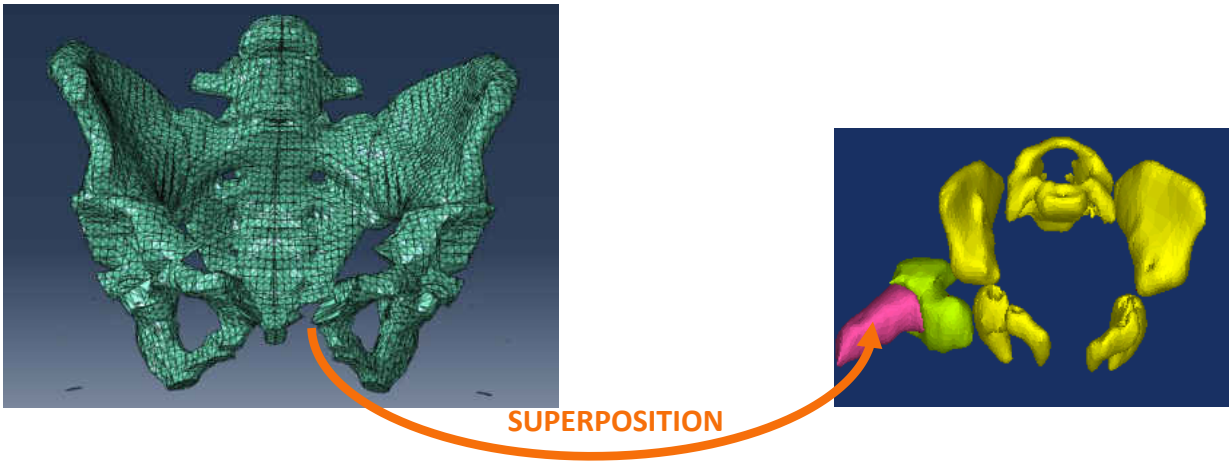

Figure 8 Hip model and its reference model of 14-years old female on the left [9].

The femur model was constructed by scaling a 38-year-old male's femur from the Visible Human Project of the National Library of Medicine (NLM) [47]. Thus, the femur was scaled anisotropically (X= 0.23, Y= 0.25, and Z= 0.22) to match the 10-week-old baby as depicted in Figure 9.

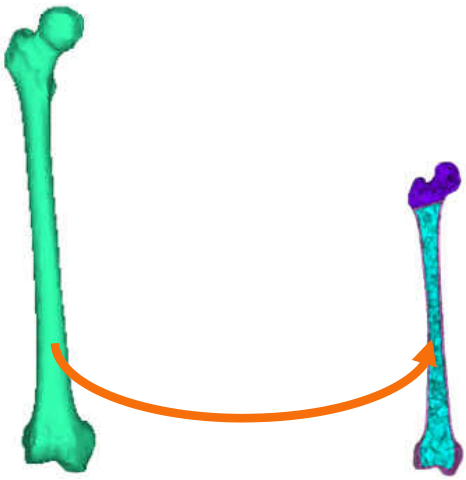

Figure 9 Femur model and its reference model of 38-years old male on the left [47].

After scaling the lower limb bones from different models as described above, the 3D model was constructed, as illustrated in Figure 10. The model includes the hip, femur, tibia, fibula, and foot. Following, five adductor muscles were added to the solid model [48]. Those muscles are the Pectineus, Adductor Brevis, Adductor Longus, Adductor Magnus, and Gracilis. They have been modeled with straight lines of action.

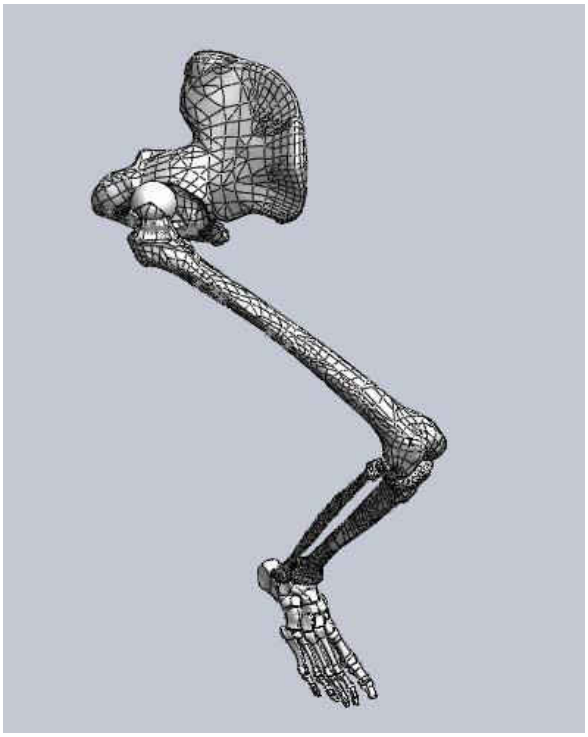

Figure 10 3D model of the lower limb bones with SolidWorks.

The knee joint was flexed at 90 degrees. For this configuration, the adductor muscles during the treatment will be stretched by the effect of the weight of the lower extremity, which will allow the head to slide anteriorly over the acetabulum rim [22].

3.1.2 Muscle Model

In the human body, there are several tissues and one of the most functional tissues is the muscle. Muscles and tendons actuate the movement by developing forces and moments about the joints. Also, muscles are made of a set of muscle fascicles that are arranged in a parallel form. Each muscle fascicle is formed from a bundle of muscle fibers, which are a similar length in each specific muscle but vary between different muscles [49, 50]. Thus, these fibers' length depends on the number and length of

sarcomeres. Those sarcomeres are arranged in a series in the fibers, which are the fundamental unit of force generation in the muscle [51].

Moreover, muscle tissue is considered a soft tissue. There are three types of muscles in the body: skeletal muscles, smooth muscles, and cardiac muscles [52]. The skeletal muscles link the skeletal bones, and then provide the action and movement of the skeleton. Smooth muscles are different from skeletal muscles and cardiac muscles. They can be found on the blood vessels and in the lymphatic vessels. The cardiac muscles are in the heart walls and contract without stimulation of the neuro-central system. Thus, the corresponding muscles for hip dysplasia studied in this research are the skeletal muscles.

The five key adductor muscles that are considered in this research (Pectineus, Adductor Brevis, Adductor Longus, Adductor Magnus, and Gracilis) are displayed in Figure 11.

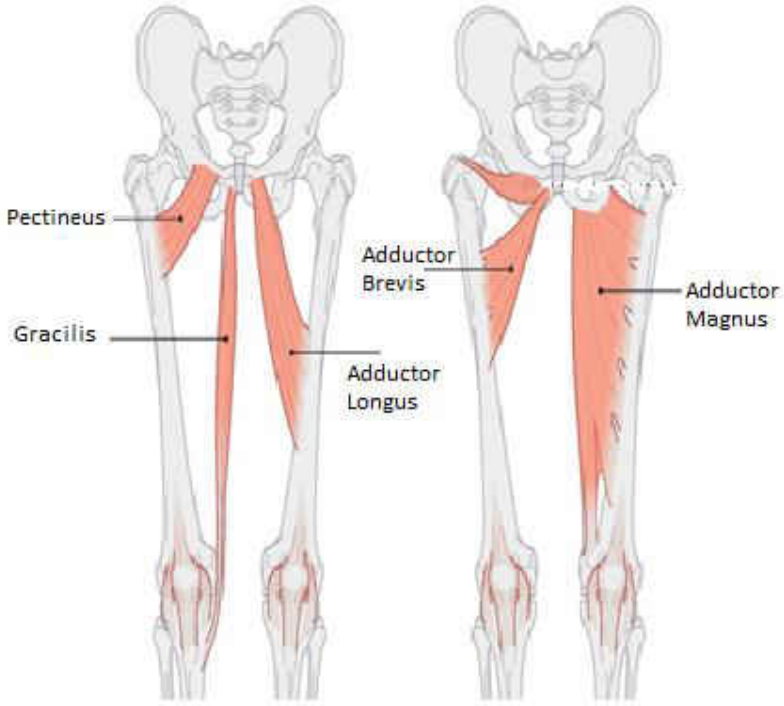

Figure 11 Five adductor muscles (Pectineus, Adductor Brevis, Adductor Longus, Adductor Magnus, and Gracilis) [53].

The adductor muscles can adduct and produce external rotation of the hip. The Pectineus muscle is a quadrangular muscle that is flat and located at the anterior part of the upper and medial of the thigh. It is the most anterior adductor muscle of the hip, and the major function of this muscle is to flex the thigh at the hip. However, the Adductor Brevis is the muscle that connects the hip at the inferior ramus of the pubis to the thigh at the pectineal line and the middle of the femur. Its function is to rotate the thigh and flex it, but the prime function is to adduct the thigh at the hip. In the same way, the Adductor Longus is located in front of the other adductor muscles on the same plane of the Pectineus. It adducts the hip along with flexion and internal rotation. The Adductor

Magnus muscle is formed in a triangle shape, and to study its behavior during this study it is divided into three different muscles (Adductor Minimus, Adductor Middle, and Adductor Posterior) [48], as displayed in Figure 12.

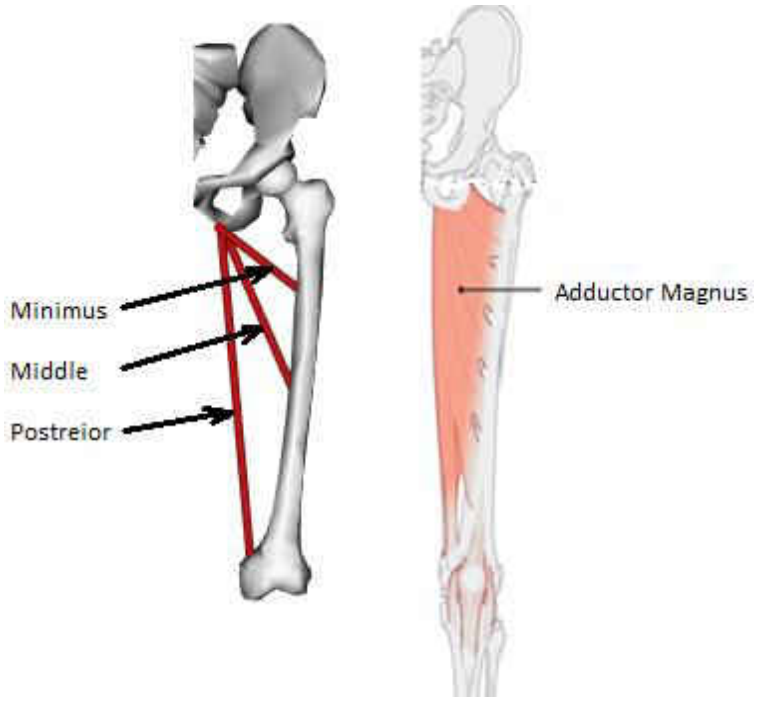

Figure 12 Adductor Magnus Muscle divided into three different muscles [53].

Finally, the Gracilis is the muscle that adducts the tibia and the femur at the hip and helps flex the leg at the knee. It originates at the lower symphysis pubis and the pubic arch and is inserted at the medial tibia [54].

3.1.3 Muscle Mechanics

The skeletal muscles produce active force (F^{CE}), the series element force (F^{SE}), and passive force (F^{PE}). The summation of the active and passive forces produces the total force of the skeletal muscles (F^{M}) [55-57].

$$F^{M} = F^{CE} + F^{SE}$$

$$F^{PE} = F^{SE}$$

The active force is generated by the interaction of actin and myosin contractile proteins. It is generated under isometric conditions while shortening the sarcomere. The sarcomere resting length occurs at the peak of the active tension curve. The passive force is obtained by lengthening the muscles and is increased exponentially by stretching the muscles [58]. This force, that starts at the sarcomere resting length, is generated by pulling the muscle fibers, as shown in Figure 13. The characteristic behaviors of the passive part of the muscle are a non-linear relation between stress and strain, incompressible behavior, and large deflection [59].

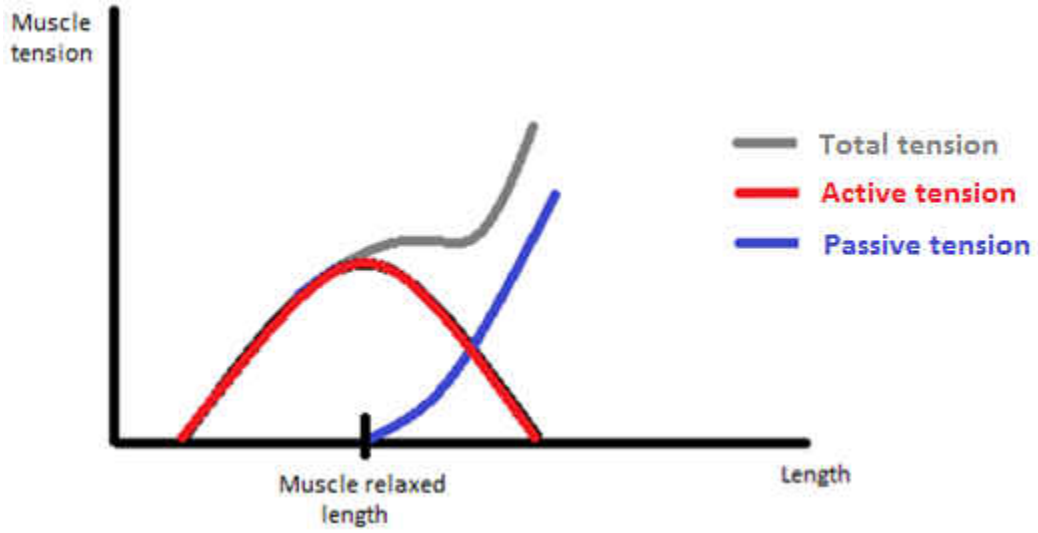

Figure 13 The behavior of active and passive forces on the muscles [60].

The mechanics of Skeletal Muscles has been studied by many researchers. One of the most well-known models is the classical three-elements Hill-Based muscle model [61, 59], as described in Figure 14.

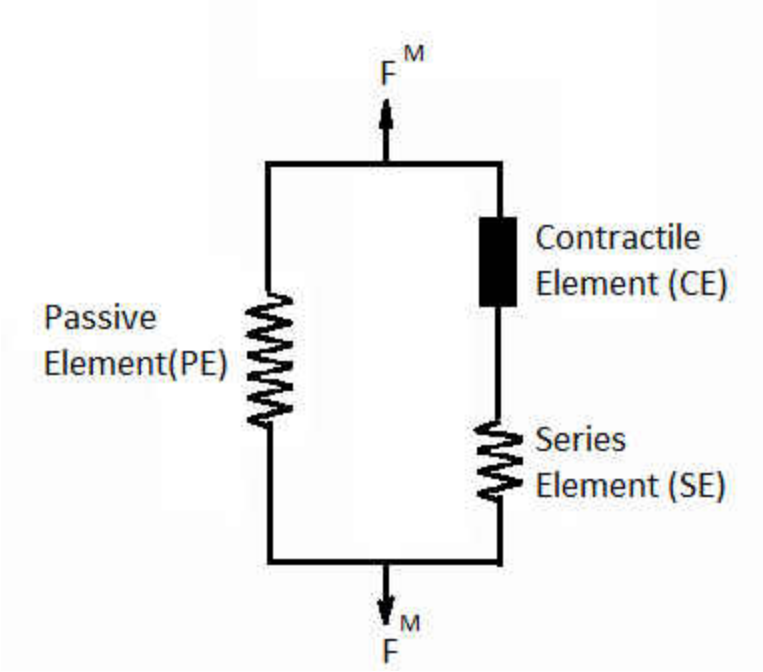

Figure 14 Hill-Based three-element muscle model [55].

The Hill-Based muscle model consists of a contractile element (CE) and two non-linear spring elements, one in series (SE) and another in a parallel form (PE). The CE element models the active force of the muscle. The SE element is a spring that is responsible for the non-linear movement of the muscle and provides an energy storing mechanism. It is also considered as a lightly-damped elastic element in series with the contractile element. The PE element was modeled as a viscoelastic or quasi-static elastic element, which is due to the very slow lengthening of the muscle fiber. This element, which is defined as the passive element, handles the stretch of the muscle [60, 55].

During the hip dysplasia treatment with the usage of the Pavlik Harness, the best results occur when the patient is asleep with no active motion [21]. According to the

research [22, 21, 46] in the manual reduction, the force to reposition the femoral head is needed, but with the usage of Pavlik Harness, the force is generated from the weight of the legs. This prevents the patients from extending the hip because the weight causes abduction. By these means, the reduction was due to passive mechanical factor. It has been shown that the passive force is considered the affecting force on the muscle due to stretching.

Muscles are modeled as nonlinear force elements positioned along the line of action of the muscles and defined by a constitutive nonlinear model named the Fung model [62]. Lately, Magid and Law gave the final model of the muscle as below [63].

$$\sigma = \frac{E_o}{\alpha}\left(e^{\alpha\,\varepsilon} - 1\right) \qquad (1)$$

Where, σ is muscle stress due to deformation, E_o is muscle elastic modulus, α is empirical constant, and ε is the muscle strain.

The muscle strain is calculated by using the reference length "L_i", which is 80% of the relaxed length at the relaxed position, as illustrated in Figure 13 above.

3.1.4 Model Scaling Factor Verification

The OpenSim model is used to verify the reconstructed SolidWorks model which has an anisotropic scaling factor of x=0.23, y=0.25, and z=0.22 for the femur of a 38-year-old male from the Visible Human Project "VHP" [47] to the 10-week-old baby. The procedure of this verification is to find the initial length of the five muscles from OpenSim along with all possible abduction and flexion angles. The muscles' initial

length (a function of abduction and flexion angles) are found from OpenSim by using the surface chart. For example, Figure 15 shows the surface chart for the Adductor Magnus Minimums muscle.

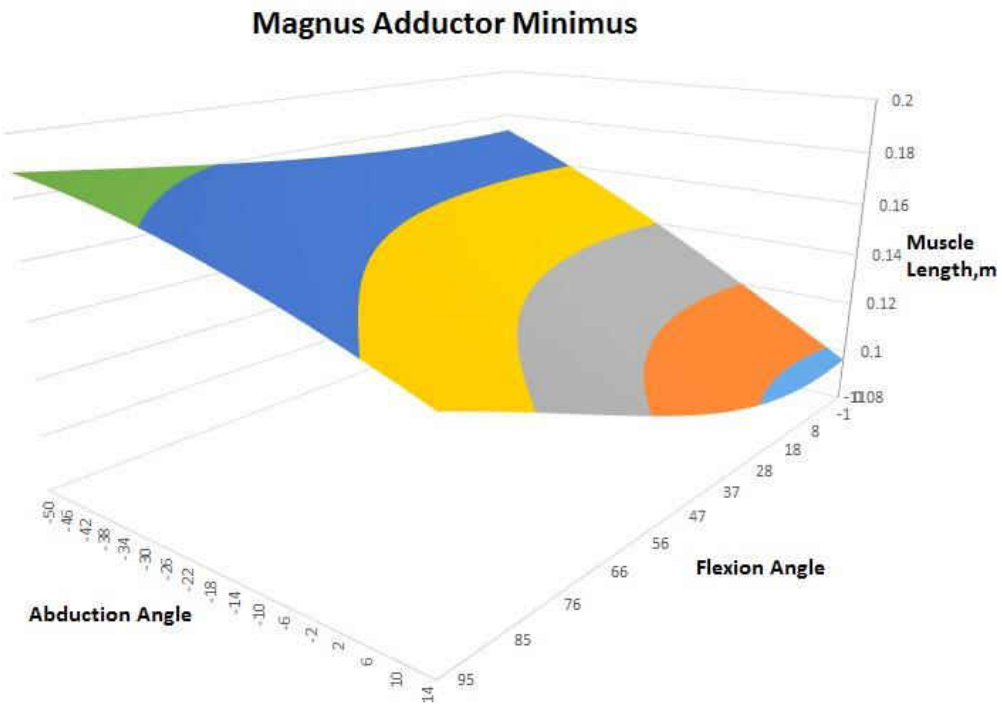

Figure 15 Adductor Magnus Minimus muscle length as a function of flexion and abduction angles (OpenSim).

After finding the initial length of all muscles, the scaling factors are then varied between 0.206 and 0.26, and they have an average scaling factor of 0.23 in the length direction, as listed in Table 1. After a comparison of the SolidWorks model and the OpenSim model is completed, it is found that the scale used has an average difference of about 8.7% in the length direction.

Table 1 Muscle length and scaling factor between OpenSim and SolidWorks model.

Muscle	Length (OpenSim)	Length (SolidWorks) @ same angles	SolidWorks initial Length	Differences in SolidWorks	Scaling factor
Pectineus	70.7 mm	18.20 mm	17.60 mm	3%	0.257
Add. Longus	170.7 mm	38.80 mm	36.37 mm	6%	0.227
Add. Brevis	114.9 mm	23.96 mm	23.79 mm	0.7%	0.208
Magnus Add. Minimus	95.3 mm	21.45 mm	20.94 mm	2.4%	0.225
Magnus Add. Middle	173.0 mm	39.88 mm	39.89 mm	≈ 0%	0.230
Magnus Add. Posterior	319.0 mm	85.53 mm	81.31 mm	5%	0.260
Gracilis	430.3 mm	87.27 mm	87.27 mm	0%	0.203

3.1.5 Constraints

There are several constraints taken in to consideration in this research. The geometrical constraints arise from the femoral head shape and the pelvic surface. The head, modeled as a sphere [46, 9], is depicted in Figure 16.

Figure 16 The femoral head in a spherical shape [9].

Moreover, the femoral head is assumed to be in contact with the pelvic surface in all locations of the hip, as shown in Figure 3 above. Thus, the distance from the femoral head center to the contact point is "*d=7mm*" (the femoral head radius).

The distance formula is used to compute the coordinates (*x,y,z*) of the femoral head center.

$$d = \sqrt{(x - x_i)^2 + (y - y_i)^2 + (z - z_i)^2} \quad (2)$$

Where, (x_i, y_i, z_i) is the contact point on the pelvic surface.

Additionally, the harness configuration is used to constrain the ranges of the femur orientation to be rotated about the flexion axis between 70 degrees and 130 degrees, as shown in Figure 17, within an abduction angle range of 0 degrees to 90 degrees, as illustrated in Figure 18, and with a hip rotation angle ranging between -30 degrees to +30 degrees, as depicted in Figure 19.

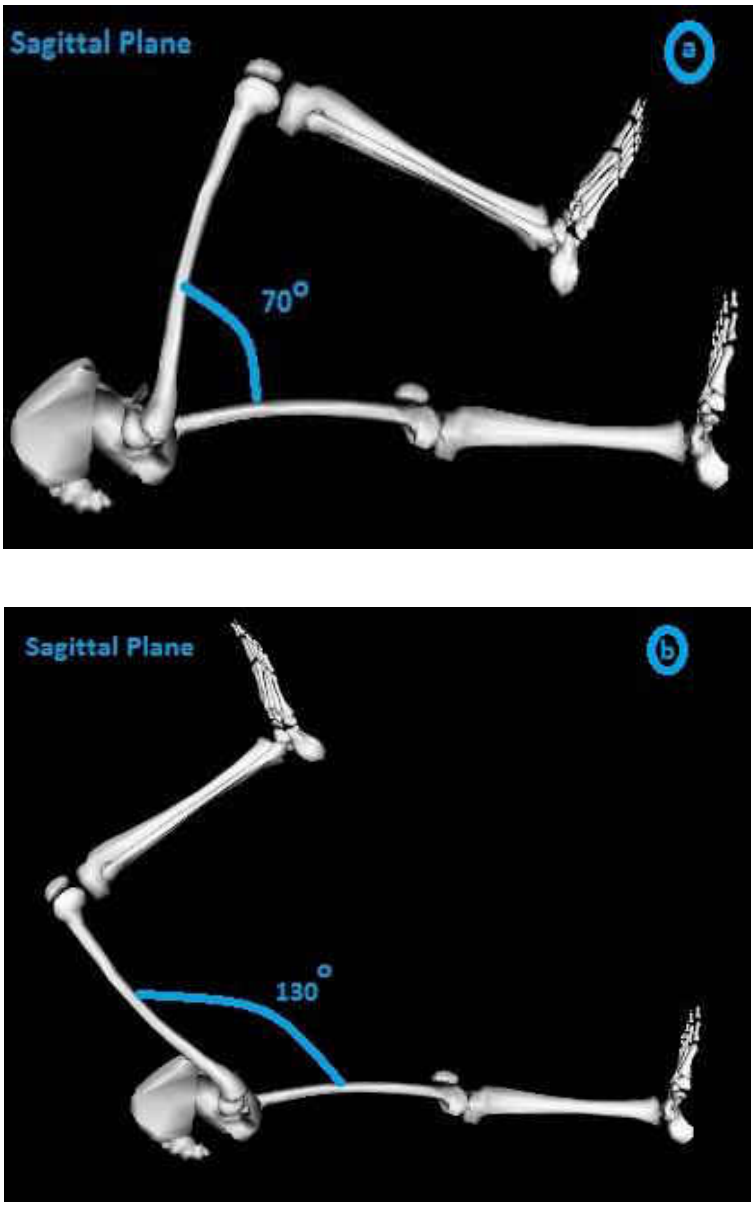

Figure 17 Flexion angle range between 70˚ and 130˚, a) 70˚, and b) 130˚.

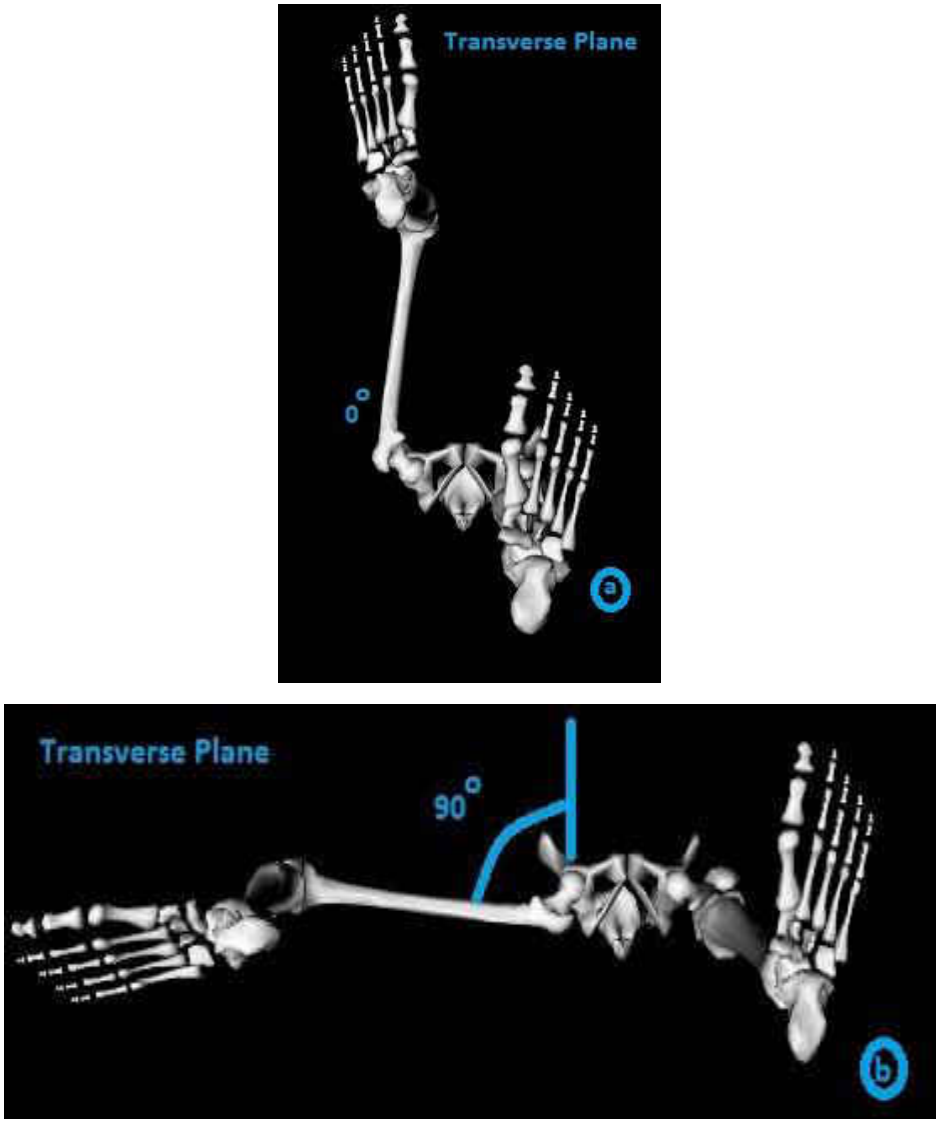

Figure 18 Abduction angle range between 0˚ and 90˚, a) 0˚, and b) 90˚.

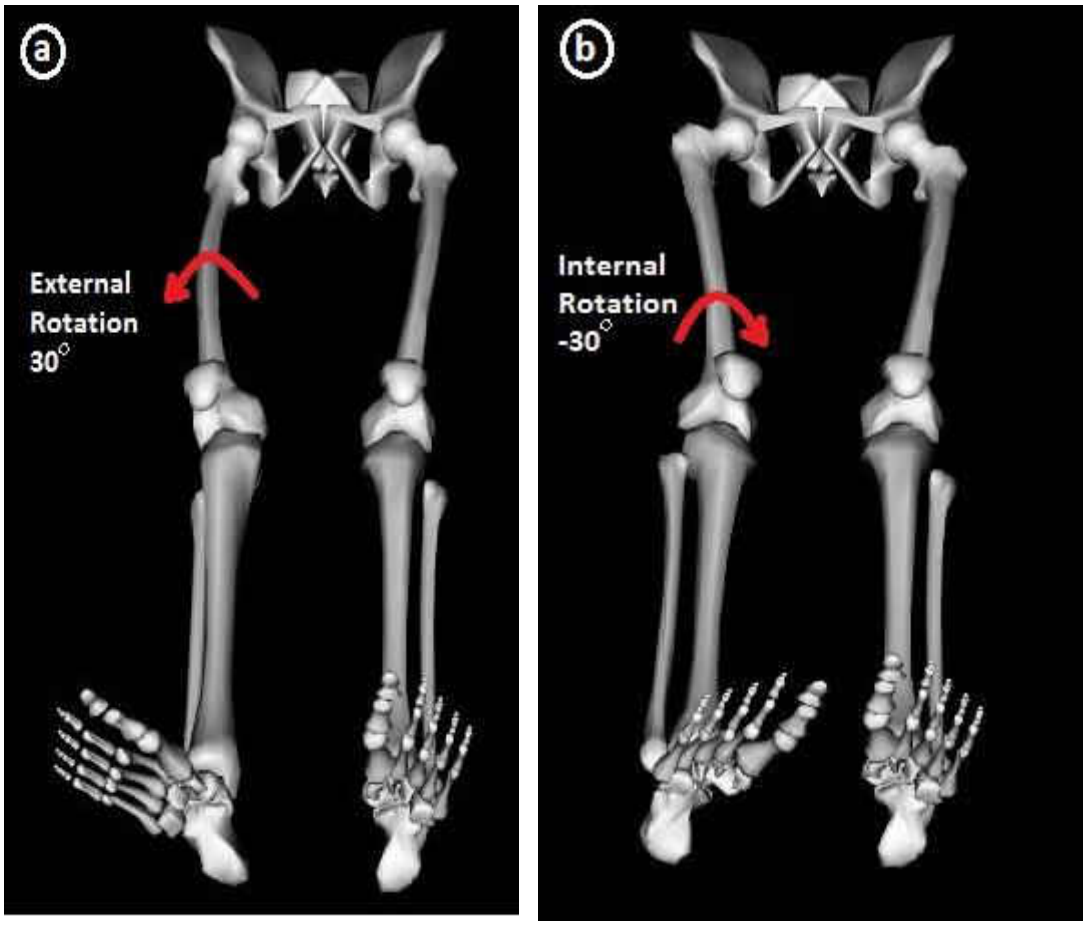

Figure 19 Hip rotation angle, (a) external rotation, and (b) internal rotation.

3.2 Energy Method

As discussed earlier, this study is based on the principle of stationary potential energy that consists of strain energy and gravitational potential energy. The strain energy is stored in the muscles due to the stretch from the dislocation and the rotation in flexion, abduction, and hip rotation angles. Whereas, the gravitational potential energy is produced by the weight of the lower extremity bones (femur, tibia, fibula, and foot).

3.2.1 Strain Energy

The strain energy of the considered muscles is computed according to the following procedure. First, a computer program is developed using the collision detection algorithm, which uses vectors from the center of the sphere (femoral head) to selected points on the pelvic surface, as illustrated in Figure 20. In this routine, the femoral head is located in the space away from the pelvic surface and moved toward each point on the surface while checking for any point of contact. Once the code finds the distance “d” is equal to 7mm, it prints out the coordinates of the femoral head center. Refer to Appendix A for details.

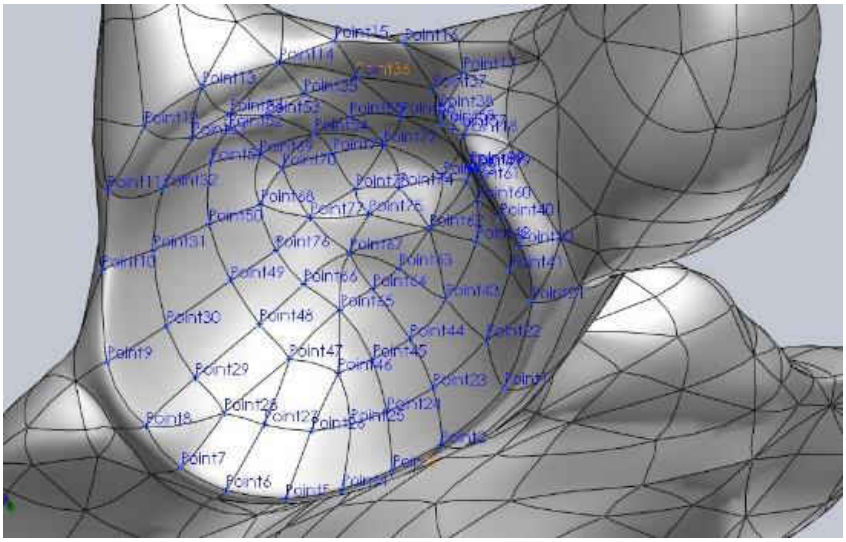

Figure 20 Points located on the wireframe of the surface by using SolidWorks®.

Second, by getting a grid of points from the collision detection routine, a further calculation is conducted. At each point of the sphere center, the lengths “L” of the selected muscles are calculated by using the distance formula between the insertion

and origin points on the femur and the hip. Following, the strain "ε" for all muscles is calculated, as described in equation 3.

$$\varepsilon = \frac{L - L_i}{L_i} \quad (3)$$

L_i is the reference muscle length and is equal to 80% of the muscle's relaxed length "L_{relax}", as shown in Figure 13 above. The relaxed lengths are assumed to be at the fetal position of the new born baby, which is observed at 120 degrees of flexion and 20 degrees of abduction.

Because muscles can only be stretched, a Heaviside function is used to exchange all negative values of the strain with zero value, as illustrated in Figure 21 and equation 4. Therefore, the effective strain can be described as shown in equation 5.

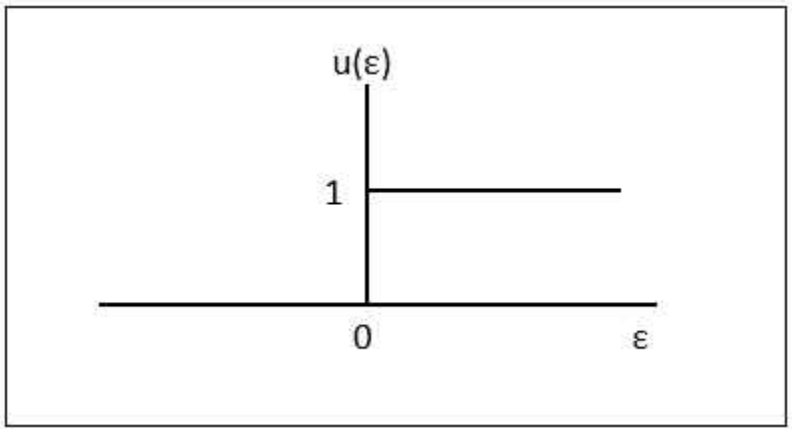

Figure 21 Heaviside function chart.

$$u(\varepsilon) = \begin{cases} 0 & if \quad \varepsilon < 0 \\ 1 & if \quad \varepsilon > 0 \end{cases} \quad (4)$$

$$\varepsilon_{eff} = \varepsilon * u(\varepsilon) \quad (5)$$

To find strain "ε" for each muscle mathematically, the following formulation is implemented for one muscle and then can be used for the other muscles by changing the origin coordinates (X_h, Y_h, Z_h), and insertion coordinates (X_f, Y_f, Z_f) for each specific muscle. For example, Figure 22 shows the origin and the insertion coordinates of the Pectineus muscle.

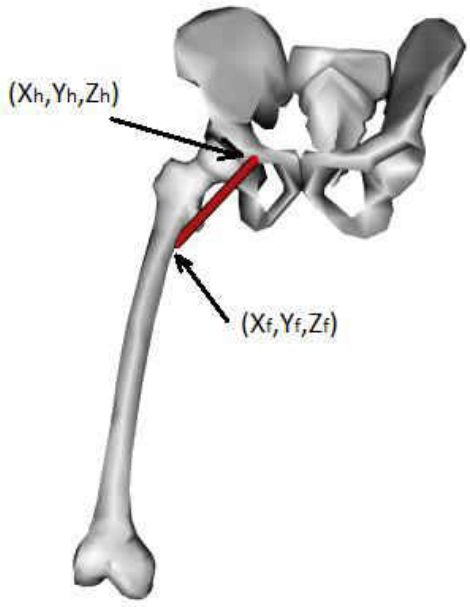

Figure 22 Origin and insertion points for the Pectineus muscle.

- (X_h, Y_h, Z_h) is the coordinate of muscle origin in the hip.
- (X_f, Y_f, Z_f) is the coordinate of muscle insertion in the femur.
- (X, Y, Z) are the coordinates of femoral head center.
- (x_1, y_1, z_1) is the first transformation of (X_f, Y_f, Z_f) about the flexion angle.
- (x_2, y_2, z_2) is the second local transformation of (x_1, y_1, z_1) about the abduction angle.
- (x_3, y_3, z_3) is the third local transformation of (x_2, y_2, z_2) about the hip rotation angle.
- θ is the flexion angle.

- Φ is the abduction angle.
- φ is the hip rotation angle.
- L_{relax} is the muscle relaxed length at the relaxed position $(\theta = 120^o \ and \ \Phi = 20^o)$ for the new born baby.
- The first transformation is about the flexion angle of the insertion coordinate (X_f, Y_f, Z_f) to the coordinate (x_1, y_1, z_1), as shown in Figure 23.

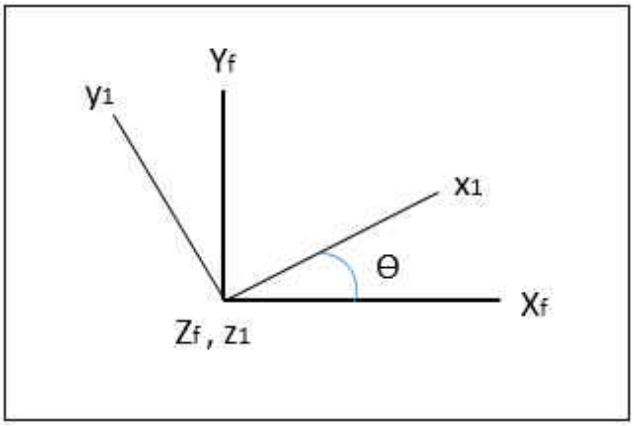

Figure 23 First transformation about the flexion angle.

$$\begin{bmatrix} x_1 \\ y_1 \\ z_1 \end{bmatrix} = \begin{bmatrix} \cos\theta & -\sin\theta & 0 \\ \sin\theta & \cos\theta & 0 \\ 0 & 0 & 1 \end{bmatrix} \begin{bmatrix} X_f \\ Y_f \\ Z_f \end{bmatrix}, \text{where } \Theta \text{ is the flexion angle.}$$

$$\boxed{\begin{aligned} x_1 &= X_f.\cos\theta - Y_f.\sin\theta \\ y_1 &= X_f.\sin\theta + Y_f.\cos\theta \\ z_1 &= z_f \end{aligned}} \qquad (6)$$

- The second transformation is about the abduction angle of the coordinate (x_1, y_1, z_1) to the coordinate (x_2, y_2, z_2), as shown in Figure 24

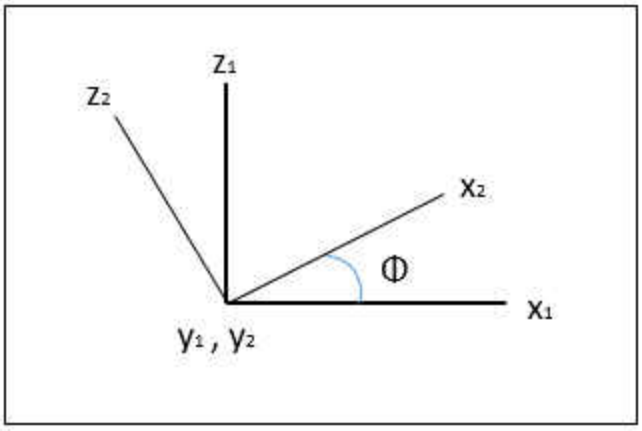

Figure 24 Second transformation about the abduction angle.

$$\begin{bmatrix} x_2 \\ y_2 \\ z_2 \end{bmatrix} = \begin{bmatrix} \cos\Phi & 0 & -\sin\Phi \\ 0 & 1 & 0 \\ \sin\Phi & 0 & \cos\Phi \end{bmatrix} \begin{bmatrix} x_1 \\ y_1 \\ z_1 \end{bmatrix}, \text{where } \Phi \text{ is the abduction angle.}$$

$$\boxed{\begin{array}{c} x_2 = x_1.\cos\Phi - z_1.\sin\Phi \\ y_2 = y_1 \\ z_2 = x_1.\sin\Phi + z_1.\cos\Phi \end{array}} \quad (7)$$

- The third transformation, which is for point (x_2,y_2,z_2), is about the hip rotation angle, as illustrated in Figure 25.

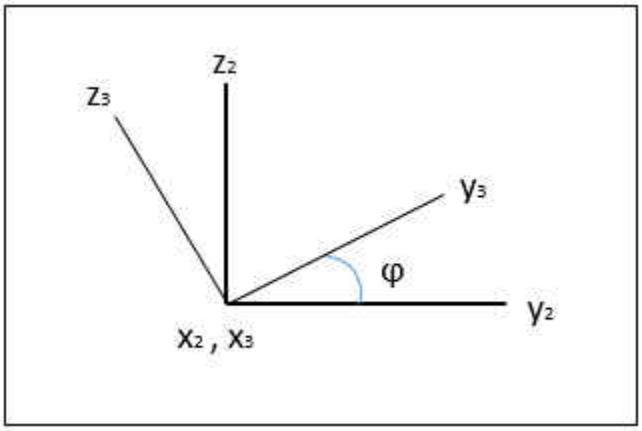

Figure 25 Third transformation about the hip rotation angle.

$$\begin{bmatrix} x_3 \\ y_3 \\ z_3 \end{bmatrix} = \begin{bmatrix} 1 & 0 & 0 \\ 0 & cos\varphi & -sin\varphi \\ 0 & sin\varphi & cos\varphi \end{bmatrix} \begin{bmatrix} x_2 \\ y_2 \\ z_2 \end{bmatrix}, \text{where } \varphi \text{ is the hip rotation angle.}$$

$$\boxed{\begin{array}{c} x_3 = x_2 \\ y_3 = y_2 cos\varphi - z_2 sinz_2 \\ z_3 = y_2 sin\varphi + z_2 cos\varphi \end{array}} \quad (8)$$

- The muscle length L is determined from the distance equation.

$$\boldsymbol{L = \sqrt{(x_h - x_3)^2 + (y_h - y_3)^2 + (z_h - z_3)^2}} \quad (9)$$

- Substituting equation 9 into equation 3 yields

$$\varepsilon = \frac{\sqrt{(x_h - x_3)^2 + (y_h - y_3)^2 + (z_h - z_3)^2} - L_i}{L_i} \quad (10)$$

- Now, substituting equations 6, 7, and 8 into equation 10, the final strain equation is derived.
- Lastly, the Fung model is used by Magid and Law [63] to formulate equation 11.

$$\sigma = \frac{E_o}{\alpha}\left(e^{\alpha\, \varepsilon_{eff}} - 1\right) \quad (11)$$

Where σ is muscle stress due to deformation, ε_{eff} is the effective strain, E_o = 2.6 x 103 N/m^2 is the initial elastic modulus, and α is an empirical constant.

However, the elastic modulus for the muscles were not defined for all muscles specifically, so equation 11 is modified to be in the form of constants “a” and “b” which are obtained by recalibrating the model for a 10-week-old female infant. These

constants are used to stiffen the exponential function to stabilize the hip joint as shown in equation 12.

$$\sigma = a\left(e^{b\,\varepsilon_{eff}} - 1\right) \quad (12)$$

Thelen [56] and Delp [51] specified these two constants for the adult model as

$$a = \frac{C}{e^{K^{PE}} - 1} = 0.466\,\frac{N}{cm^2} \quad (13)$$

$$b = \frac{K^{PE}}{\varepsilon_o^M} = 6.667 \quad (14)$$

Where, $C = 25\ N.cm^2$ is the specific muscle tension, $K^{PE} = 4$ is the exponential shape factor, and $\varepsilon_o^M = 0.6$ is the passive muscle strain.

For the 10-week-old female infant model, the value of "b" is assumed to be 13.95, and the value of "a" is recalibrated for the infant model to achieve the equilibrium at the flexion angle of 90 degrees, abduction angle of 80 degrees, and hip rotation angle at 0 degrees, where a = 0.00078 MPa.

Moreover, integrating the stress with respect to strain, the strain energy density "U_o" is determined as shown in equation 15.

$$U_o = \int_0^{\varepsilon} \sigma\, d\varepsilon \quad (15)$$

The final strain energy density is

$$U_o = \frac{a}{b}\left(e^{b.\varepsilon_{eff}} - b.\,\varepsilon_{eff} - 1\right) \quad (16)$$

Finally, the strain energy values "*U*" are computed for all femoral head center locations with variant flexion, abduction, and hip rotation angles. The strain energy function is determined as shown in equation 17.

$$U = U_o * V \ = f(X, Y, Z, \theta, \Phi, \varphi) \qquad (17)$$

Where *V* is the volume of each muscle (*V = physiological cross-sectional area *L*).

To estimate the physiological cross-sectional area (PCSA) for the studied muscles, MRI data for the Adductor Brevis of the infant model is utilized with an area of 41 mm^2. In general, the PCSA is proportional to the force in the muscles, and this area is varied along each muscle. It is calculated by dividing the volume of the muscle by the length. Next, the PCSA of the adult Adductor Brevis muscle from the OpenSim software is found equal to 11.52 cm^2. Therefore, the scaling factor is computed between the adult and infant models to be 3.56. This scaling factor is used to scale the PCSA of all muscles from the OpenSim model. Table 2 lists the physiological cross-sectional areas of the OpenSim and scaled infant models.

Table 2 The scaled muscles' cross-sectional areas from the OpenSim model.

Muscle	OpenSim PCSA cm^2	Scaled PCSA mm^2
Pectineus	9.03	32.14
Adductor Longus	22.73	80.90
Adductor Brevis	11.52	41.00
Add. Magnus Min.	25.52	90.83
Add. Magnus Mid.	18.35	65.31
Add. Magnus Post.	16.95	60.33
Gracilis	3.72	13.27

3.2.2 Gravitational Potential Energy

The second part of the potential energy calculation is to find the gravitational potential energy value for each femoral head center's location. This potential energy (Ω) is the negative of the work done by the weight of the lower extremity bones (femur, tibia, fibula, and foot). Moreover, the lower limb bones are assumed to be fixed relatively to each other as one rigid body. The gravitational potential energy is calculated by defining the center of gravity height "*X*", as illustrated in Figure 26, for all locations on the hip with different flexion, abduction, and hip rotation angles. Hence, the reference axis for calculating the height is the horizontal line that passes through the acetabulum center while the baby is lying horizontally.

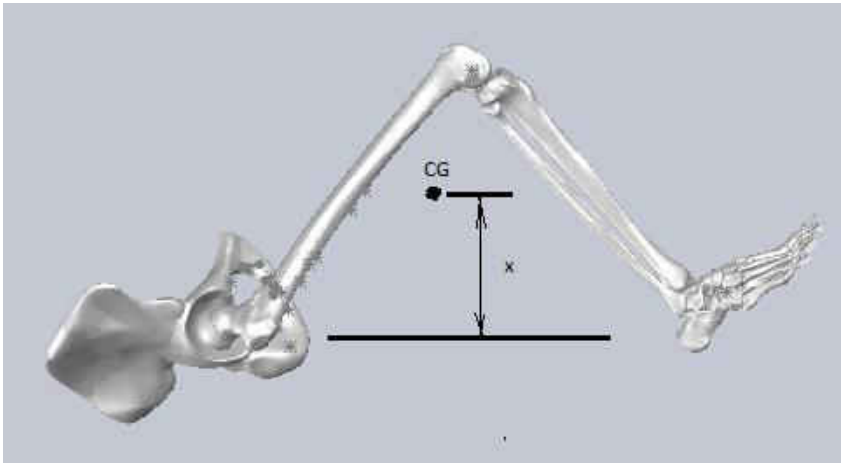

Figure 26 Height "X" of the center of gravity for lower extremity bones.

The mass "m_{total}" is the total mass of the femur, tibia, fibula, and foot. Therefore, a computer code is modified to calculate the gravitational potential energy by changing the location of the femoral head center and changing the femur orientation for all possible flexion, abduction, and external rotation angles.

$$\Omega = -m_{total}.g.X \qquad (18)$$

$$m_{total} = 0.65\ Kg$$

This gravitational potential energy is a function of femoral head center coordinate *(X,Y,Z)*, flexion angle "θ", abduction angle "Φ", and hip rotation angle "φ".

3.2.3 Stationary Potential Energy

The potential energy "Π" consists of elastic strain energy "*U*", stored in the muscles, and gravitational potential energy "Ω", which is the work done "-W" by the weight in the gravitational field, and it is a function of $(X,Y,Z,\theta,\Phi,\varphi)$.

$$\Pi(X,Y,Z,\theta,\Phi,\varphi) = U + \Omega \qquad (19)$$

There are an infinite number of paths between any two positions $\overrightarrow{r_1}$ and $\overrightarrow{r_2}$. The path with least energy is the true path and leads to an equilibrium state, and the paths with slight differences are the varied paths, as shown in Figure 27.

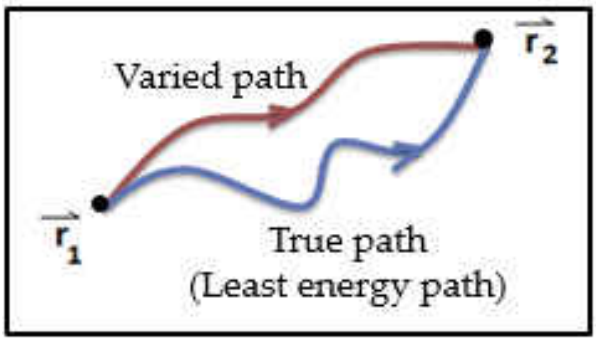

Figure 27 Energy path.

Furthermore, the energy path between any two positions ($\overrightarrow{r_1}$ and $\overrightarrow{r_2}$) can be defined as

$$EP = \int_{\overrightarrow{r_1}}^{\overrightarrow{r_2}} \Pi \, dr \quad ; \quad \Pi = \Pi(X, Y, Z, \theta, \Phi, \varphi) \tag{20}$$

Moreover, the least energy path is attained when

$$\delta \int_{\overrightarrow{r_1}}^{\overrightarrow{r_2}} \Pi \, dr = \int_{\overrightarrow{r_1}}^{\overrightarrow{r_2}} \delta\Pi \, dr = 0 \tag{21}$$

Thus,

$$\delta\Pi = 0 \tag{22}$$

Lastly, equation 22 leads to

$$\frac{\partial \Pi}{\partial q_i} = 0 \tag{23}$$

Where $\mathrm{q_i}$ are the generalized coordinates.

3.3 Potential Energy Calculation

Several methods are utilized to calculate the potential energy values and to compute the local minima of the potential energy for all femoral head center locations.

3.3.1 Proper Orthogonal Decomposition (POD)

POD is a curve fitting method. This method creates snapshots of a POD decomposition matrix and uses radial basis functions (RBF) for creating an interpolation network, which is used to predict the solution. Therefore, the POD and the RBF will be stored in a database that can be accessed any time to retrieve the solutions.

The first step in this method is creating the snapshot matrix "$\boldsymbol{U}$", which is a collection of *N* values of femoral head locations and *M* values of different femur orientations. In this case, the snapshot matrix is $\boldsymbol{U}_{NxM}$. The goal of this matrix "$\boldsymbol{U}$" is to find the POD basis "$\boldsymbol{\Phi}_j$", which is an orthonormal vector (j=0, 1, 2 … M), and given by

$$\boldsymbol{\Phi} = \boldsymbol{U}.\boldsymbol{V} \qquad (24)$$

Where $\boldsymbol{V}$ is eigenvectors of the covariance matrix $\boldsymbol{C}$ and can be computed by using a nontrivial solution of the general eigenvalue problem represented as

$$\boldsymbol{C}\cdot\boldsymbol{V} = \boldsymbol{\Lambda}\cdot\boldsymbol{V} \qquad (25)$$

Where $\boldsymbol{\Lambda}$ is a diagonal matrix that stores the eigenvalues "λ" of matrix $\boldsymbol{C}$, $\boldsymbol{C}$ is symmetric and positive and can be defined as

$$\boldsymbol{C} = \boldsymbol{U}^T.\boldsymbol{U} \qquad (26)$$

Where λ is real, positive, and graphed in descending order, as shown in Figure 28.

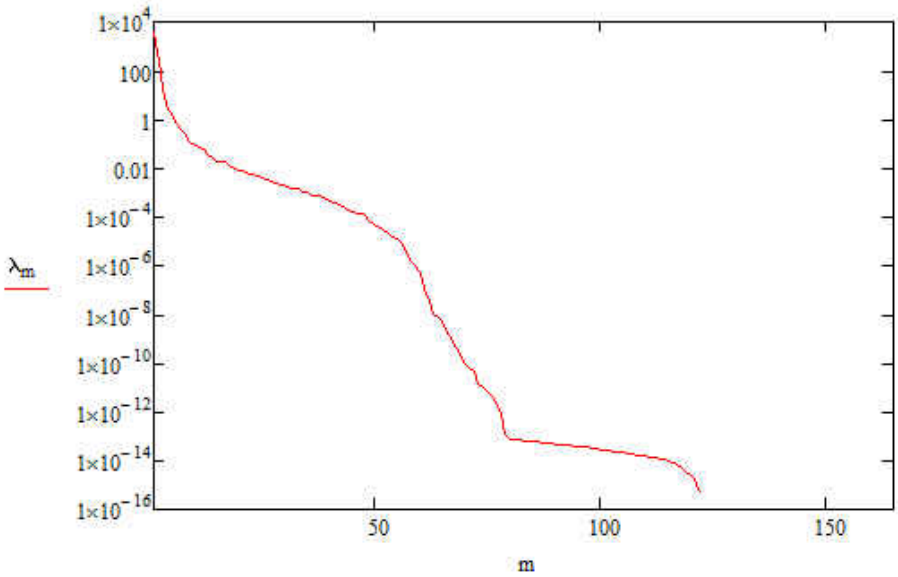

Figure 28 Eigenvalues are sorted.

From Figure 28, the eigenvalues decrease rapidly while increasing the mode number. High modes can be discarded from the data without influencing the accuracy because they hold little data. Moreover, this step is called truncating of the POD basis, and the result is a truncated POD basis, which consists of K<<M vectors and given by

$$\widehat{\boldsymbol{\Phi}} = \boldsymbol{U}.\widehat{\boldsymbol{V}} \qquad (27)$$

Where the eigenvectors are truncated with K^{th} eigenvectors. The truncated POD basis is orthogonal, where

$$\boldsymbol{\Phi}^{\boldsymbol{T}}.\boldsymbol{\Phi} = \boldsymbol{I} \qquad (28)$$

After getting the truncated POD basis, the snapshot matrix is regenerated by

$$\boldsymbol{U} = \widehat{\boldsymbol{\Phi}}.\boldsymbol{A} \qquad (29)$$

Where $\boldsymbol{A}$ is the amplitudes associated with u^j, which can be defined by

$$\mathbf{A} = \widehat{\mathbf{\Phi}}^{\mathbf{T}}.\mathbf{U} \qquad (30)$$

The data should be extrapolated by considering a vector ***P***, which stores the parameters of the problem, which are flexion angles "θ" and abduction angle "Φ". To proceed with the extrapolation, a coefficient matrix **B** should be calculated from ***A*** = ***B***·***F***, where ***F*** is the matrix of interpolation functions, and the set of interpolation functions "$f_i(\boldsymbol{p})$" can be chosen arbitrarily.

$$\boldsymbol{B} = \boldsymbol{A}.\boldsymbol{F}^{-1} \qquad (31)$$

For better approximation and smoothing properties, a radial basis function (RBF) can be used as the interpolating function. Therefore, an inverse multiquadric RBF is created and defined by

$$f_i(\boldsymbol{p}) = f_i\left(\left|\boldsymbol{p} - \boldsymbol{p}^i\right|\right) = \frac{1}{\sqrt{\left|\boldsymbol{p}-\boldsymbol{p}^i\right|^2 + c^2}} \qquad (32)$$

Where *c* is defined as the RBF smoothing factor and $\boldsymbol{p}^i$ is parameter ***p*** at different u^i *(for i = 1, 2 … M)*. By using all the above relations, the POD basis function can be derived as

$$\boldsymbol{\Phi}^T \cdot \boldsymbol{U} = \boldsymbol{B} \cdot \boldsymbol{F} \qquad (33)$$

Lastly, by using the orthogonality of the truncated POD basis, the snapshot matrix is

$$u(\boldsymbol{p}) \approx \boldsymbol{\Phi} \cdot \boldsymbol{B} \cdot \boldsymbol{F}(\boldsymbol{p}) \qquad (34)$$

Moreover, this model can be described as the trained POD-RBF network to find any unknown data at any given parameter ***p***. This function can be used as the curve fitted potential energy function.

3.3.2 Genetic Algorithm Code and Eureqa Software

The Genetic algorithm is a well-known optimization method. It is used to find the minimum potential energy for all femoral head center locations. At each location, the Genetic Algorithm code is conducted to find the minimum potential energy with respect to the flexion and abduction angles. Therefore, it is required to define the function of the potential energy with respect to the desired variables. Eureqa software is used to find the function of the potential energy. It uses genetic programming with symbolic regression to determine the mathematical equation which represents the dataset.

The Genetic algorithm code, as illustrated in Appendix B1 and B2, is conducted for each femoral head location (x,y,z) for the ranges of 70 to 130 degrees of flexion and 0 to 90 degrees of abduction. These ranges are constrained by the Pavlik Harness straps. The code uses a random population of both angles and ranks the chromosomes according to their fitness, and it is used to find the minimum energy values of the energy function. Moreover, the code mates and mutates the population as per the definition given in the code. After the process of the genetic algorithm is finished, the outputs will be the local minima potential energy for all points with respect to the flexion and abduction angles.

3.3.3 MATLAB Code

A MATLAB code [64] is created for calculating the potential energy values for all femoral head center locations of the model with regards to the three angles of rotation. First, the femoral head center location’s coordinates are defined in the code. Second, the muscle insertion and origin coordinates are added. Third, the three-dimensional

rotation is applied to the insertion coordinates of the muscles to find the new position of each insertion point. The rotation is started about the flexion angle between 70 degrees and 130 degrees, then rotated about the abduction angle between 0 degrees and 90 degrees, and finally rotated about the hip rotation angle between -30 degrees and 30 degrees. Fourth, the mathematical model and the values of equilibrium constants “a” and “b” are introduced into the code to calculate the potential energy values for all locations. Lastly, the code finds the minimum energy at a specific femur orientation.

3.4 Dijkstra’s Algorithm and Least Energy Path Method

After finding the local minimum potential energy for all femoral head center locations, Dijkstra’s algorithm code [65] is modified to find the least energy path for the hip dysplasia reduction. First, the coordinates of all femoral head center locations (x,y,z) are identified in the program. Second, the points’ numbers in the code for each point are assigned. The third required input is the edges between the points, which can be determined by addressing the adjacent points for each point. Finally, the local minimum potential energy for all points is assigned. The program requires the source point number and the target point number to be inputted. The program then calculates two variables: the absolute value of the energy difference between the source point and all adjacent points, and the distance. This process is repeated until all points in the field are covered, and a path tree is created by the program. Finally, it picks the path of least energy required for reduction. It should be noted that in case the paths between the source and the target have the same amount of energy differences, which are independent of the path, the code will check for the second condition, which is the

shortest path, as illustrated in Figure 29. Thus, the program will follow the same process but for the shortest distance between the source and the target points.

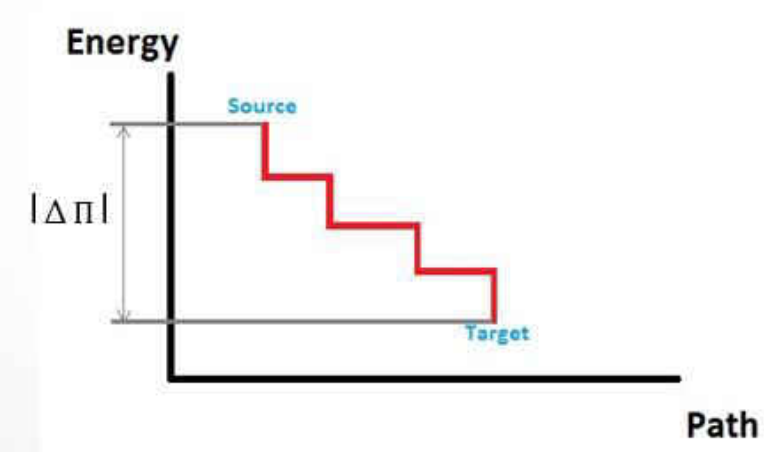

Figure 29 The absolute energy difference of the path.

Figure 30 below depicts the program window of the inputs. This window has three required inputs to be given. The first input is the file name that has the points' numbers, the points' coordinates, the local minima potential energy, and the adjacent points for each point. The second input, listed in Table 3, is the number of the source points, which is the location of the femoral head at each hip dysplasia grades' location. The last input is the target point number, which is the center of the acetabulum where the femoral head should be relocated. The results from this program are each points' number that the path goes through, the energy required for the reduction of the hip dysplasia, and the total length between the source point and the target point.

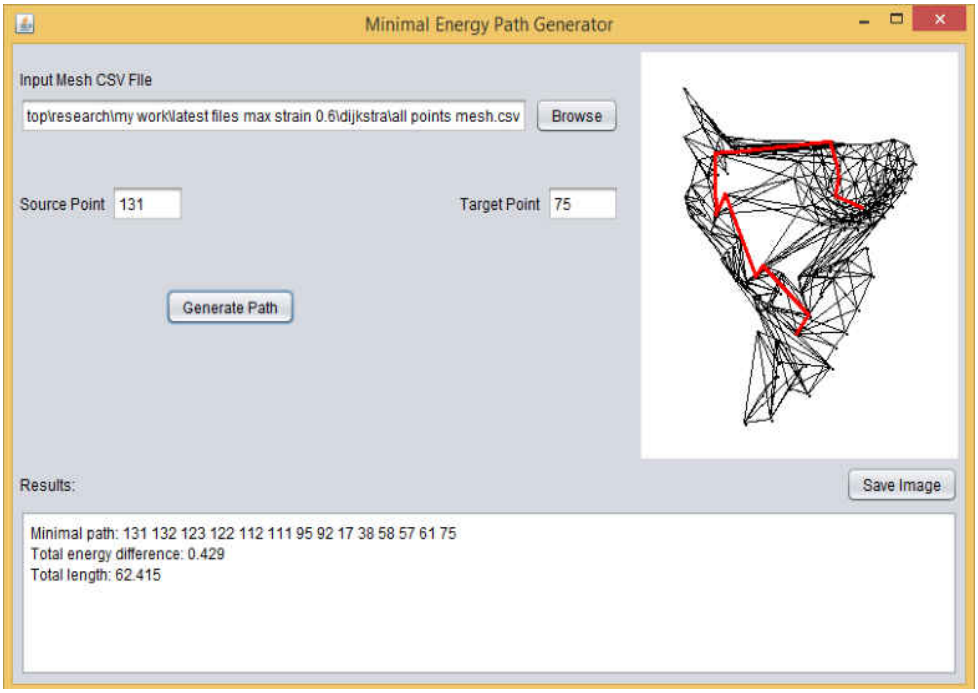

Figure 30 Dijkstra's algorithm sample window to find the hip dysplasia reduction path.

Table 3 Source points and target point definition.

Point #	Definition
75	Natural location of the femoral head at the Center of the acetabulum
66	Femoral head center location at Grade I
27	Femoral head center location at Grade II
5	Femoral head center location at Grade III
131	Femoral head center location at Grade IV

CHAPTER 4: RESULTS

This chapter presents the results of the implemented computer codes, potential energy map, and the optimal path for hip dysplasia reduction. Initially, the model with two angles of rotation (flexion and abduction angles) is considered. Moreover, another study is implemented by adding the third femur orientation (hip rotation angle). The later investigation yielded more accurate results by determining the least energy path (LEP). To re-iterate, there are two types of analyses carried out in this research: the first analysis has two angles of rotation and the second one considers all three angles of rotation.

4.1 Two Angle Model

In this section, the potential energy values for all femoral head locations are calculated by using the mathematical model that was described in the previous chapter. A curve fitting for the dataset of the potential energy values is conducted by using two methods: Proper Orthogonal Decomposition (POD) and Eureqa software. Following, the potential energy map is created by using MATLAB software. Finally, the Dijkstra's algorithm code is applied to find the LEP for the hip dysplasia reduction for all grades.

4.1.1 Potential Energy Calculation

In the previous chapter, the mathematical model was created to calculate the potential energy values for all femoral head locations (i.e., acetabulum points, and pelvis points) by using equation 19, changing flexion angles between 70 and 130 degrees and abduction angles between 0 and 90 degrees. After calculating the energy

values for all locations of the femoral head with different orientations of the femur, a mathematical function is formulated by using the curve fitting method of the dataset.

As previously described, there are two groups of datasets from potential energy calculation. The first group is the acetabulum surface points, which are between 1 and 78, as shown in Figure 31.

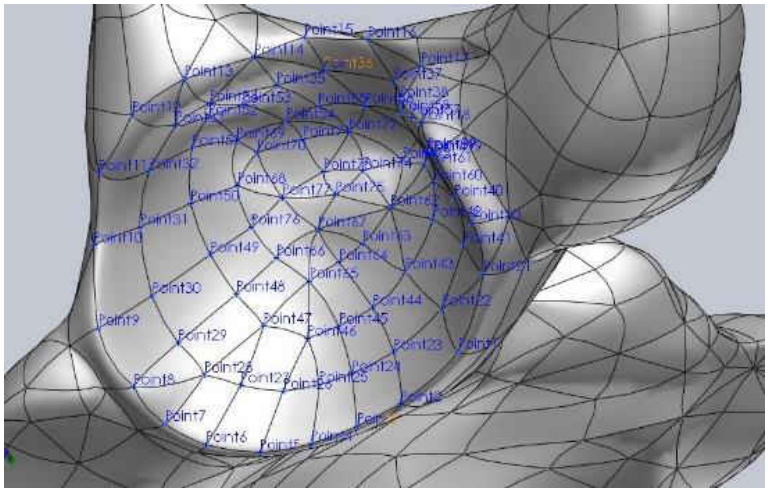

Figure 31 Points located on the acetabulum surface.

The second group is the pelvis surface points. Figure 32 shows the pelvis points, which are between 79 and 155.

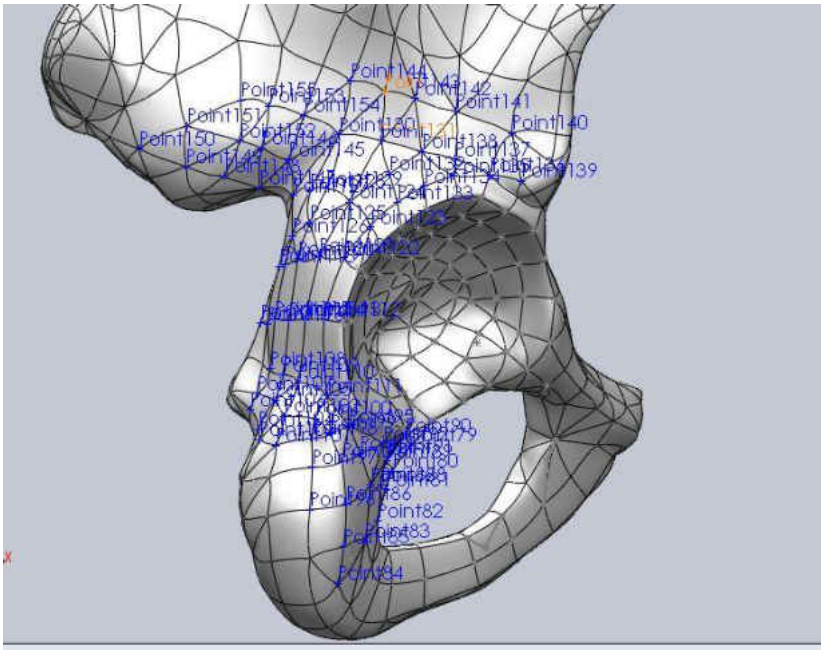

Figure 32 Points located on the pelvis surface.

The next key step is to determine the potential energy function. This function will lead to finding the local minima of potential energy, thus creating the potential energy map and developing the LEP.

4.1.2 Potential Energy Function and Local Minima

Two results are presented in this section by using the POD and the Genetic algorithm. After creating the POD_RBF, the local minima of the potential energy for all femoral head locations are found. At each femoral head location, the POD plotted a chart of the potential energy versus different angles, and the smallest value is the local minimum energy at that location. Figure 33 shows the plot of the calculated potential energy values for all points. Table 4 has a sample of several points of the femoral head

location in the acetabulum surface and the corresponding local minima of potential energy at different flexion and abduction angles.

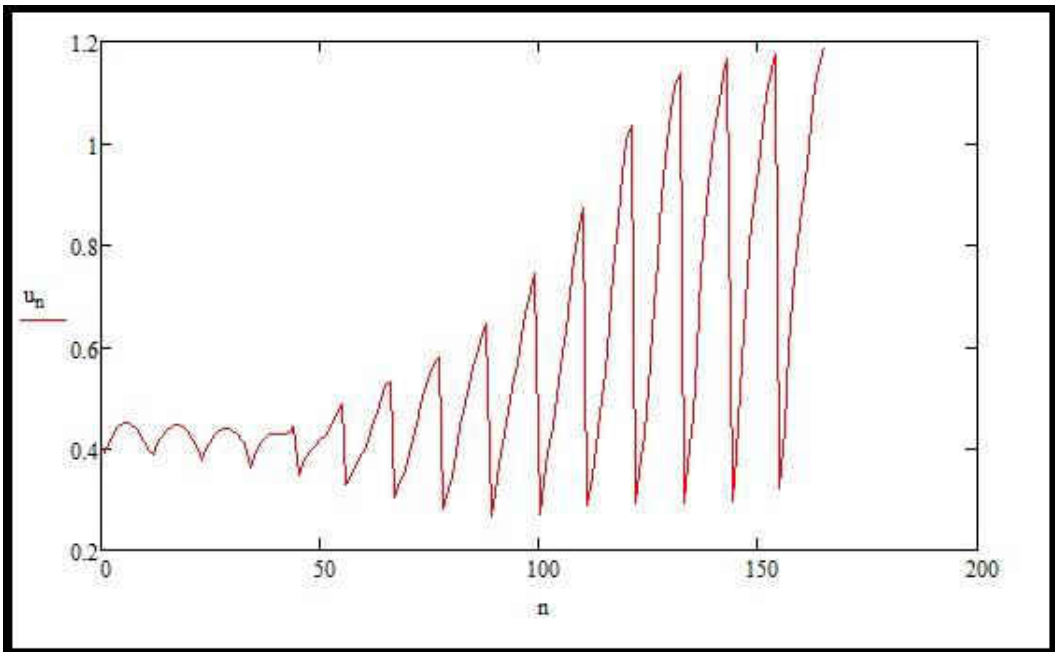

Figure 33 POD results show the potential energy at the specific femoral head location to get the minimum energy.

Table 4 Sample of acetabulum points with local minimum potential energy at flexion and abduction angles.

N	Flexion	Abduction	Potential Energy (J)
1	70	84	0.20
2	70	54	0.27
3	70	48	0.32
4	70	42	0.36
5	70	30	0.40
6	70	24	0.43
7	70	12	0.45

The local minima of potential energy can be shown in the following figures, which are the acetabulum surface and four regions in the pelvic area. Figure 34 displays the corresponding flexion and abduction angles where the local minima occur at the acetabulum points. Figure 35 shows the corresponding flexion and abduction angles where the local minima occur at the first region of the pelvis surface. Figure 36 displays the corresponding flexion and abduction angles where the local minima occur at the second area of the pelvis surface. Figure 37 displays the corresponding flexion and abduction angles where the local minima occur in the third area of the pelvis surface. Finally, Figure 38 shows the corresponding flexion and abduction angles where the local minima occur for the last area of the pelvic surface.

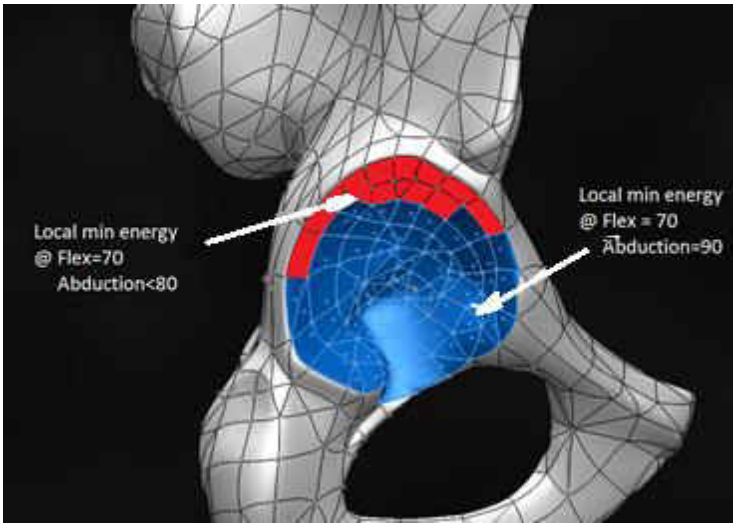

Figure 34 Acetabulum surface that has two regions, the top one, and the bottom one.

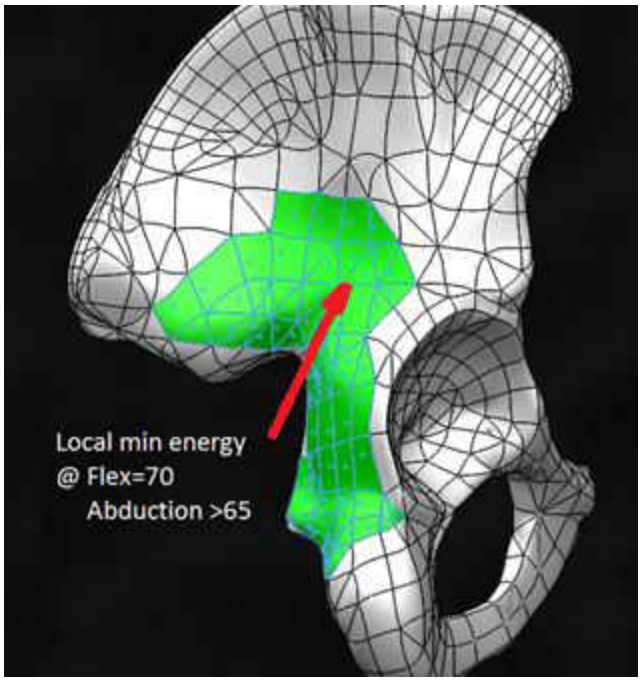

Figure 35 Pelvis first region.

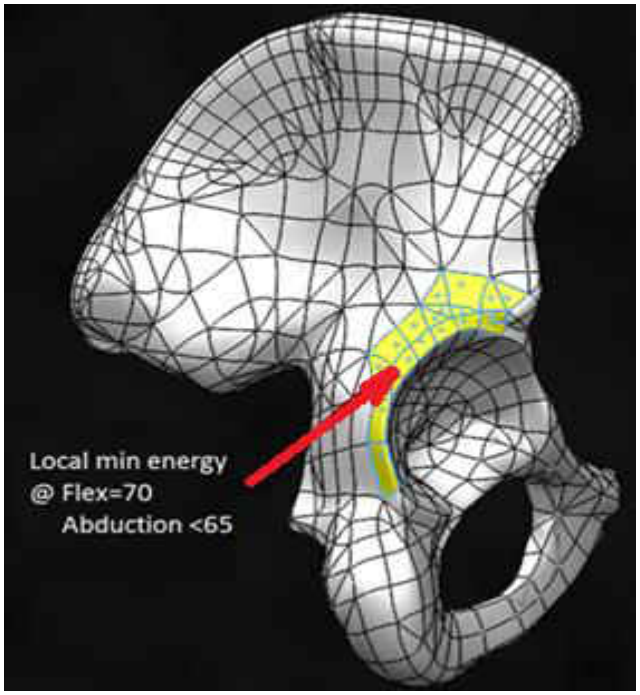

Figure 36 Pelvis second region.

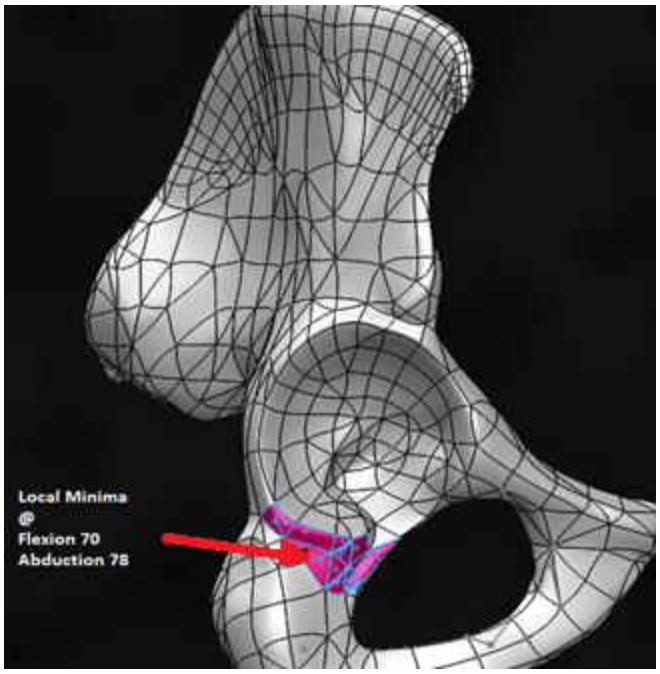

Figure 37 Pelvis third region.

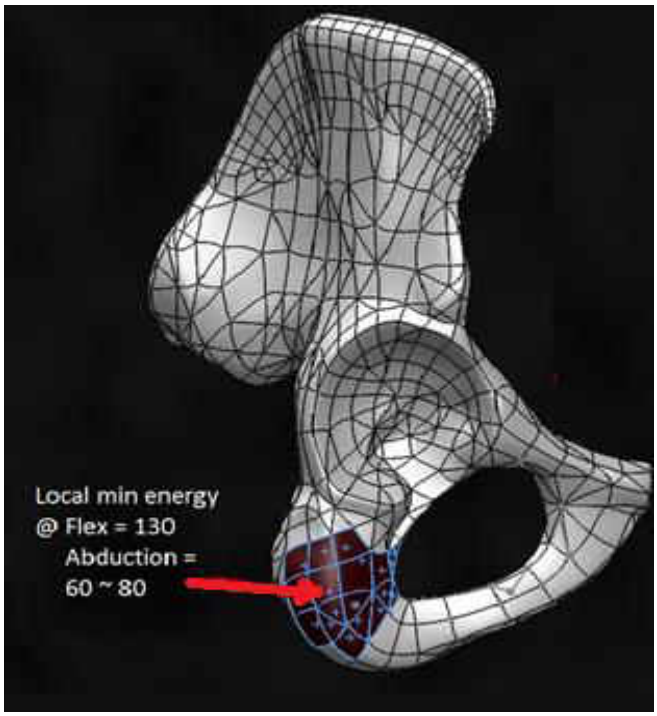

Figure 38 Pelvis fourth region.

The Genetic algorithm is used to find the minimum potential energy for all femoral head locations. Therefore, Eureqa software is used to find the function of the potential energy. Figure 39 shows two colored points: the blue dots are the calculated potential energy values and the red dots are the curve fitted points. Hence, the software finds the most curve fitted data to the given values and prints out the curve fitted function, as illustrated in equation 35 and 36.

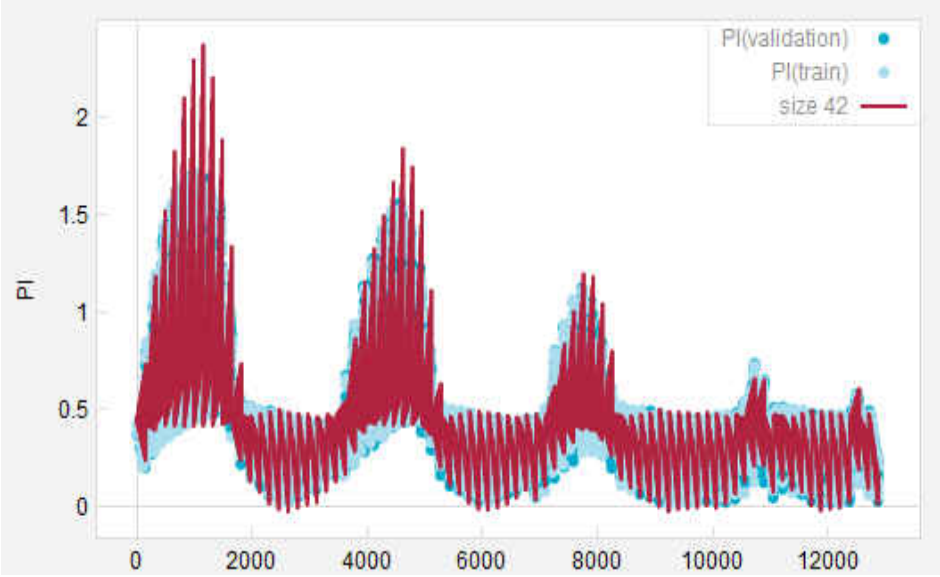

Figure 39 Eureqa curve fitting data for acetabulum surface.

The potential energy function for the first surface points (acetabulum points) is:

$$\pi_{1-78} = 0.5 + 0.001 * z * \theta + 0.0235 * z * \theta * \Phi - 0.34 * \theta / \Phi + 0.001 * z * \Phi * \theta\text{^}2 + 0.0015 * \Phi * z\text{^}2 * \theta\text{^}2 - 0.013 * z \quad (35)$$

Where, *(x,y,z)* is the femoral head center coordinates, θ is the flexion angle (in radian), and Φ is the abduction angle (in radian).

Moreover, the corresponding curve fitted function for the pelvic surface points (79 – 155), is displayed in equation 36.

$$\pi_{1-78} = 0.45 + 1.51 * \theta * \Phi + 0.07 * x * \theta * \Phi + 0.003 * \Phi * x^2 - 0.07 * \theta - 1.4 * \Phi \quad (36)$$

Table 5 listed a sample of the points with corresponding minimum potential energy at the selected angles.

Table 5 Sample of Genetic Algorithm results.

X	Y	Z	Abduction (Rad)	Flexion (Rad)	Potential Energy (J)
-6.75	0.69	3.71	0.10	2.28	2.52E-03
-4.41	2.62	5.95	0.11	2.20	2.57E-03
-2.90	2.98	7.31	0.11	1.55	2.52E-03
-1.43	3.26	8.42	0.11	2.30	2.56E-03
0.28	3.35	9.33	0.10	2.29	2.51E-03
2.19	2.87	9.94	0.10	2.29	2.52E-03
3.61	1.80	10.17	0.11	2.30	2.53E-03

4.1.3 Potential Energy Map

The potential energy map is one of the most important steps in finding the LEP. This map is a representation of minimum potential energy for all femoral head locations on the hip. In order to display the values of the local minima of potential energy, a

numerical code is created by using MATLAB software, which uses the coordinates of the wireframe's nodes in the SolidWork model and assigns the potential energy value for each node. Next, the code plotted the wireframe and developed different colors for each node as per its energy value, as shown in Figure 40.

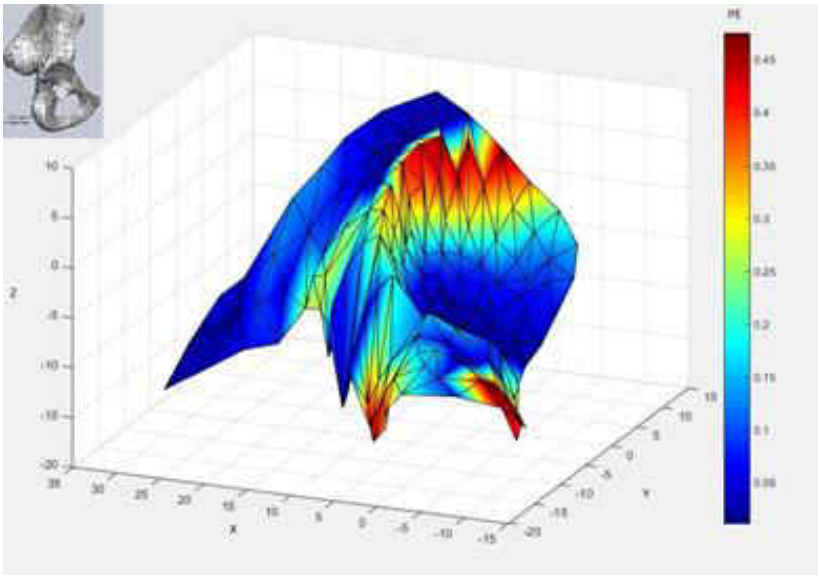

Figure 40 Potential energy map for the model with two angles of rotation.

After defining the local minima of the potential energy for all points by using the POD method, the LEP is identified for the four hip dysplasia grades. The Dijkstra's algorithm is utilized to find the LEP for the hip dysplasia reduction.

4.1.4 Two Angle Model Results

As a result of using the Dijkstra's algorithm program that was defined in the previous chapter, the four grades of hip dysplasia are studied separately. The first grade of hip dysplasia, as identified by IHDI, is shown in Figure 41.

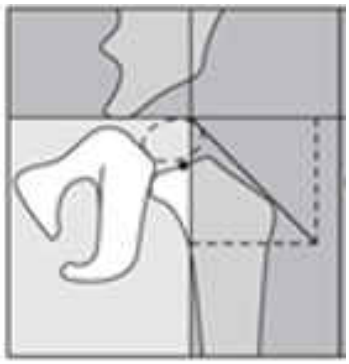

Figure 41 International Hip Dysplasia Institute classification of Grade I.

As seen in the figure, the source point is located just above the natural position of the femoral head. After identifying the source point and the target point, the result of the code is the LEP of hip dysplasia reduction and is shown in Figure 42. The hip dysplasia reduction path should be through the points identified in the picture while keeping the femur orientation at a flexion angle of 70 degrees and abduction angle of 90 degrees for the LEP.

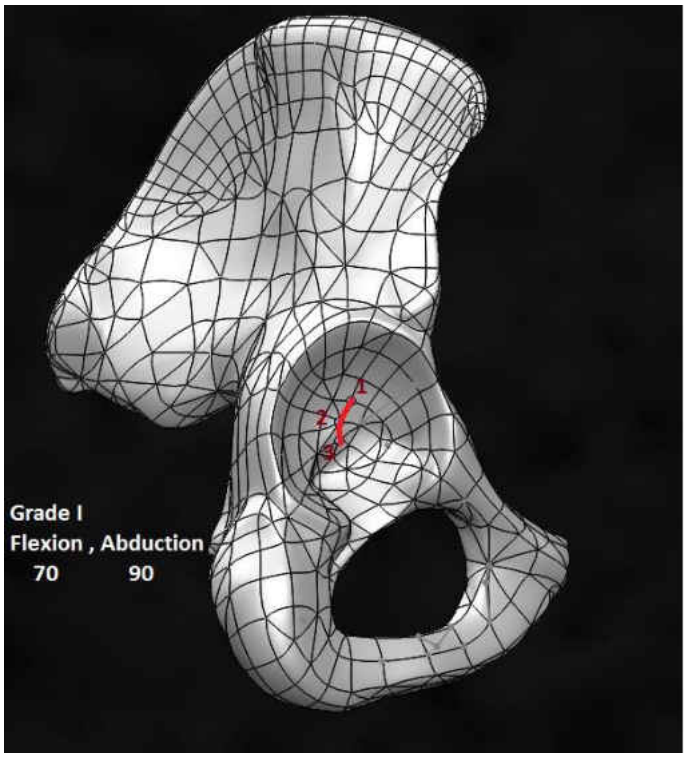

Figure 42 Grade I: Hip Dysplasia reduction path.

For grade II, the IHDI defined the femoral head as being located underneath the acetabulum rim, as depicted in Figure 43. After identifying the source point and the target point, the LEP is created from the Dijkstra's algorithm, as shown in Figure 44. The hip dysplasia reduction path should be through the points where identified in the picture while keeping the femur orientation at a flexion angle of 70 degrees and an abduction angle of 90 degrees.

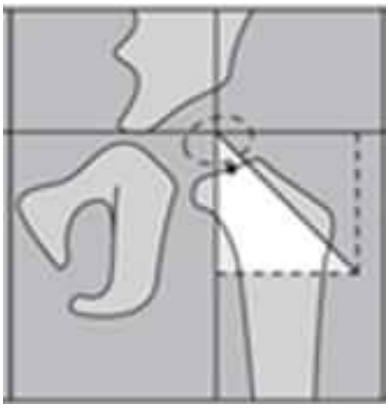

Figure 43 International Hip Dysplasia Institute classification of grade II.

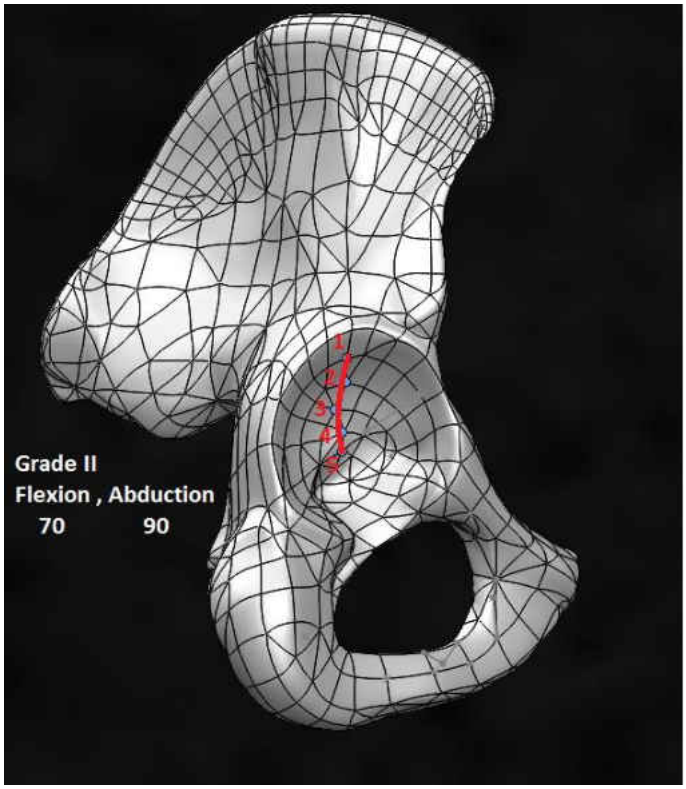

Figure 44 Grade II: Hip Dysplasia reduction path.

For grade III, the IHDI explained that the femoral head is located on the acetabulum rim, as displayed in Figure 45. After identifying the source point and the target point, the resulted LEP is shown in Figure 46. However, the femur is flexed at 70

degrees with 54 degrees of abduction. Then the femur is abducted to 90 degrees at the end of the LEP.

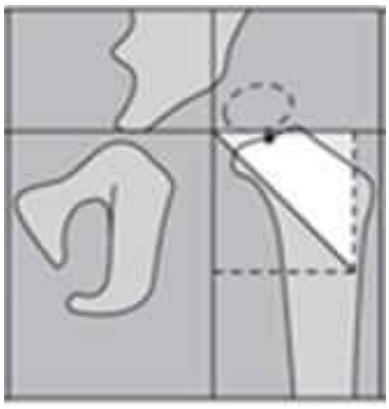

Figure 45 International Hip Dysplasia Institute classification of grade III.

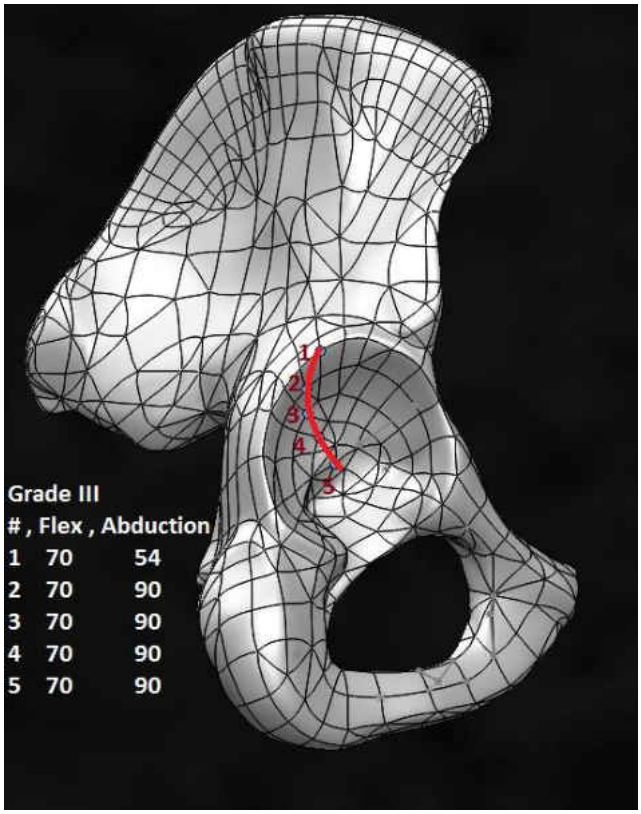

Figure 46 Grade III: Hip Dysplasia reduction path.

According to IHDI, the femoral head in grade IV is located outside the acetabulum rim, as shown in Figure 47, where it is in non-equilibrium condition. This grade is considered to be the most severe hip dysplasia grade. Moreover, it is quite a big challenge for the physician to treat babies with this kind of dislocation. In this research, the main goal is to identify the path of all grades—the most significant of which is grade IV.

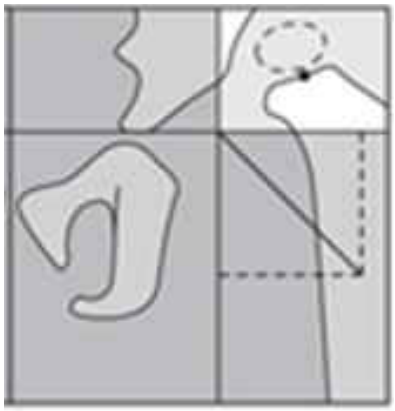

Figure 47 International Hip Dysplasia Institute classification of grade IV.

Therefore, the source point and the target point are identified for grade IV, which are node number 131 and node number 75, as defined in Table 3 above. The resulted path has the route of the femoral head moving along specific points with a specific femur orientation. As listed in Table 6, the femur should be flexed at 70 degrees during the reduction, but the abduction angle has changed. Furthermore, the femoral head is moved from the source point to the acetabulum rim by increasing the abduction angle gradually to 60 degrees. Following, the femur is moved along the rim by increasing the abduction angle gradually until it reaches the acetabulum notch with an abduction angle of 90 degrees. Finally, the femur is passed the acetabulum notch to reach the

acetabulum center with flexion angle of 70 degrees and abduction angle of 90 degrees. Figure 48 shows the reduction path of Grade IV.

Table 6 Grade IV hip dysplasia reduction path and orientation.

#	Point No.	Flexion	Abduction
1	131	70	54
2	132	70	42
3	123	70	54
4	122	70	60
5	112	70	60
6	111	70	66
7	95	70	72
8	92	70	78
9	17	70	90
10	38	70	90
11	58	70	90
12	57	70	90
13	61	70	90
14	75	70	90

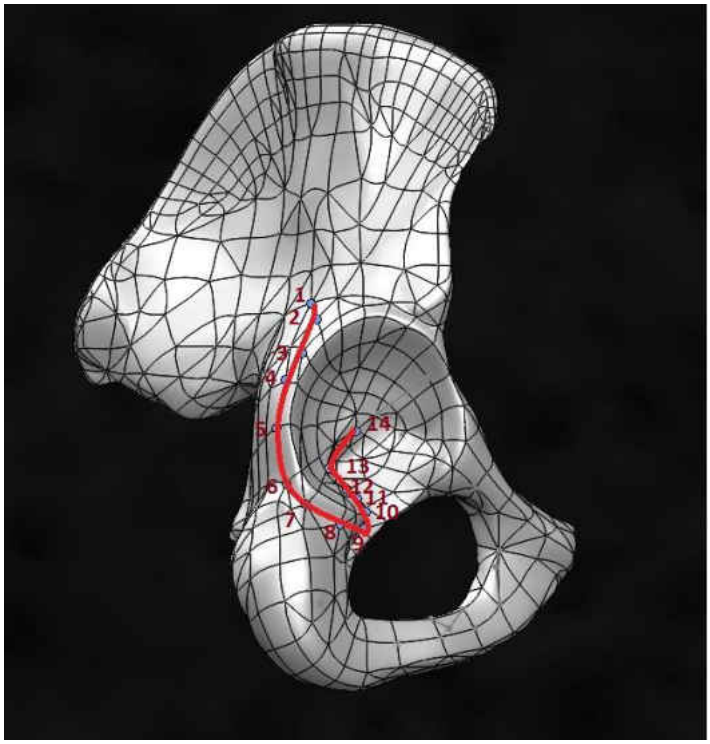

Figure 48 Grade IV: Hip dysplasia reduction path.

4.2 Three Angle Model

To provide accuracy for the hip dysplasia reduction path, the third femur orientation angle (hip rotation angle) is added to the study. In the hip dysplasia treatment using the Pavlik Harness, the femur is free to rotate in three angles as specified previously. However, in the previous model that has only two angles of rotation, the model was studied and analyzed for the verification of the proposed method. Therefore, the third rotation angle is added to examine the reduction of the femur.

4.2.1 Potential Energy Calculation and Local Minima

A MATLAB code [64] is created for calculating the potential energy values for all 155 points (femoral head center locations on the hip). First, the femoral head center locations' coordinates are defined in the code. Second, the muscle insertion and origin coordinates are added. Third, the three-dimensional rotation is applied to the insertion coordinates of the muscles to find the new position of the insertion points after rotation. The rotation is started about the flexion angle between 70 degrees and 130 degrees, then rotated about the abduction angle between 0 degrees and 90 degrees, and finally rotated about the hip rotation angle between -30 degrees and 30 degrees. Fourth, the mathematical model and the values of the equilibrium constants "a" and "b" are introduced into the code to calculate the potential energy values for all femoral head locations. Lastly, the code finds the minimum energy for a specific femur orientation. Table 7 lists a sample of the local minimum energy for several points at a required femur orientation based on the three angles of rotation.

Table 7 Sample table of the MATLAB code results of several femoral head points.

Point No.	Flexion	Abduction	External Rotation	Potential Energy (J)
1	70	45	25	0.48
2	70	35	15	0.54
3	70	25	5	0.57
4	70	15	0	0.60
5	70	0	5	0.62
6	70	0	10	0.64
7	70	0	15	0.65

4.2.2 Potential Energy Map for the Model with Three Angles of Rotation

This map, which is a representation of the minimum potential energy for all femoral head locations, displays the local minima and the global minimum. Figure 49 shows the hip points that are considered in the study with the representation color of the local potential energy values. The dark blue represents the lowest energy values, and the dark red is the highest energy values. Thus, the center of the acetabulum shows the lowest energy value, which is compatible with the initial idea that the center of the acetabulum should have the global minimum of the potential energy.

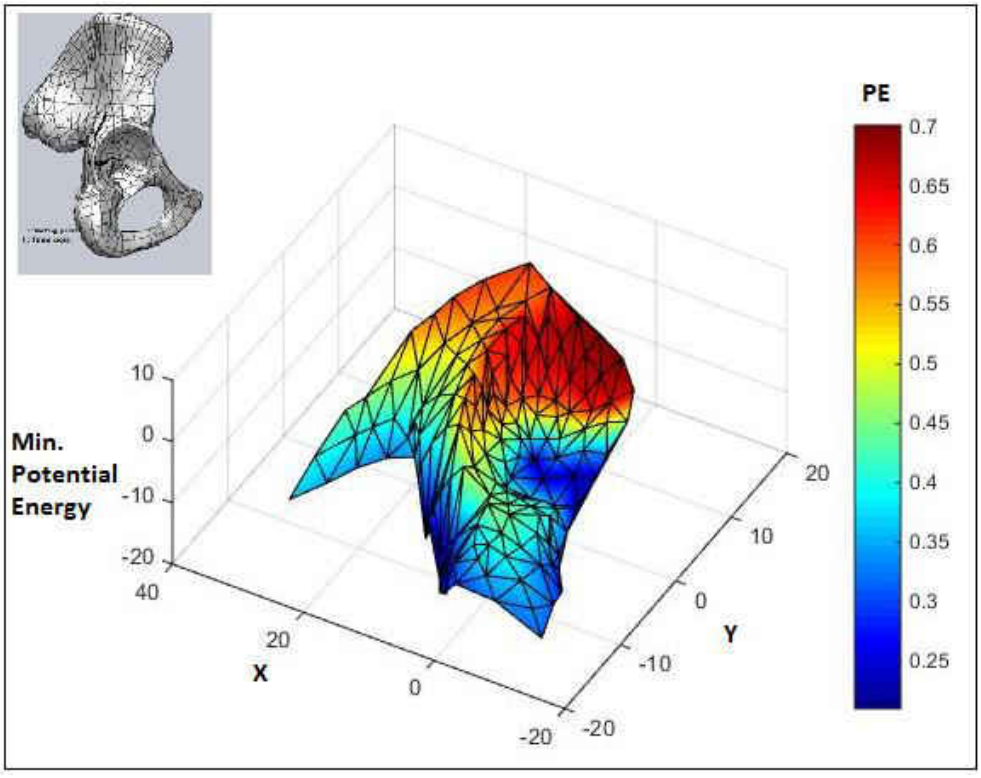

Figure 49 Potential energy map.

4.2.3 Three Angle Model Results

After finding the local minimum of the potential energy for the specified femoral head locations on the hip, Dijkstra's algorithm program is used to create the reduction path for all four hip dysplasia grades.

a. Grade I

Dijkstra's algorithm is used to find the reduction path with the required femur orientation, as listed in Table 8. Figure 50 shows the LEP of hip dysplasia reduction for grade I. The femur should be flexed at 90 degrees during the reduction but abducted gradually from 40 degrees to 80 degrees with external rotation between 10 and 0 degrees until it reaches the center of the acetabulum.

Table 8 Grade I: required femur orientation for the hip dysplasia reduction.

#	Point #	Flexion	Abduction	Hip Rotation
1	66	70	40	10
2	67	70	60	0
3	75	70	80	10

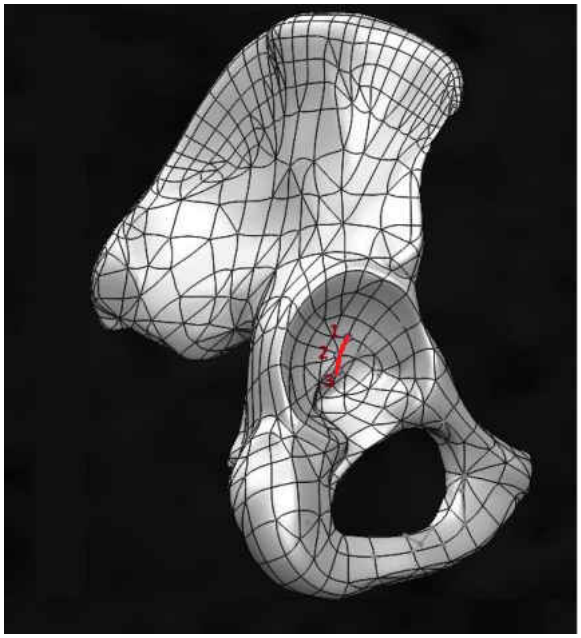

Figure 50 Grade I: Hip Dysplasia reduction path with using three angles of rotation.

b. Grade II

Table 9 lists the required femur orientation angles for the reduction. Thus, the femur should be flexed at an angle of 70 degrees during the reduction and abducted gradually from 0 degrees to 60 degrees while changing the hip rotation externally between 0 and 5 degrees during the reduction path. Figure 51 shows the LEP of hip dysplasia reduction for grade II by using the Dijkstra's program.

Table 9 Grade II: required femur orientation for the hip dysplasia reduction.

#	Point #	Flexion	Abduction	Hip Rotation
1	27	70	0	5
2	47	70	20	0
3	65	70	40	5
4	67	70	60	0
5	75	70	80	10

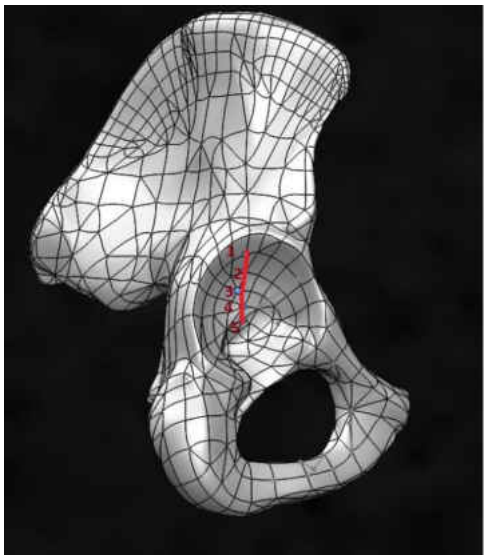

Figure 51 Grade II: Hip Dysplasia reduction path with using three angles of rotation.

c. Grade III

The path is created by using the Dijkstra's algorithm code. Table 10 shows the required femur orientation angles for the reduction. Figure 52 displays the least-action path of hip dysplasia reduction for grade III of hip dysplasia. As previous grades, the flexion angles is 70 degrees for the minimum energy path, and gradually abducted from the initial angle to 80 degrees while changing the external rotation between 0, 5, and 10 degrees as described below.

Table 10 Grade III: required femur orientation for the hip dysplasia reduction.

#	Point #	Flexion	Abduction	Hip Rotation
1	5	70	0	5
2	26	70	15	0
3	46	70	25	0
4	65	70	40	5
5	67	70	60	0
6	75	70	80	10

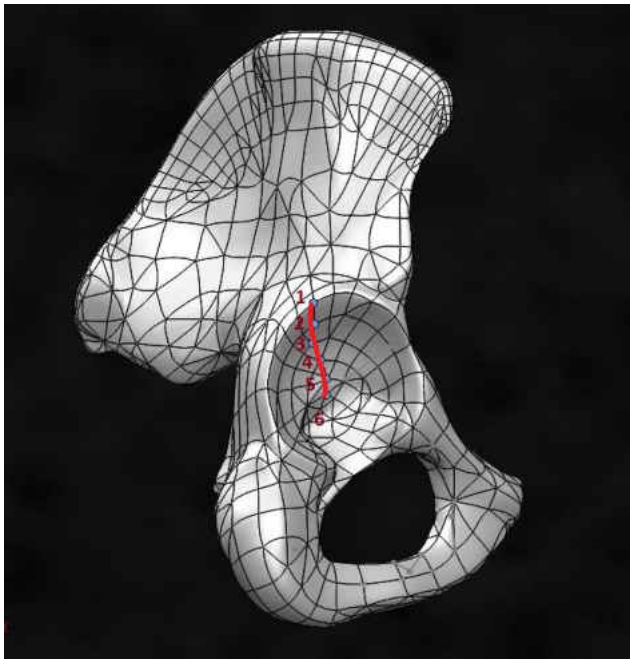

Figure 52 Grade III: Hip Dysplasia reduction path with using three angles of rotation.

d. Grade IV

Two types of analysis are implemented for grade IV. The first analysis determined the LEP from the starting point of a Grade IV dislocated hip to the acetabulum center (direct path). The second analysis is implemented to determine the required energy of the two-stage pathway (indirect path) that follows the modified Hoffman-Daimler result, which is a path that goes to the intermediate point on the ischium near the acetabular notch. Furthermore, in each analysis, the effect of the Pectineus is computationally switched off to evaluate the reduction pathways and to illustrate the changes in the required energy between the reduction of a model with all muscles intact and one without the effect of the Pectineus.

For the purpose of studying the reduction pathway, the Dijkstra's algorithm program is used to find the direct LEP with the presence of all muscles. Table 11 lists the evaluated LEP with the required femur orientation. The reduction path starts with a flexed femur at an angle of 70 degrees and continues along the path. The femur is guided to be abducted at 40 degrees, and then increased gradually to 80 degrees while changing the hip rotation angle internally from 30 degrees to -30 degrees ending up with an external rotation of 10 degrees at the center of the acetabulum. The resulting pathway is shown in Figure 53. Figure 54 shows the potential energy map with the LEP for this analysis.

Table 11 Grade IV: required femur orientation for the hip dysplasia reduction (Direct path) with the effect of all muscles.

#	Point #	Flexion	Abduction	Hip Rotation
1	131	70	40	30
2	124	70	50	30
3	121	70	55	30
4	112	70	55	30
5	111	70	55	30
6	99	75	55	30
7	93	130	70	30
8	19	70	60	-30
9	39	70	60	-30
10	59	70	65	-30
11	60	70	60	-30
12	62	70	70	5
13	75	70	80	10

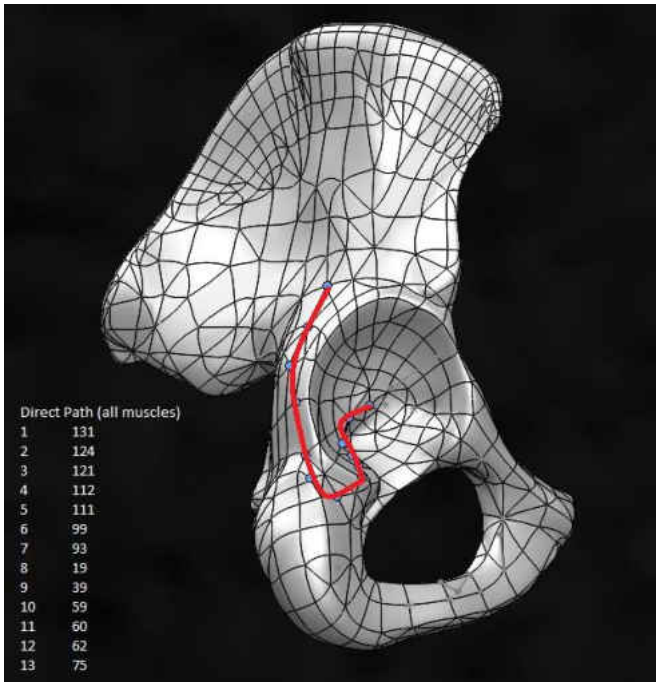

Figure 53 Grade IV: Hip Dysplasia direct reduction pathway for the model with all muscles intact.

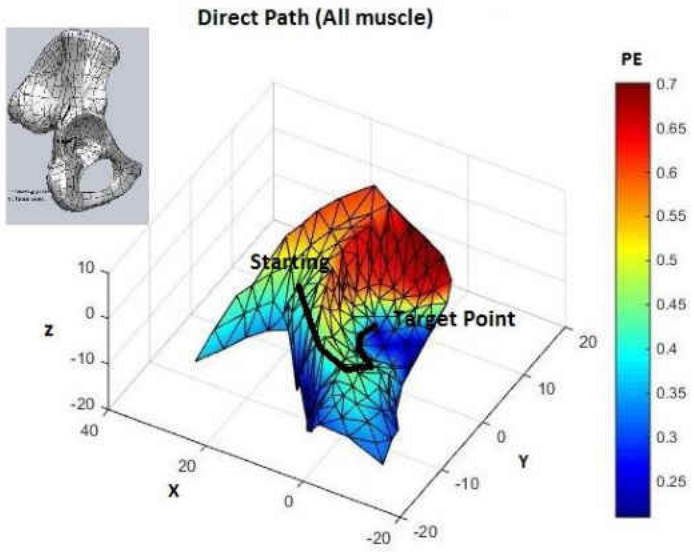

Figure 54 Potential energy map for the direct reduction path for the model with all muscles intact.

For demonstration purposes, the lower limb bones are scaled down by a scaling factor of 4:10. Then, at each point on the reduction pathway, the femur is rotated as determined from the results of the Dijkstra's algorithm, as shown in Figure 55.

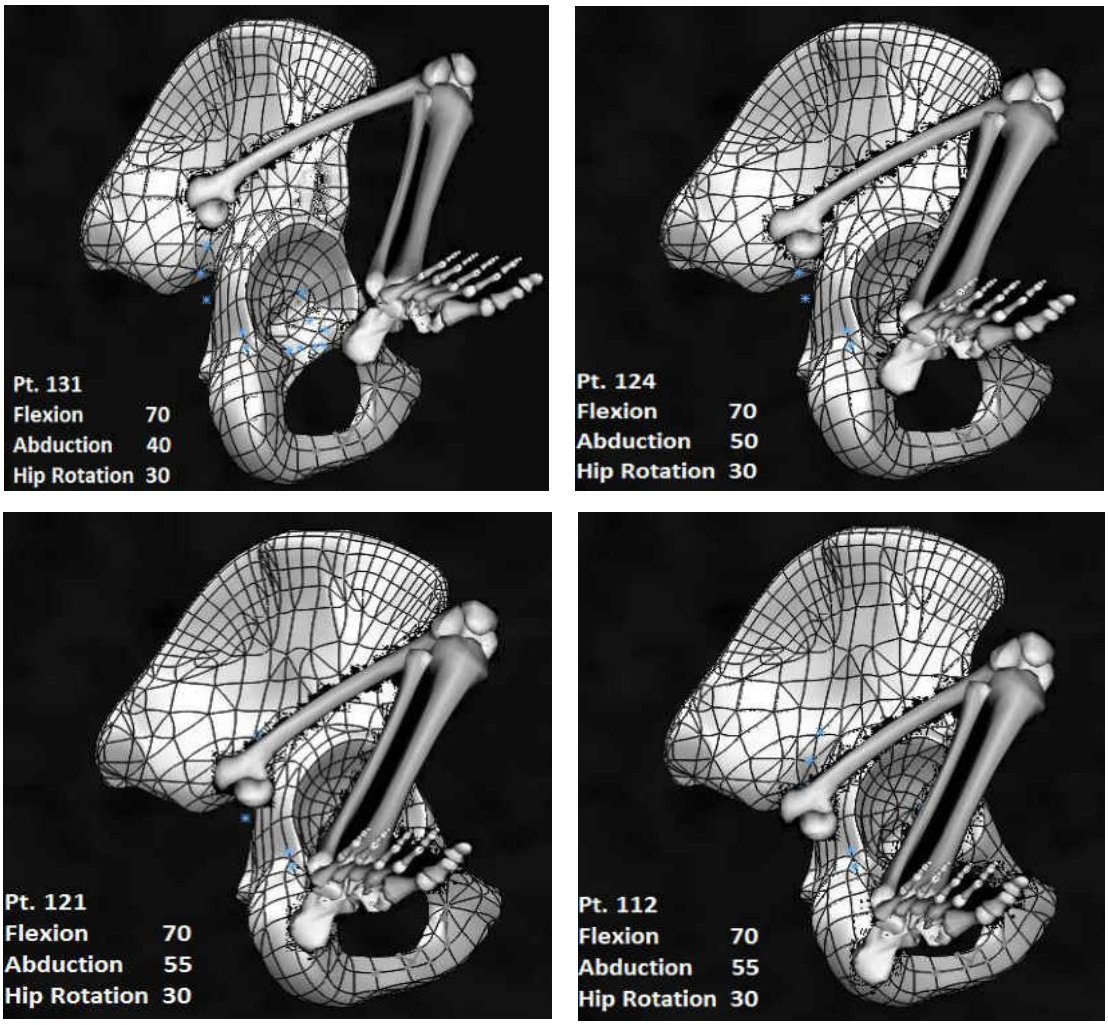

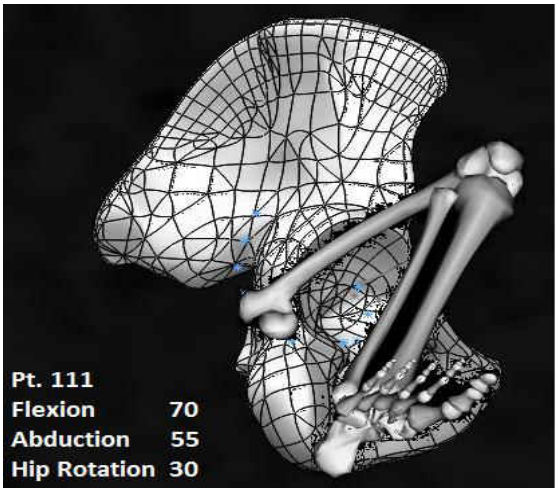
Pt. 111
Flexion 70
Abduction 55
Hip Rotation 30

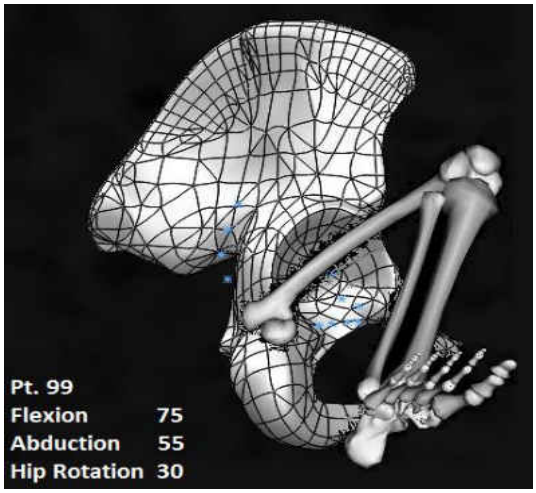
Pt. 99
Flexion 75
Abduction 55
Hip Rotation 30

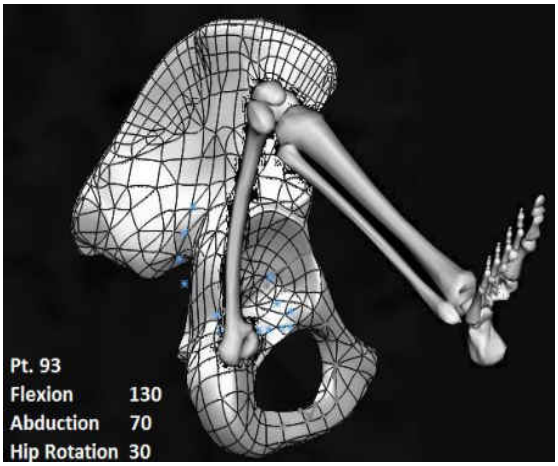
Pt. 93
Flexion 130
Abduction 70
Hip Rotation 30

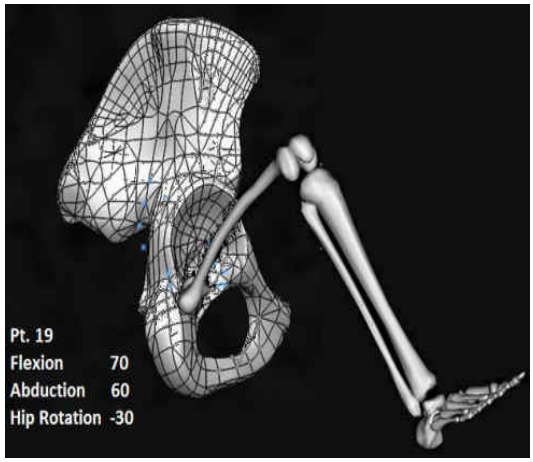
Pt. 19
Flexion 70
Abduction 60
Hip Rotation -30

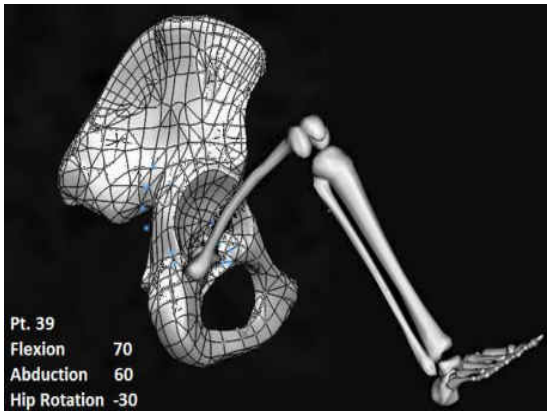
Pt. 39
Flexion 70
Abduction 60
Hip Rotation -30

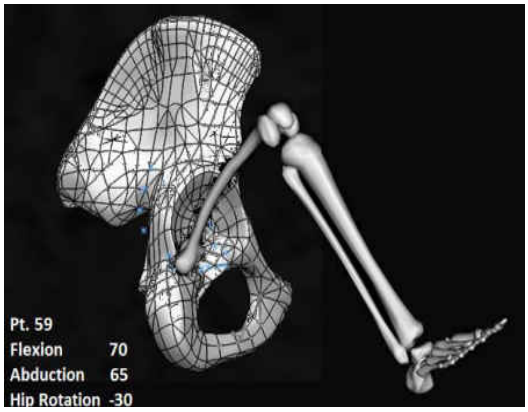
Pt. 59
Flexion 70
Abduction 65
Hip Rotation -30

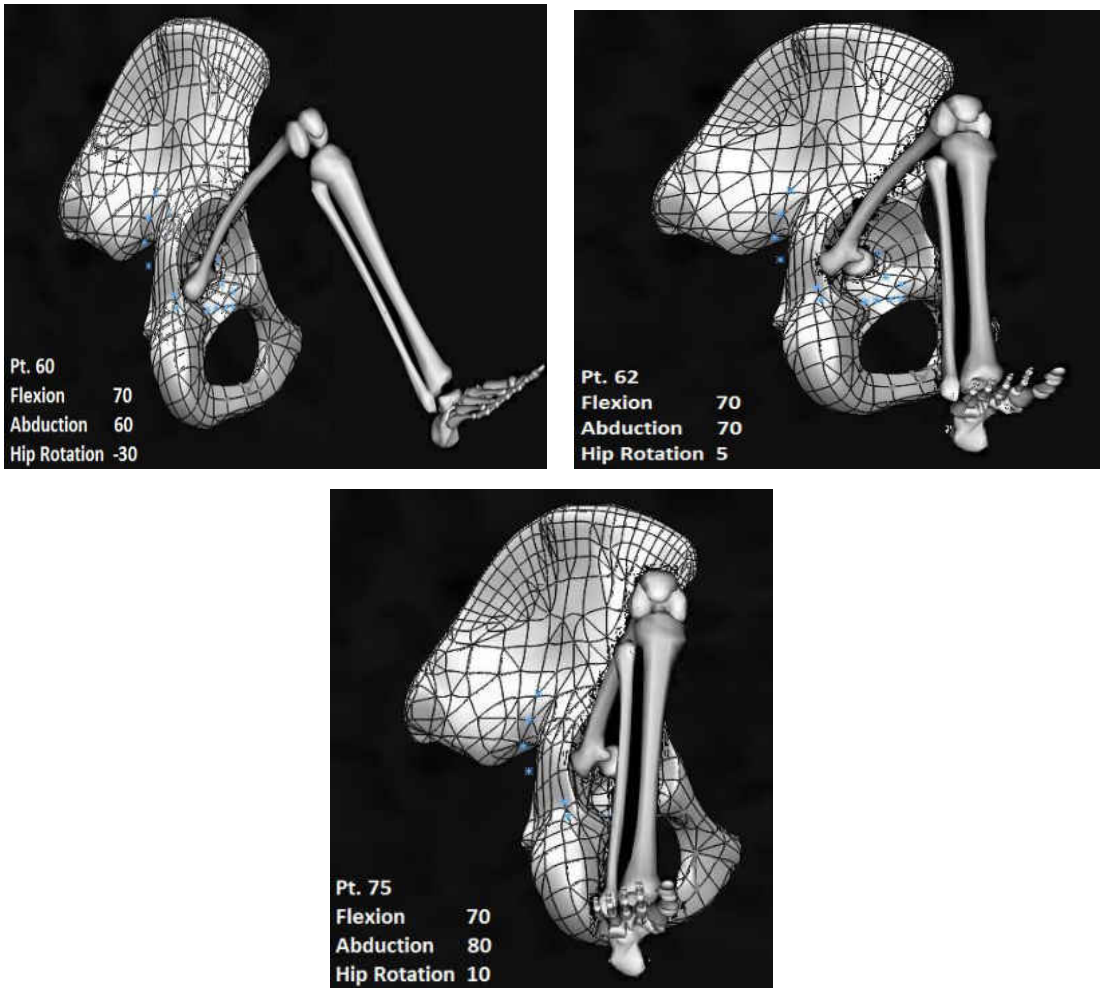

Figure 55 Grade IV direct reduction path with femur orientation for the model with all muscles.

Table 12 lists the computed direct pathway points with the required femur orientation angles to achieve the least energy path for the model that does not have the effect of the Pectineus. Figure 56 shows the resulting pathway that closely followed the direct pathway proposed by Iwasaki and was documented by Suzuki. To achieve reduction with the lowest energy, the femur should be flexed at 70 degrees along the path. However, the abduction angle is changed from 40 to 90 degrees while the hip is

rotated internally from 0 degrees to -30 degrees. Figure 57 shows the potential energy map with the LEP for this analysis.

Table 12 Grade IV: required femur orientation for the hip dysplasia direct reduction of the model without the effect of the Pectineus.

#	Point #	Flexion	Abduction	hip rotation
1	131	70	40	0
2	124	70	50	-15
3	122	70	50	-30
4	1	70	50	-30
5	22	70	55	-30
6	43	70	60	-30
7	63	70	70	-30
8	75	70	90	-30

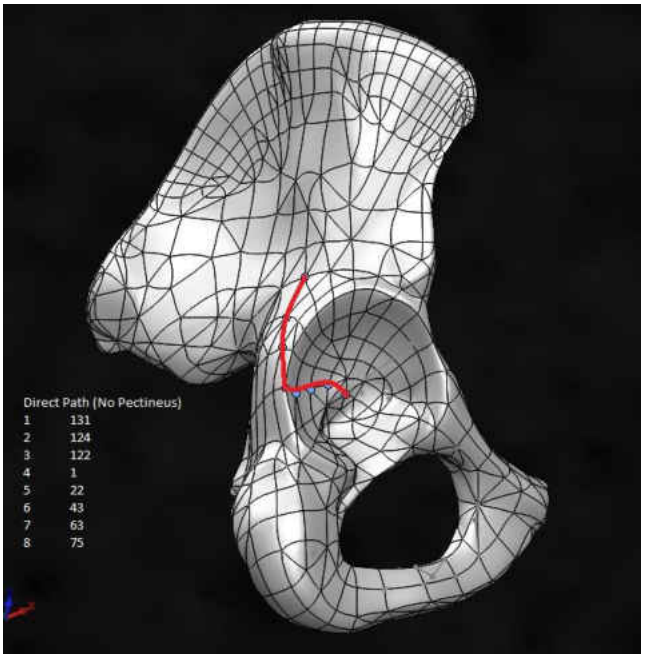

Figure 56 Grade IV: Hip Dysplasia direct reduction path for the model without the effect of the Pectineus.

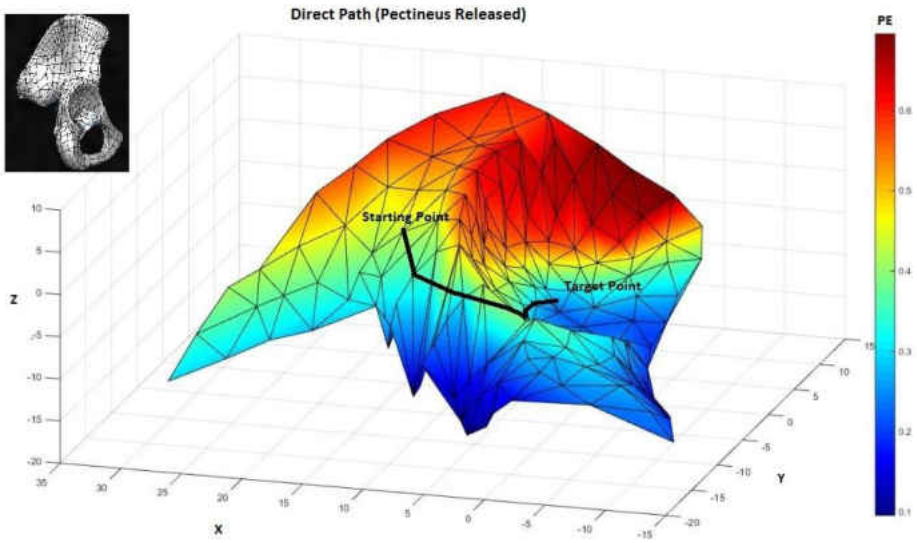

Figure 57 Potential energy map for the direct reduction path for the model without the effect of the Pectineus muscle.

For demonstration purposes, the lower limb bones are scaled down with a scaling factor of 4:10 and rotated as found from the Dijkstra's algorithm program to show the femur orientation during the reduction path. Figure 58 shows different images which are presenting the required femur orientation for the reduction at each point in the path.

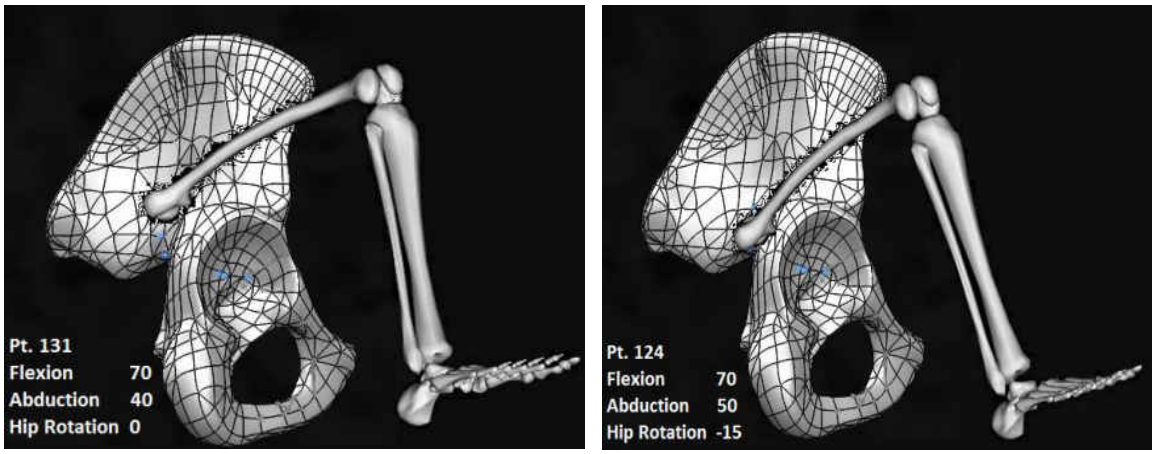

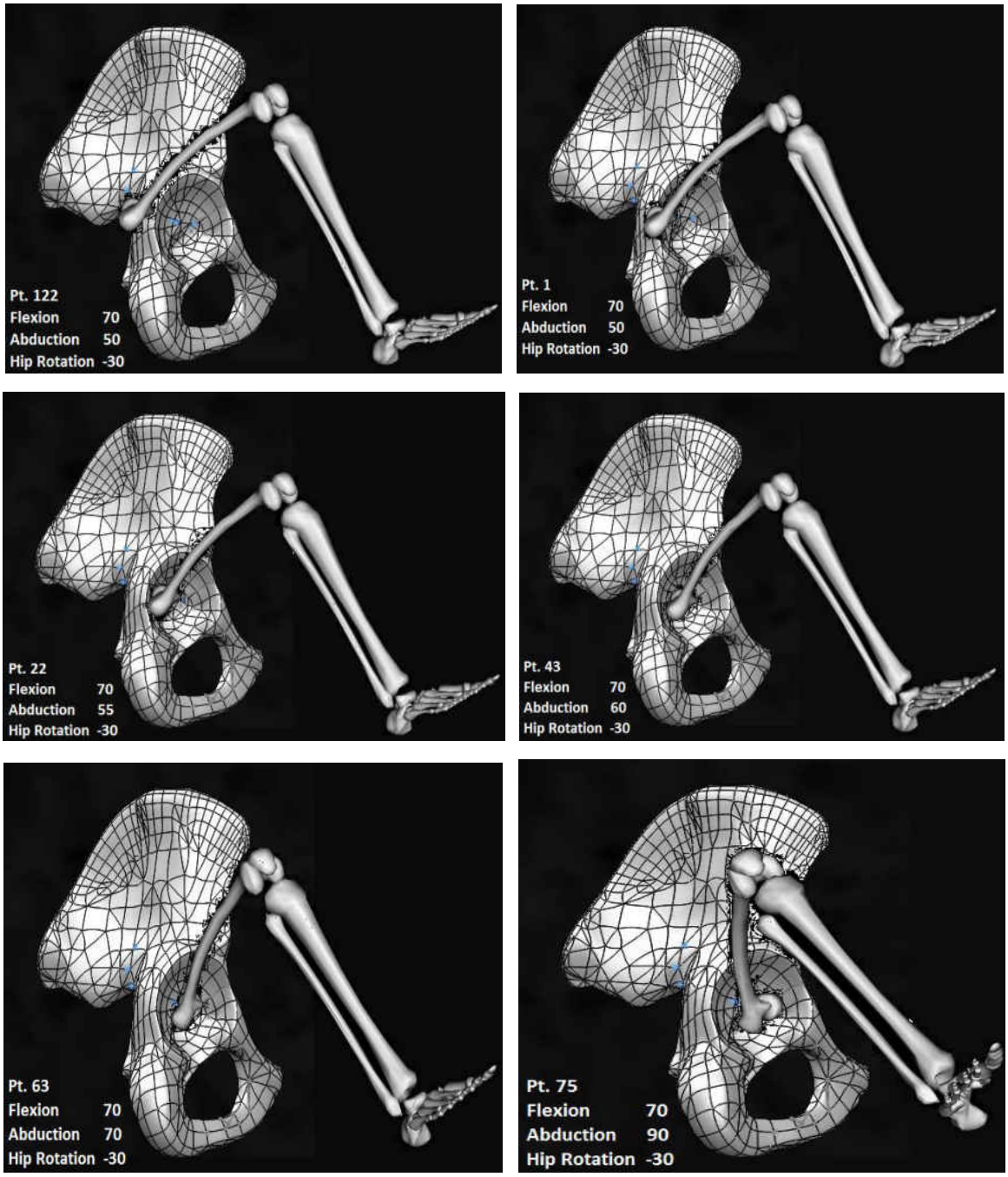

Figure 58 Grade IV direct reduction path with femur orientation for the model without the effect of the Pectineus.

Table 13 shows the difference in the required energy for the direct pathway between the model with all muscles and the model without the effect of the Pectineus. In addition to the pathway change, the percentage of energy drop between the two cases is 5.2% when the effect of the Pectineus is removed.

Table 13 The difference between the two cases in the first analysis (Direct path).

Model	Required Energy (J)
All muscles intact	0.231
No Pectineus	0.219

The Modified Hoffman-Daimler pathway proposed by Papadimitriou, et. al. is further evaluated by defining a path that goes to the intermediate point on the ischium near the acetabular notch, and then continues to the center of the acetabulum. The required energy for the reduction is determined and compared with the results of the model that does not have the effect of the Pectineus. For the model with all muscles intact, the femur should be flexed at 70 degrees during the reduction, but it is increased to 130 degrees at the acetabulum notch and returned to 70 degrees to continue the reduction. Additionally, the femur should be abducted at 40 degrees at the beginning of the path, and then increased to 90 degrees until it reaches the acetabulum center, and then end at an 80-degree angle. Finally, the hip rotation angle should be changed from positive 30 degrees to negative 30 degrees at the acetabular notch and then rotated externally at the end of the reduction pathway, as listed in Table 14. Figure 59 shows

the resulted least energy path for the indirect pathway for the model with all muscles intact. Figure 60 shows the potential energy map with the LEP for this analysis.

Table 14 Grade IV: required femur orientation for the hip dysplasia indirect reduction pathway of the model with all muscles intact.

#	Pt. #	Flexion	Abduction	Hip Rotation
1	131	70	40	30
2	124	70	50	30
3	121	70	55	30
4	112	70	55	30
5	111	70	55	30
6	99	75	55	30
7	93	130	70	30
8	92	130	75	30
9	17	130	90	30
10	16	70	90	-30
11	36	70	90	-30
12	56	70	90	-30
13	74	70	85	5
14	75	70	80	10

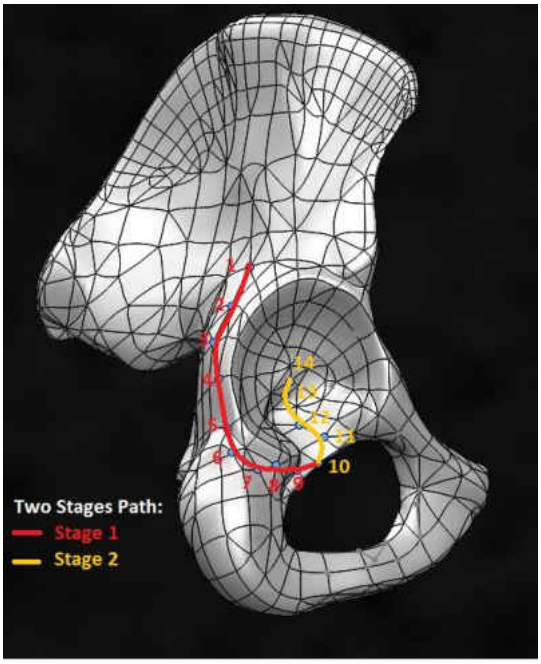

Figure 59 Grade IV: Hip Dysplasia indirect reduction pathway with the effect of all muscles.

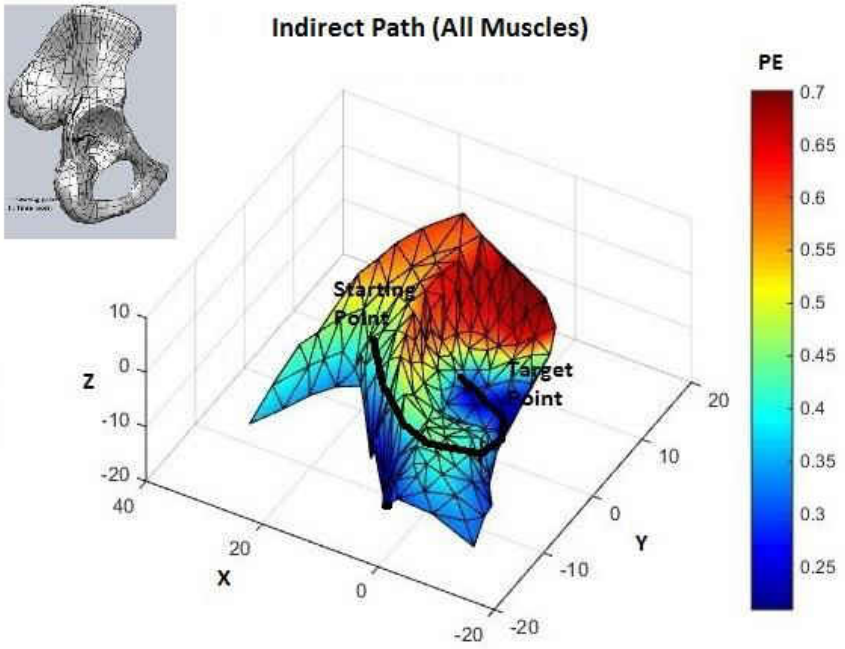

Figure 60 Potential energy map for the indirect reduction path for the model with all muscles intact.

As specified previously for the direct reduction path in grade IV, the lower limb bones are scaled by 4:10. For the indirect pathway of hip dysplasia reduction, the femur is rotated as specified from the Dijkstra's algorithm program. Figure 61 shows different images which present the required femur orientation for the reduction at each point in the pathway.

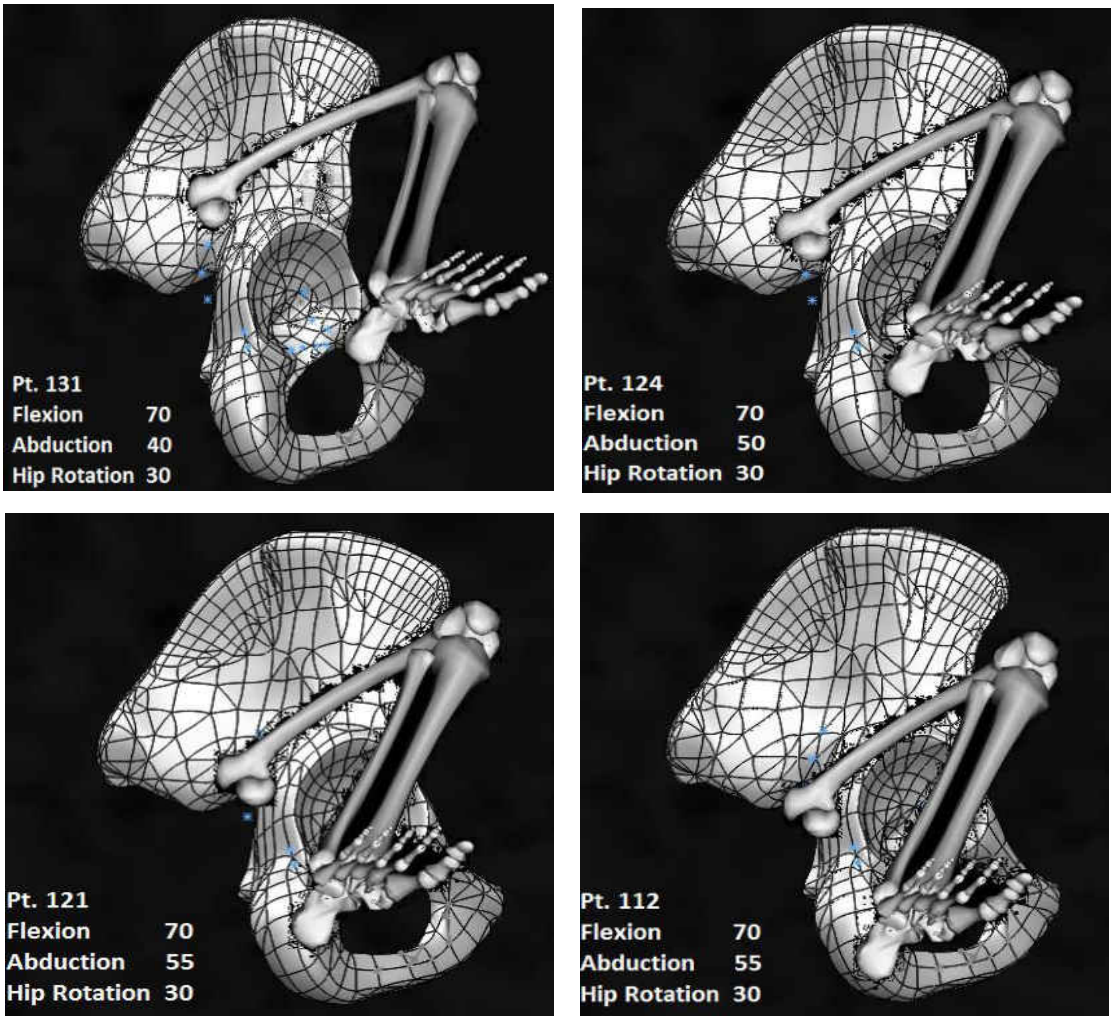

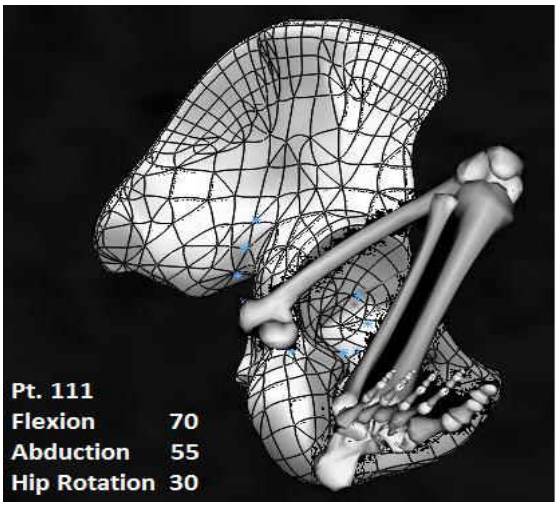
Pt. 111
Flexion 70
Abduction 55
Hip Rotation 30

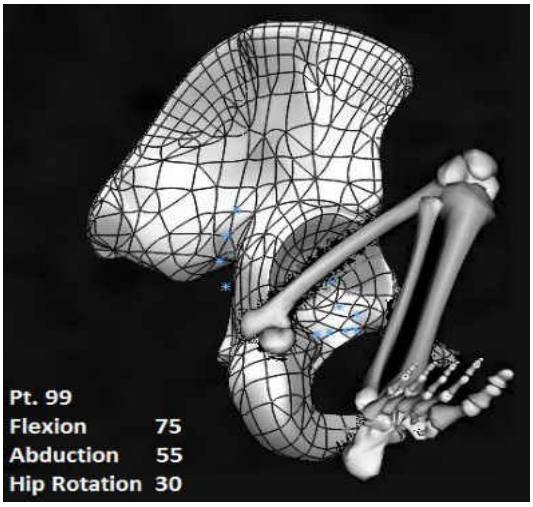
Pt. 99
Flexion 75
Abduction 55
Hip Rotation 30

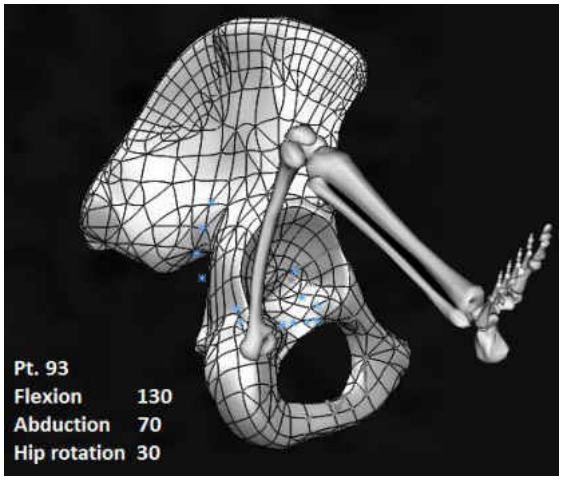
Pt. 93
Flexion 130
Abduction 70
Hip rotation 30

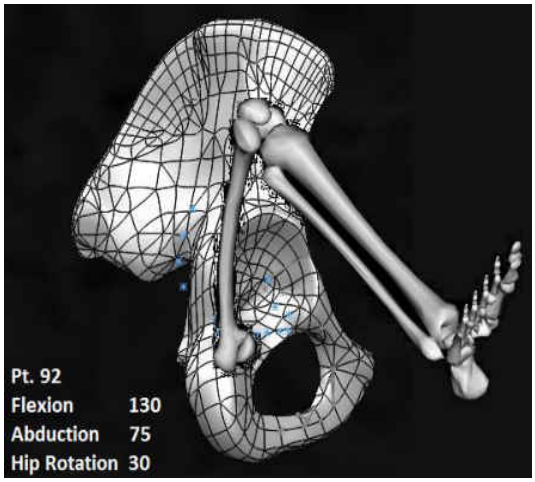
Pt. 92
Flexion 130
Abduction 75
Hip Rotation 30

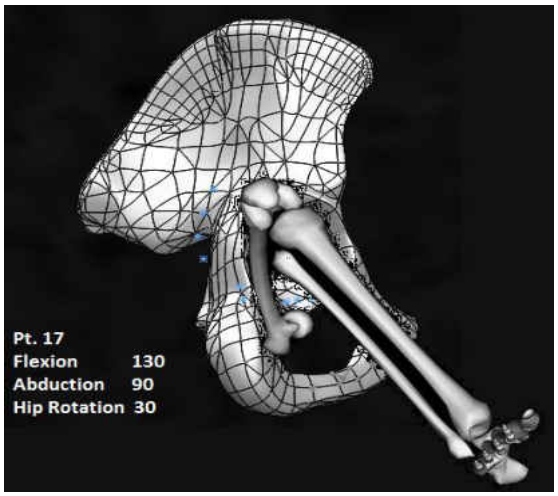
Pt. 17
Flexion 130
Abduction 90
Hip Rotation 30

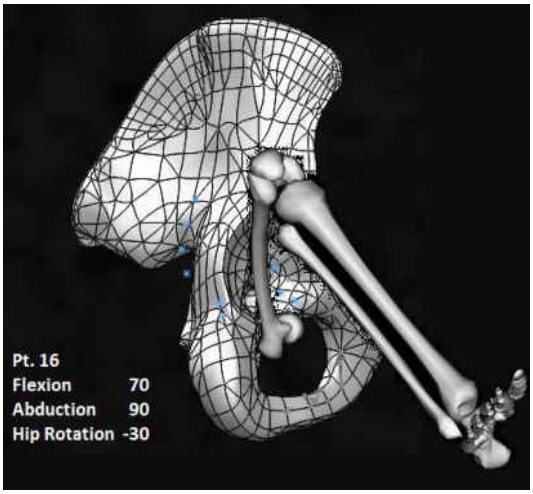
Pt. 16
Flexion 70
Abduction 90
Hip Rotation -30

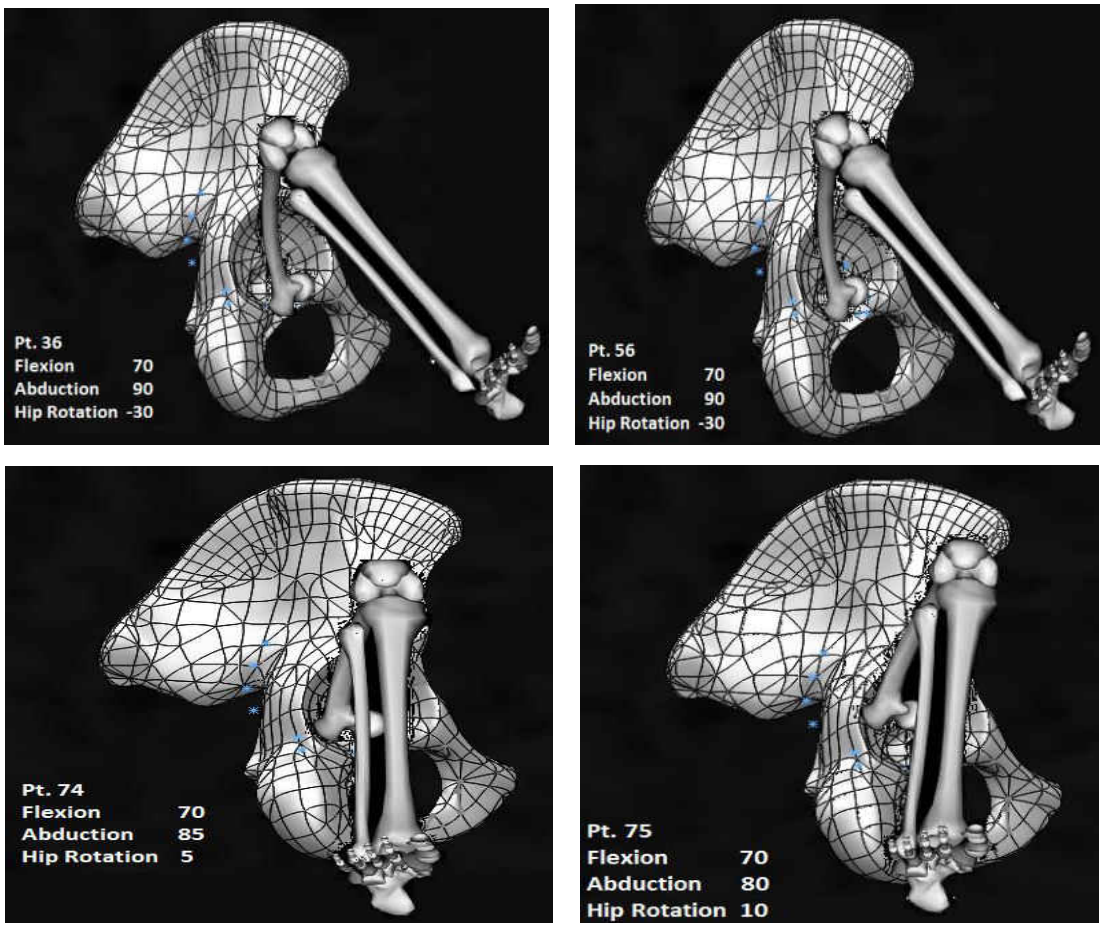

Figure 61 Grade IV: indirect reduction path with femur orientation for the model with all muscles intact.

Table 15 lists the computed indirect pathway points with the required femur orientation angles to achieve the least energy path for the model that does not have the effect of the Pectineus. For the least energy path, the femur should be flexed at 70 degrees along the pathway and abducted from 40 to 90 degrees while the hip is rotated internally from 0 to -30 degrees. Figure 62 shows the indirect reduction pathway that goes through the acetabular notch. Figure 63 shows the potential energy map with the LEP for this analysis.

Table 15 Grade IV: required femur orientation for the hip dysplasia indirect reduction path of the model without the effect of the Pectineus.

#	Pt. #	Flexion	Abduction	Hip Rotation
1	131	70	40	0
2	124	70	50	-15
3	121	70	55	-30
4	112	70	60	-30
5	111	70	65	-30
6	99	70	65	-30
7	93	70	75	-30
8	92	70	80	-30
9	17	70	90	-30
10	16	70	90	-30
11	36	70	90	-30
12	55	70	90	-30
13	71	70	90	-30
14	78	70	90	-30
15	75	70	90	-30

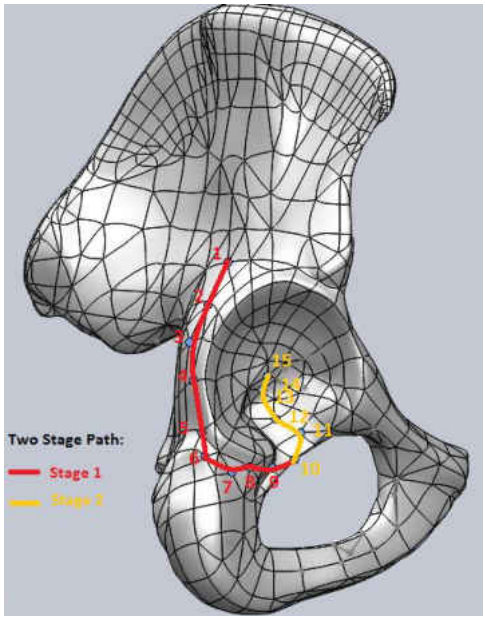

Figure 62 Grade IV: Hip Dysplasia indirect reduction path without the effect of the Pectineus.

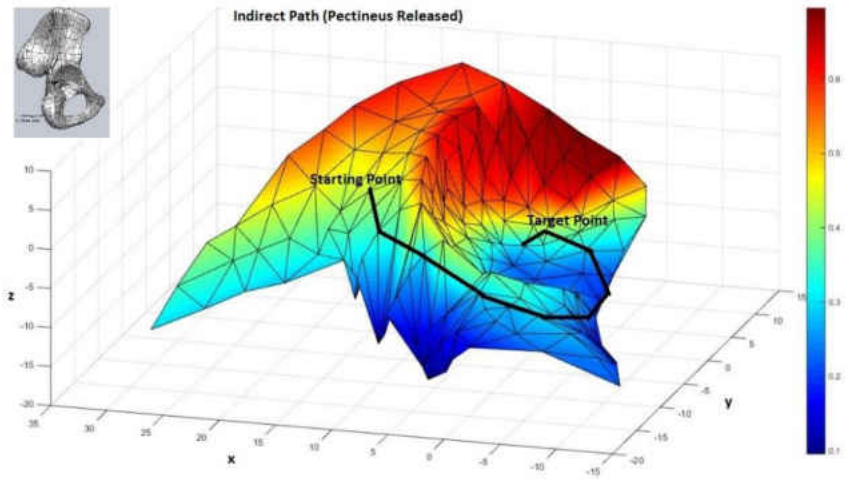

Figure 63 Potential energy map for the indirect reduction path for the model without the effect of the Pectineus muscle.

As specified previously for demonstration purposes, the lower limb bones are scaled at 4:10. In the indirect path of hip dysplasia reduction without the effect of the Pectineus, the femur is rotated as specified from the Dijkstra's algorithm program. Figure 64 shows different images present the required femur orientation for the reduction at each point on the least energy path.

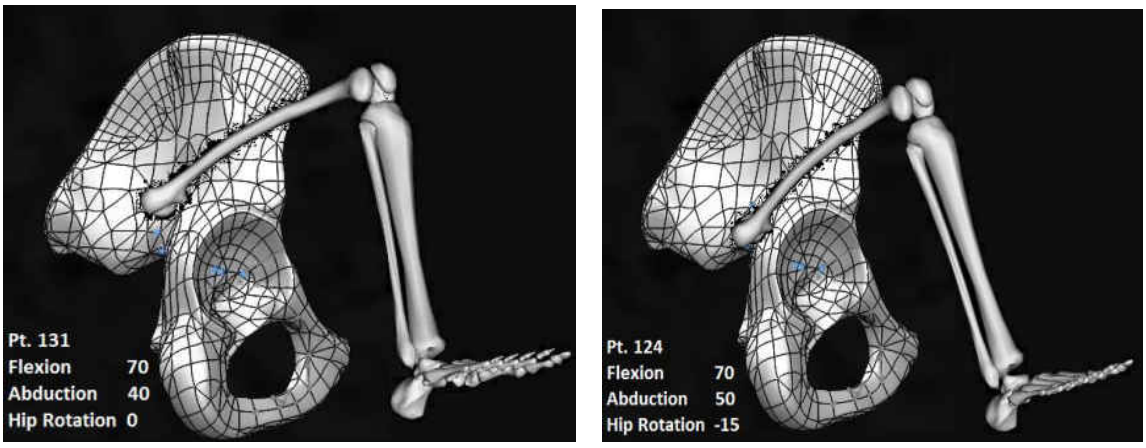

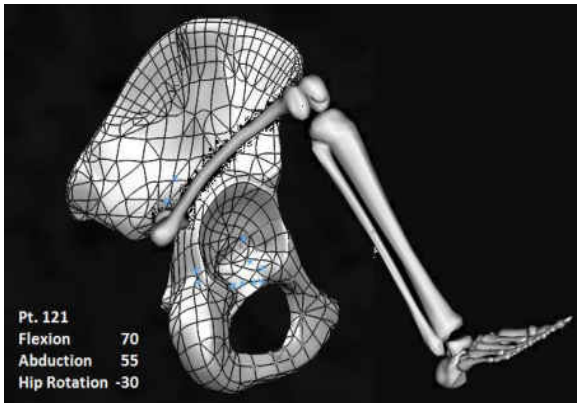
Pt. 121
Flexion 70
Abduction 55
Hip Rotation -30

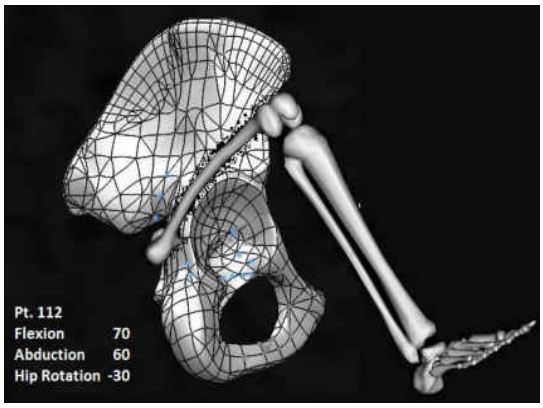
Pt. 112
Flexion 70
Abduction 60
Hip Rotation -30

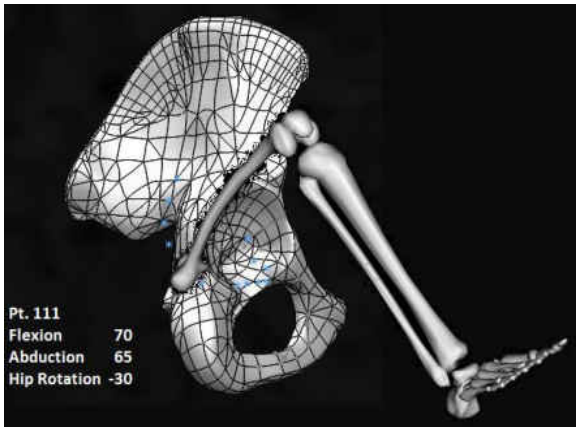
Pt. 111
Flexion 70
Abduction 65
Hip Rotation -30

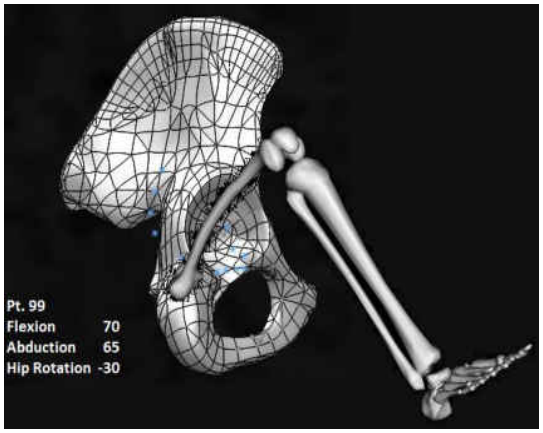
Pt. 99
Flexion 70
Abduction 65
Hip Rotation -30

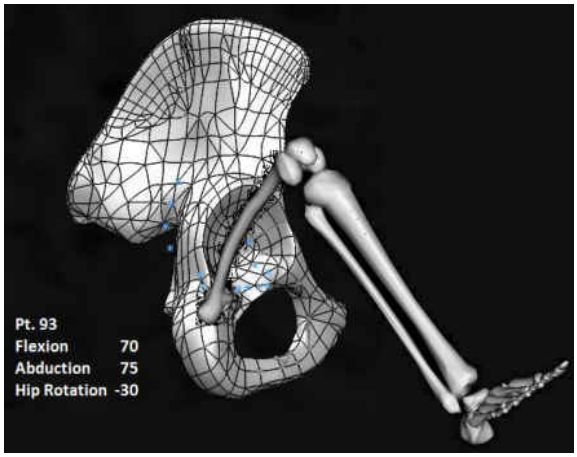
Pt. 93
Flexion 70
Abduction 75
Hip Rotation -30

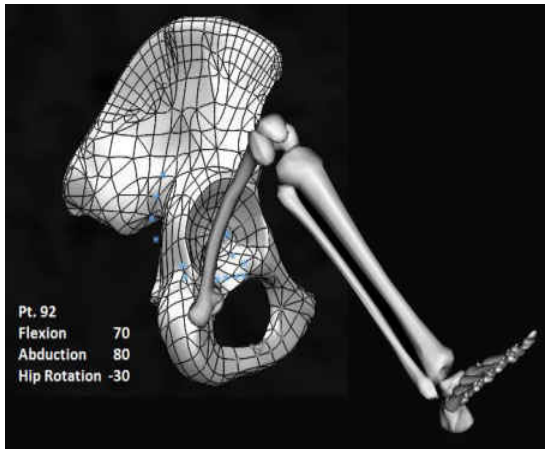
Pt. 92
Flexion 70
Abduction 80
Hip Rotation -30

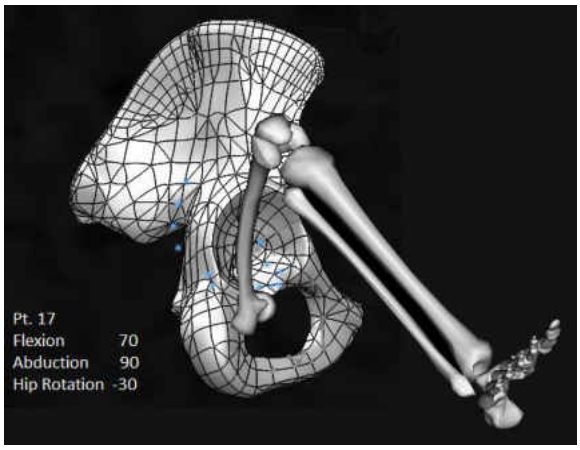
Pt. 17
Flexion 70
Abduction 90
Hip Rotation -30

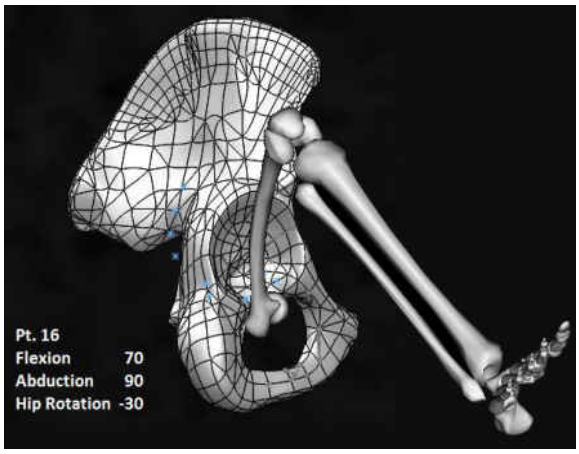
Pt. 16
Flexion 70
Abduction 90
Hip Rotation -30

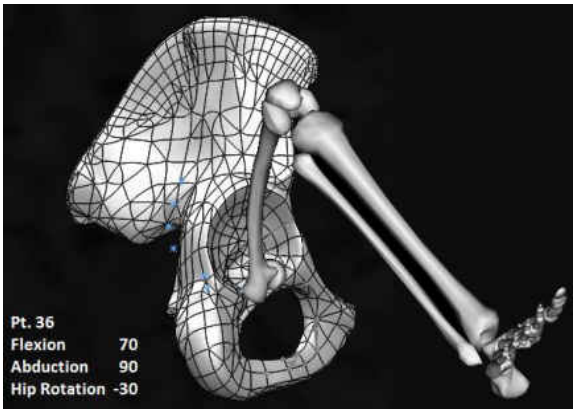
Pt. 36
Flexion 70
Abduction 90
Hip Rotation -30

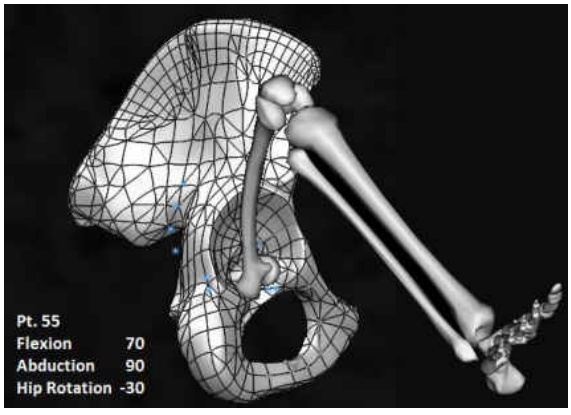
Pt. 55
Flexion 70
Abduction 90
Hip Rotation -30

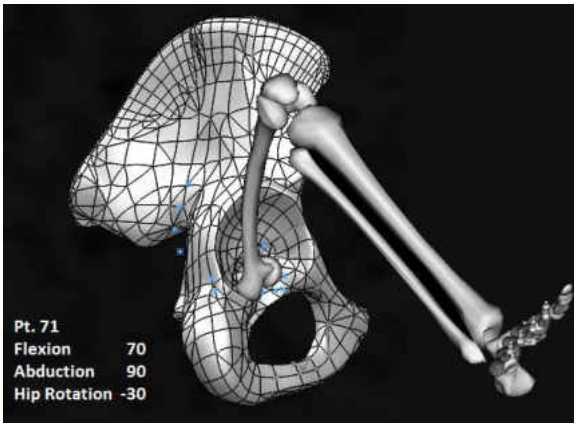
Pt. 71
Flexion 70
Abduction 90
Hip Rotation -30

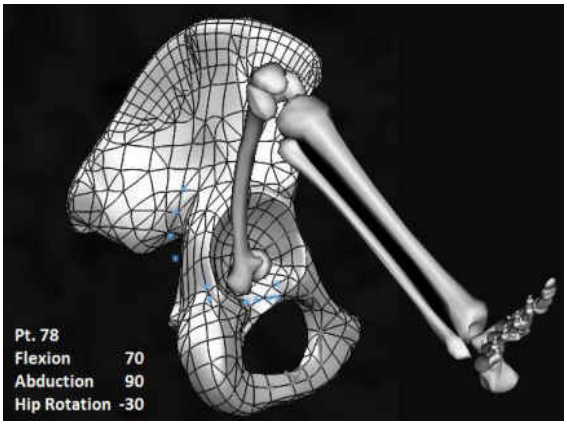
Pt. 78
Flexion 70
Abduction 90
Hip Rotation -30

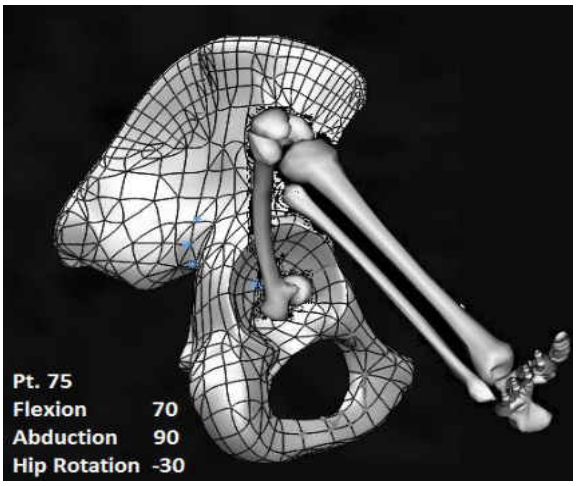

Figure 64 Grade IV indirect reduction paths with femur orientation for the model without the effect of the Pectineus.

Table 16 shows the difference in the required energy of the indirect path between the model with all muscles intact and the model without the effect of the Pectineus. The percentage of energy drop between the two analyses is 9.2% when the effect of the Pectineus is eliminated.

Table 16 The difference between the third and fourth analysis (indirect path).

Model	Required Energy (J)
All Muscles effect	0.509
No Pectineus	0.462

A fifth calculation is determined by identifying the least energy path from the dislocated position to the center of the acetabulum without the effect of the Pectineus. Since this path closely approximated the direct path proposed by Iwasaki, the energy requirement for this path is determined by all muscles intact. The results indicate that

additional energy is required for the femoral head to pass directly over the rim of the posterior acetabulum when the Pectineus muscle is intact. This supports the findings of Suzuki that the traction or manual reduction may be needed for the direct reduction of Grade IV hip dislocation. Table 17 lists the pathway points with the required femur orientation angles to achieve the least energy path.

Table 18 shows the difference in energy between the second and fifth analysis that followed the direct pathway proposed by Iwasaki and documented by Suzuki.

Table 17 Least energy path with the required femur orientation for the model with all muscles to follow the proposed pathway by Iwasaki.

#	Pt. #	Flexion	Abduction	Hip Rotation
1	131	70	40	30
2	124	70	50	30
3	122	70	50	30
4	1	70	45	25
5	22	70	50	25
6	43	70	55	15
7	63	70	60	5
8	75	70	80	10

Table 18 The difference between the second and the fifth analysis (Direct pathway).

Model	Required Energy (J)
All Muscles effect	0.241
No Pectineus	0.219

CHAPTER 5: DISCUSSION AND CONCLUSION

5.1 Discussion

The developed method in this dissertation identifies the least energy path endorsing the clinical observations of reduction for the four grades of hip dysplasia. There were several analyses conducted for the severe hip dislocation (Grade IV). Generally, two different pathways of reduction were considered. The first pathway is the direct path that starts from the dislocated location to the center of the acetabulum. The second pathway is the two-stage path that is considered the indirect pathway, which initially starts from the dislocated location to a point proximal to the ischial tuberosity and then proceeds to enter the acetabulum from an inferior position. Furthermore, eliminating the effect of the Pectineus, by numerically switching it off, has demonstrated a major influence on the required energy for the reduction of Grade IV.

In the first analysis of Grade IV that has the effect of all considered adductor muscles (Pectineus, Adductor Brevis, Adductor Longus, Adductor Magnus, and Gracilis), the resulted pathway of least energy closely approximated the indirect pathway proposed by Papadimitriou, et al [29]. With the studied method, the femoral head enters the acetabulum at the posterior margin of the lunate articular surface instead of through the center of the acetabular notch as described in the Modified Hoffman-Daimler method. Eliminating the effect of the Pectineus in the second analysis changed the pathway to closely follow the direct pathway proposed by Iwasaki and documented by Suzuki [22, 21]. This model also demonstrated that eliminating the force of the Pectineus muscle decreases the energy required for reduction.

For the purpose of studying the pathway that was described by the Modified Hoffman-Daimler method, the computational model was forced to follow a path that goes through a point proximal to the ischial tuberosity. In this type of study, the resulted pathways in the two proposed models (the all muscles intact model and the model with the Pectineus released) successfully followed the pathway of Modified Hoffman-Daimler, and the effect of eliminating the Pectineus gave the same conclusion of lowering the required power for the hip reduction.

In the last analysis, the direct pathway of the model with the effect of all muscles intact was forced to follow the Iwasaki pathway. The femoral head initially shifts to the posterior part of the acetabulum, slides directly over the acetabular rim, and finally slides into the acetabulum. The amount of energy required for this reduction path was higher than the initial one that closely followed the Papadimitriou two-stage result, and even higher than the one proposed by Iwasaki.

5.2 Conclusion

The reduction of all hip dysplasia grades was successfully achieved by applying the developed method that is based on the principle of stationary potential energy. This method leads to the identification of a least energy path. Several computer codes were developed for implementing this study by starting with the collision detection algorithm that used the three dimensional SolidWorks model of a 10-week-old female infant to find the femoral head location centers' coordinates. Next, the muscle mechanics was introduced by using the non-linear constitutive Fung model that was defined as Hill-type

muscle model. They defined the muscle behavior function as an exponential function of the muscle strain that used the passive effect only. This function was used along with the gravitational potential energy to develop the potential energy, which is a function of the femoral head center coordinates and the three angles of rotation of the femur. Following the development of the mathematical model of the muscle and specifying all model constraints, the Dijkstra's algorithm program was modified to identify the least energy path.

At the beginning of the analysis, a model with two angles of rotation (flexion and abduction) was analyzed and then the least energy path for the four grades were computed. These results were demonstrated by using optimization methods that calculated the potential energy values at each femoral head location and found the local minimum energy at those locations. The resulting least energy paths were presented by producing the pathway along with the required femur orientation and the required energy for the reduction. Thus, each grade had its least energy path with the required femur orientation and required energy for reduction.

The model was further enhanced by including a third angle (hip rotation). The MATLAB code was developed to compute the local minimum energy at each femoral head location with respect to the three angles of rotation. The Dijkstra's algorithm program was then used to outline the least energy path for all four grades.

Additional analyses were carried out for Grade IV. Two types of pathways were defined: the first was specified by Iawaski and it was noted as the direct path, and the

second was defined from the result of the Modified Hoffman-Daimler pathway that was an indirect path. The direct pathway was started from the dislocated position of the hip and ended at the center of the acetabulum, while the indirect pathway followed a path that entered the acetabulum through the acetabular notch. For both analyses, the effect of the Pectineus was computationally switched off to compare the required energy for the reduction. Hence, the findings of this study suggest that release of the Pectineus muscle may also be considered to facilitate the hip reduction in Grade IV dislocations.

In conclusion, the developed biomechanical computational method is consistent with the clinical observations stated in the literature, especially the Iwasaki result for the direct reduction and the Modified Hoffman-Daimler result for the indirect reduction. It could theoretically provide physicians resources to modify the existing treatment methods and may lead to new visions of non-surgical management of developmental dysplasia of the hip.

5.3 Future Work

The work developed in this research improves the prospects of the hip dysplasia treatment. Furthermore, the results of the developed least energy method will change the thoughts on hip dysplasia treatments.

It is important to mention that the functionality and design of the harness have not been modified in more than half a century. The developed mathematical model and the principle of the stationary potential energy will not only optimize the harness use, but it will also lead to future development of a new harness. A synthesized harness through

the use of inverse methods could be very promising for treating hip dysplasia, especially for grade IV. The synthesized harness can be a modification of any existing treatment method by using the computed least energy path along with the required femur orientation. For instance, the Pavlik Harness's straps are used to fix the femur in different orientations at different locations during the reduction. The straps' setups were identified as explained in the literature. However, by using the developed method along with the proven least energy path, the straps with their configuration could be modified to achieve hip dysplasia reduction as per the achievements of this study.

APPENDIX A: COLLISION DETECTION ALGORITHM

Appendix A introduced the Collision detection algorithm routine. It is used to finding the coordinates of the femoral head center when the head is in contact with the pelvis surface.

```
Sub FindCenters()
Dim source As Worksheet
Dim destination As Worksheet
Set source = Sheets("Input")
Set centers = Sheets("FHeadCenters")
Const nump = 78 'number of points in the acetabulum
Const r = 7
Const fapp = 30 '% of aproach for each iteration
Dim i, j, L As Integer
Dim D, Min, Min2, magV, magVV, AA(2, nump - 1) As Double
Dim VV(2, nump - 1), V(2), B(2, nump - 1), A(2, nump - 1), CC(2, nump - 1), CCC(2) As Double
Dim M, c As Variant

c = Array(-0.36, -10.05, 17.8)
For i = 0 To nump - 1
  B(0, i) = source.Cells(i + 2, 2)
  B(1, i) = source.Cells(i + 2, 3)
  B(2, i) = source.Cells(i + 2, 4)
Next i

Count2 = 0
For L = 0 To nump - 1
   'Calculate the vector of direction of displacement
```

```
V(0) = B(0, L) - c(0)
V(1) = B(1, L) - c(1)
V(2) = B(2, L) - c(2)
magV = (V(0) ^ 2 + V(1) ^ 2 + V(2) ^ 2) ^ 0.5
CC(0, L) = c(0)
CC(1, L) = c(1)
CC(2, L) = c(2)
Min = 1000000
Count = 0
Do While (Min > 0.000000001 And Count < 100)
   Count = Count + 1
   Min = 1000000
   Min2 = 1000000
   'Advancing in V direction find the maximum amount to advance without
   'collision for each point, then pick the minimum of all those distances.
   For i = 0 To nump - 1
      VV(0, i) = B(0, i) - CC(0, L)
      VV(1, i) = B(1, i) - CC(1, L)
      VV(2, i) = B(2, i) - CC(2, L)
      magVV = (VV(0, i) ^ 2 + VV(1, i) ^ 2 + VV(2, i) ^ 2) ^ 0.5
      VVdotV = V(0) * VV(0, i) + V(1) * VV(1, i) + V(2) * VV(2, i)
      cosT = VVdotV / (magV * magVV)
      D = (magVV - r) / cosT
      If Abs(D) < Abs(Min) Then
         Min = D
      End If
   Next i
   If Abs(Min) > Abs(Min2) Then 'In case that we have pennetration
```

```
    Min = -Min
  End If
  Min2 = Abs(Min)
  CC(0, L) = fapp / 100 * V(0) * Min / magV + CC(0, L)
  CC(1, L) = fapp / 100 * V(1) * Min / magV + CC(1, L)
  CC(2, L) = fapp / 100 * V(2) * Min / magV + CC(2, L)
  CCC(0) = CC(0, L)
  CCC(1) = CC(1, L)
  CCC(2) = CC(2, L)
Loop
centers.Cells(L + 3, 2).Value = CC(0, L)
centers.Cells(L + 3, 3).Value = CC(1, L)
centers.Cells(L + 3, 4).Value = CC(2, L)
If Count > Count2 Then
Count2 = Count
End If
If 1 Then 'Just to check distances
  'Calculate all the possible points of contact
  For i = 0 To nump - 1
    VV(0, i) = B(0, i) - CC(0, L)
    VV(1, i) = B(1, i) - CC(1, L)
    VV(2, i) = B(2, i) - CC(2, L)
    magVV = (VV(0, i) ^ 2 + VV(1, i) ^ 2 + VV(2, i) ^ 2) ^ 0.5
    A(0, i) = VV(0, i) * r / magVV + CC(0, L)
    A(1, i) = VV(1, i) * r / magVV + CC(1, L)
    A(2, i) = VV(2, i) * r / magVV + CC(2, L)
  Next i
  Min = 1000000
```

```
        For i = 0 To nump - 1
            For j = 0 To nump - 1
                D = (A(0, i) - B(0, j)) ^ 2 + (A(1, i) - B(1, j)) ^ 2 + (A(2, i) - B(2, j)) ^ 2
            If D < Min Then
                Min = D
                Anode = i
                Bnode = j
            End If
            Next j
        Next i
        Min = Min ^ 0.5
        centers.Cells(L + 3, 9).Value = Min
        centers.Cells(L + 3, 11).Value = Anode
        centers.Cells(L + 3, 12).Value = Bnode
    End If
Next L
centers.Cells(2, 7).Value = Count2
End Sub
```

APPENDIX B: GENETIC ALGORITHM

Appendix B1: Genetic Algorithm Code:

```
Const PopulationSize As Integer = 100
Const MatingPop As Double = 0.2 'Only the best 20% mates and the best mutation
Dim MaxGenerations, BestPop, posBestMutated As Integer
Dim MutationRate As Double
Dim x, Y, Z As Double
Dim CurrentGeneration(1 To PopulationSize) As Chromosome
Dim Offspring(1 To PopulationSize) As Chromosome
Dim Generation As Integer
Dim SumFitnessScores As Double

Private Sub ShowProgressCheckBox_Click()
End Sub

Private Sub Evolve_Click()
    Dim i, j As Integer
    Application.ScreenUpdating = ShowProgressCheckBox.Value
    Randomize
    MaxGenerations = Worksheets("Genetic").Range("MaxGenerations")
    MutationRate = Worksheets("Genetic").Range("MutationRate")
    BestPop = CInt(MatingPop * PopulationSize)
    i = Worksheets("Genetic").Cells(3, 7) 'Starting point in X,Y and Z so you can continue
calculating later
    Dim a As Boolean
    a = IsEmpty(Worksheets("results").Cells(i + 1, 1))
    Do While (Not (IsEmpty(Worksheets("results").Cells(i + 1, 1))))
        Worksheets("Genetic").Cells(3, 7) = i 'Starting point modified automatically
```

```
        x = Worksheets("results").Cells(i + 1, 1)
        Y = Worksheets("results").Cells(i + 1, 2)
        Z = Worksheets("results").Cells(i + 1, 3)
        For j = 1 To PopulationSize
            Set CurrentGeneration(j) = New Chromosome
            Set Offspring(j) = New Chromosome
            CurrentGeneration(j).x = x
            CurrentGeneration(j).Y = Y
            CurrentGeneration(j).Z = Z
            CurrentGeneration(j).MutationRate = MutationRate
        Next
        DoGeneticAlgorithm
        Application.ScreenUpdating = True
        Application.ActiveWorkbook.Save
        With Worksheets("results")
                .Cells(1 + i, 4) = Worksheets("Genetic").Cells(3, 2)
                .Cells(1 + i, 5) = Worksheets("Genetic").Cells(3, 3)
                .Cells(1 + i, 6) = Worksheets("Genetic").Cells(3, 4)
        End With
        i = i + 1
    Loop
End Sub

Public Sub DoGeneticAlgorithm()
    Dim i As Integer
    Dim mom As Integer
    Dim dad As Integer
    'Dim m As Integer
```

```
    Generation = 0
    posBestMutated = -1
    Do While (Generation <= MaxGenerations)
        EvaluteFitness
        DisplayResults 'Here we also arrange the points in Energy order
        posBestMutated = -1 'Just to initialize it and use -1 as reference to know there is
no mutation
        For i = 1 To BestPop
            Offspring(i).Copy CurrentGeneration(Worksheets("Genetic").Cells(i + 2, 1))
        Next
        For i = BestPop + 1 To PopulationSize
            mom = SelectChromosome
            dad = SelectChromosome
            Offspring(i).Mate CurrentGeneration(mom), CurrentGeneration(dad)
            If Offspring(i).Bmutated = True Then 'If a mutation happen during mate
                Offspring(i).EvaluateE
                If posBestMutated = -1 Then
                    posBestMutated = i
                Else
                    If Offspring(i).E <= Offspring(posBestMutated).E Then
                        posBestMutated = i
                    Else
                        Offspring(i).Bmutated = False
                    End If
                End If
            End If
        Next
```

```
        For i = 1 To PopulationSize
            CurrentGeneration(i).Copy Offspring(i)
        Next
        Generation = Generation + 1
    Loop
End Sub

Public Sub EvaluteFitness()
    Dim i, pos As Integer
    Dim MinE As Double
    Dim MaxE As Double
    CurrentGeneration(1).EvaluateE
    MinE = CurrentGeneration(1).E
    MaxE = CurrentGeneration(1).E
    pos = 1
    For i = 2 To PopulationSize
        CurrentGeneration(i).EvaluateE
        If CurrentGeneration(i).E > MaxE Then
            MaxE = CurrentGeneration(i).E
        End If
        If CurrentGeneration(i).E < MinE Then
            MinE = CurrentGeneration(i).E
        End If
    Next
    SumFitnessScores = 0
    For i = 1 To PopulationSize
        CurrentGeneration(i).FitnessScore = 1 - _
            (CurrentGeneration(i).E - MinE) / (MaxE - MinE)
```

```
        SumFitnessScores = SumFitnessScores + CurrentGeneration(i).FitnessScore
    Next
End Sub


Public Function SelectChromosome() As Integer
    SelectChromosome = CInt(Rnd * (MatingPop * PopulationSize + (1))) + 1   'The (1)is
to include also the best mutation
End Function


Public Sub DisplayResults()
    Dim i As Integer
    Dim r As Integer
    Dim found As Boolean
    r = 3
    For i = 1 To PopulationSize
        With Worksheets("Genetic")
            .Cells(r, 1) = i
            .Cells(r, 2) = CurrentGeneration(i).Ab
            .Cells(r, 3) = CurrentGeneration(i).Fl
            .Cells(r, 4) = CurrentGeneration(i).E
            .Cells(r, 5) = CurrentGeneration(i).mutant
        End With
        r = r + 1
    Next
    ' Sort the results:
    Range("A2", Range("E" & Rows.Count).End(xlUp).Address).Sort Key1:=Range("D3"),
_
    Order1:=xlAscending, Header:=xlYes
```

```
   Worksheets("Genetic").Range("Generation") = Generation 'Shows in which
generation we are
   If posBestMutated <> -1 Then
      ' Put the mutated Chromosome at the end of the list of the best Population if it was
not in the best population
      found = False
      'Plot best mutated
      Worksheets("Genetic").Cells(2, 15) = CurrentGeneration(posBestMutated).Ab
      Worksheets("Genetic").Cells(2, 16) = CurrentGeneration(posBestMutated).Fl
      For i = 1 To BestPop
         If Worksheets("Genetic").Cells(2 + i, 1) = posBestMutated Then
            Worksheets("Genetic").Cells(2 + i, 5) = "Best Mutant" 'this line should not be
necessary
            found = True
            Exit For
         End If
      Next
      If found = False Then
         With Worksheets("Genetic")
               .Cells(BestPop + 3, 1) = posBestMutated
               .Cells(BestPop + 3, 2) = CurrentGeneration(posBestMutated).Ab
               .Cells(BestPop + 3, 3) = CurrentGeneration(posBestMutated).Fl
               .Cells(BestPop + 3, 4) = CurrentGeneration(posBestMutated).E
               .Cells(BestPop + 3, 5) = "Best Mutant"
         End With
      End If
   End If
End Sub
```

Appendix B2: The Chromosome:

```
Public Ab As Double
Public Fl As Double
Public E As Double
Public x As Double
Public Y As Double
Public Z As Double
Public Bmutated As Boolean 'For the best mutant
Public mutant As Boolean 'For sons of one of the best mutanted
Public MaxAb As Double
Public MinAb As Double
Public MaxFl As Double
Public MinFl As Double
Public MutationRate As Double
Public FitnessScore As Double

Private Sub Class_Initialize()
    MutationRate = Worksheets("Genetic").Cells(2, 7)
    Bmutated = False
    mutant = False
    MaxAb = 90 * Pi / 180
    MinAb = 6 * Pi / 180
    MaxFl = 132 * Pi / 180
    MinFl = 70 * Pi / 180
    Ab = (MaxAb - MinAb - 1) * Rnd + MinAb
    Fl = (MaxFl - MinFl - 1) * Rnd + MinFl
    EvaluateE
```

```
End Sub
Public Sub EvaluateE()
   E =
End Sub

Public Sub Mutate()
   Dim num As Double
   Const both = 0.15 'Intersecting range will vary both parameters, not 1
   Bmutated = False
   num = Rnd
   If (num < MutationRate) Then
      Bmutated = True 'I asume will be the best mutated this will change after the mate
      num = Rnd
      If num < (1 - both) Then
         Ab = (MaxAb - MinAb - 1) * Rnd + MinAb
      End If
      If num > both Then
         Fl = (MaxFl - MinFl - 1) * Rnd + MinFl
      End If
   End If
End Sub

Public Sub Mate(mom As Chromosome, dad As Chromosome)
   Dim num As Double
   num = Rnd
   Ab = (1 - num) * mom.Ab + num * dad.Ab
   num = Rnd
   Fl = (1 - num) * mom.Fl + num * dad.Fl
```

```
    ' Mutate the result
    Mutate
    ' To show if one of the parents were the best mutated of the parents generation
    If mom.Bmutated = True Or dad.Bmutated = True Then
        mutant = True
    Else
        mutant = False
    End If
End Sub

Public Sub Copy(dup As Chromosome)
    Ab = dup.Ab
    Fl = dup.Fl
    E = dup.E
    MaxAb = dup.MaxAb
    MinAb = dup.MinAb
    MaxFl = dup.MaxFl
    MinFl = dup.MinFl
    MutationRate = dup.MutationRate
    FitnessScore = dup.FitnessScore
    mutant = dup.mutant
    Bmutated = dup.Bmutated
End Sub
```

LIST OF REFERENCES

1. Ortolani, M., *Congenital hip dysplasia in the light of early and very early diagnosis.* Clinical Orthopaedics And Related Research, 1976(119): p. 6-10.
2. Seringe, R., J.C. Bonnet and E. Katti, *Pathogeny and natural history of congenital dislocation of the hip.* Orthopaedics & Traumatology: Surgery & Research, 2014. **100**(1): p. 59-67.
3. Barlow, T.G., *EARLY DIAGNOSIS AND TREATMENT OF CONGENITAL DISLOCATION OF THE HIP.* Journal of Bone & Joint Surgery, British Volume, 1962. **44-B**(2): p. 292-301.
4. Weinstein, S.L., S.J. Mubarak and D.R. Wenger, *Developmental Hip Dysplasia and Dislocation*. Part I. Vol. 85. 2003. 1824-1832.
5. Ardila, O.J., Eduardo A. Divo, Faissal A. Moslehy, George T. Rab, Alain J. Kassab, and Charles T. Price, *Mechanics of hip dysplasia reductions in infants using the Pavlik harness: A physics-based computational model.* Journal of Biomechanics, 2013. **46**(9): p. 1501-1507.
6. Price, C., Castanedo, P., Clarke, N., Cundy, P., Herarro-Soto, J., Hosalkar, H., Kasser, J., Mubarak, S., Wedege, J., and Narayanan, U., *Reliability of a New Radiographic Classification of Developmental Hip Dysplasia.* Journal of Child Orthopaedics, 2011. **5**(1): p. 1-35.
7. Stuart L. Weinstein, M., Scott J. Mubarak, MD, AND Dennis R. Wenger, MD, *Developmental Hip Dysplasia and Dislocation*, ed. S.L. Weinstein, S.J. Mubarak and D.R. Wenger. Vol. 85. 2003. 2024-2035.

8. Kitoh, H., M. Kawasumi and N. Ishiguro, *Predictive Factors for Unsuccessful Treatment of Developmental Dysplasia of the Hip by the Pavlik Harness.* JOURNAL OF PEDIATRIC ORTHOPAEDICS, 2009. **29**(6): p. 552-557.

9. Huayamave, V., C. Rose, S. Serra, B. Jones, E. Divo, F. Moslehy, A.J. Kassab and C.T. Price, *A patient-specific model of the biomechanics of hip reduction for neonatal Developmental Dysplasia of the Hip: Investigation of strategies for low to severe grades of Developmental Dysplasia of the Hip.* Journal of Biomechanics, 2015.

10. Tibrewal, S., V. Gulati and M. Ramachandran, *The Pavlik method: a systematic review of current concepts*.

11. Pavlik, A., *The functional method of treatment using a harness with stirrups as the primary method of conservative therapy for infants with congenital dislocation of the hip. 1957.* Clinical Orthopaedics And Related Research, 1992(281): p. 4-10.

12. Mubarak, S.J. and V. Bialik, *Pavlik: The man and his method*.

13. Pavlik, A., *Stirrups as an aid in the treatment of congenital dysplasias of the hip in children. By Arnold Pavlik, 1950.* Journal Of Pediatric Orthopedics, 1989. **9**(2): p. 157-159.

14. Bin, K., J.M. Laville and F. Salmeron, *Developmental dysplasia of the hip in neonates: Evolution of acetabular dysplasia after hip stabilization by brief Pavlik harness treatment.* Orthopaedics & Traumatology: Surgery & Research, 2014. **100**(4): p. 357-361.

15. Mubarak, S., S. Garfin, R. Vance, B. McKinnon and D. Sutherland, *PITFALLS IN THE USE OF THE PAVLIK HARNESS FOR TREATMENT OF CONGENITAL DYSPLASIA SUB LUXATION AND DISLOCATION OF THE HIP.* Journal of Bone and Joint Surgery American Volume, 1981. **63**(8): p. 1239-1248.

16. Grill, F., H. Bensahel, J. Canadell, P. Dungl, T. Matasovic and T. Vizkelety, *THE PAVLIK HARNESS IN THE TREATMENT OF CONGENITAL DISLOCATING HIP REPORT ON A MULTICENTER STUDY OF THE EUROPEAN PEDIATRIC ORTHOPEDIC SOCIETY.* JOURNAL OF PEDIATRIC ORTHOPAEDICS, 1988. **8**(1): p. 1-8.

17. Guille, J.T., P.D. Pizzutillo and G.D. MacEwen, *Development dysplasia of the hip from birth to six months.* The Journal Of The American Academy Of Orthopaedic Surgeons, 2000. **8**(4): p. 232-242.

18. Peled, E., V. Bialik, A. Katzman, M. Eidelman and D. Norman, *Treatment of Graf's ultrasound class III and IV hips using Pavlik's method*.

19. Kalamchi, A. and R. Macfarlane, III, *THE PAVLIK HARNESS RESULTS IN PATIENTS OVER 3 MONTHS OF AGE.* Journal of Parenteral Science and Technology, 1982. **2**(1): p. 3-8.

20. Atalar, H., U. Sayli, O.Y. Yavuz, I. Uraş and H. Dogruel, *Indicators of successful use of the Pavlik harness in infants with developmental dysplasia of the hip.* International Orthopaedics, 2007. **31**(2): p. 145-150.

21. Suzuki, S., *Reduction of CDH by the Pavlik harness. Spontaneous reduction observed by ultrasound.* The Journal Of Bone And Joint Surgery. British Volume, 1994. **76**(3): p. 460-462.

22. Iwasaki, K., *TREATMENT OF CONGENITAL DISLOCATION OF THE HIP BY THE PAVLIK HARNESS MECHANISMS OF REDUCTION AND USAGE.* Journal of Bone and Joint Surgery American Volume, 1983. **65**(6): p. 760-767.

23. Viere, R.G., J.G. Birch, J.A. Herring, J.W. Roach and C.E. Johnston, *USE OF THE PAVLIK HARNESS IN CONGENITAL DISLOCATION OF THE HIP AN ANALYSIS OF FAILURES OF TREATMENT.* Journal of Bone and Joint Surgery American Volume, 1990. **72**(2): p. 238-244.

24. Miller, B., *Hip Dysplasia.* Pediatrics for Parents, 2007. **23**(5): p. 12-13.

25. Seidl, T., J. Lohmaier, T. Holker, J. Funk, R. Placzek and H.H. Trouillier, *Reduction of unstable and dislocated hips applying the Tubingen hip flexion splint?* 2012.

26. Bernau, A., *[The Tübingen hip flexion splint in the treatment of hip dysplasia].* Zeitschrift Für Orthopädie Und Ihre Grenzgebiete, 1990. **128**(4): p. 432-435.

27. Atalar, H., C. Gunay and M. Komurcu, *Functional treatment of developmental hip dysplasia with the Tübingen hip flexion splint.* Hip International: The Journal Of Clinical And Experimental Research On Hip Pathology And Therapy, 2014. **24**(3): p. 295-301.

28. Wilkinson, A.G., D.A. Sherlock and G.D. Murray, *The efficacy of the Pavlik harness, the Craig splint and the von Rosen splint in the management of neonatal dysplasia of the hip - A comparative study*.

29. Papadimitriou, N.G., A. Papadimitriou, J.E. Christophorides, T.A. Beslikas and P.K. Panagopoulos, *Late-Presenting Developmental Dysplasia of the Hip Treated with the Modified Hoffmann-Daimler Functional Method*. Vol. 89. 2007. 1258-1268.

30. Lewars, E., *Computational chemistry [electronic resource] : introduction to the theory and applications of molecular and quantum mechanics / Errol Lewars*. 2010: Dordrecht ; London : Springer, 2010. 2nd ed.

31. Huayamave, V., Ceballos, A, Divo, E, Kassab, A, Barkaszi, S, Seigneur, H, Barriento, *POD-accelerated CFD analysis of wind loads on PV systems*, in *10th International Conference on Heat Transfer, Fluid Mechanics and Thermodynamics*. 2014, International Conference on Heat Transfer, Fluid Mechanics and Thermodynamics: Florida.

32. Ostrowski, Z., R. Białecki and A. Kassab, *Estimation of constant thermal conductivity by use of Proper Orthogonal Decomposition.* Computational Mechanics, 2005. **37**(1): p. 52-59.

33. Quapp, W. and D. Heidrich, *Analysis of the concept of minimum energy path on the potential energy surface of chemically reacting systems.* Theoretica chimica acta, 1984. **66**(3-4): p. 245-260.

34. Scharfenberg, P., *Analysis of critical points on the potential energy surface.* Theoretica chimica acta, 1980. **58**(1): p. 73-79.

35. Smidstrup, S., A. Pedersen, K. Stokbro and H. Jónsson, *Improved initial guess for minimum energy path calculations.* Journal of Chemical Physics, 2014. **140**(21): p. 214106-214101-214106-214106.

36. Schlegel, H.B., *Geometry optimization on potential energy surfaces.* Modern Electronic Structure Theory, 1995. **2**: p. 459-500.

37. Nichols, J., H. Taylor, P. Schmidt and J. Simons, *Walking on potential energy surfaces.* Journal of Chemical Physics, 1990. **92**(1): p. 340.

38. Basilevsky, M.V. and A.G. Shamov, *The local definition of the Optimum ascent path on a multi-dimensional potential energy surface and its practical application for the location of saddle points.* Chemical Physics, 1981. **60**(3): p. 347-358.

39. Kiryati, N. and G. Szekely, *Estimating shortest paths and minimal distances on digitized three-dimensional surfaces.* Pattern Recognition, 1993. **26**(11): p. 1623-1637.

40. Stefanakis, E. and M. Kavouras, *On the determination of the optimum path in space.* SPATIAL INFORMATION THEORY, 1995. **988**: p. 241-257.

41. Mitchell, J.S., D.M. Mount and C.H. Papadimitriou, *The discrete geodesic problem.* SIAM Journal on Computing, 1987. **16**(4): p. 647-668.

42. Aleksandrov, L., H. Djidjev, A. Maheshwari and J.R. Sack, *An Approximation Algorithm for Computing Shortest Paths in Weighted 3-d Domains*. 2011.

43. Kimmel, R. and N. Kiryati, *Finding the shortest paths on surfaces by fast global approximation and precise local refinement*.

44. Delp, S.L., F.C. Anderson, A.S. Arnold, P. Loan, A. Habib, C.T. John, E. Guendelman and D.G. Thelen, *OpenSim: Open-Source Software to Create and Analyze Dynamic Simulations of Movement.* Biomedical Engineering, IEEE Transactions on, 2007. **54**(11): p. 1940-1950.

45. Arnold, E., S. Ward, R. Lieber and S. Delp, *A Model of the Lower Limb for Analysis of Human Movement.* Annals of Biomedical Engineering, 2010. **38**(2): p. 269-279.

46. Huayamave, V., Rose, C., Zwawi, M., Divo, E., Moslehy, F., Kassab, A.J., Price, C., *Mechanics of Hip Dysplasia Reduction in Infants with the Pavlik Harness using Patient Specific Geometry*, in *Proceedings of ASME-IMECE 2014*. 2014: Montreal, Canada.

47. *The Visible Human Project, Us National Library of Medicine*. 1994; Available from: http://www.nlm.nih.gov/research/visible/.

48. Dostal, W.F. and J.G. Andrews, *A three-dimensional biomechanical model of hip musculature.* Journal of Biomechanics, 1981. **14**(11): p. 803-812.

49. Wickiewicz, T.L., R.R. Roy, P.L. Powell and V.R. Edgerton, *Muscle architecture of the human lower limb.* Clinical Orthopaedics And Related Research, 1983. **179**: p. 275-283.

50. Friederich, J.A. and R.A. Brand, *Muscle fiber architecture in the human lower limb.* Journal of Biomechanics, 1990. **23**(1): p. 91-95.

51. Delp, S.L., *Surgery simulation: a computer graphics system to analyze and design musculoskeletal reconstructions of the lower limb*. 1990, Stanford University.

52. Marieb, E.N., *Human anatomy & physiology*. 1998: Menlo Park, Calif. : Benjamin/Cummings, c1998.

4th ed.

53. Drake, R.L., *Gray's atlas of anatomy*. 2015: Philadelphia, PA : Churchill Livingstone, [2015]

Second edition.

54. Agur, A.M.R., A.F. Dalley and J.C.B. Grant, *Grant's atlas of anatomy. [electronic resource]*. 2013: Philadelphia : Wolters Kluwer Health/Lippincott Williams & Wilkins, c2013.

13th ed.

55. Martins, J.A.C., E.B. Pires, R. Salvado and P.B. Dinis, *A numerical model of passive and active behavior of skeletal muscles.* Computer Methods in Applied Mechanics and Engineering, 1998. **151**(3–4): p. 419-433.

56. Thelen, D.G., *Adjustment of Muscle Mechanics Model Parameters to Simulate Dynamic Contractions in Older Adults.* Journal of Biomechanical Engineering, 2003. **125**(1): p. 70-77.

57. Calvo, B., A. Ramirez, A. Alonso, J. Grasa, F. Soteras, R. Osta and M.J. Munoz, *Passive nonlinear elastic behaviour of skeletal muscle: Experimental results and model formulation.* Journal of Biomechanics, 2010. **43**(2): p. 318-325.

58. Gajdosik, R.L., *Passive extensibility of skeletal muscle: Review of the literature with clinical implications.* Clinical Biomechanics, 2001. **16**(2): p. 87-101.

59. Herzog, W., *Skeletal muscle mechanics : from mechanisms to function*. 2000: Chichester ; New York : John Wiley & Sons, c2000.

60. Winters, J.M., *Hill-based muscle models: a systems engineering perspective*, in *In, Winters, J.M. and Woo, S.L-Y. (eds.), Multiple muscle systems: biomechanics and movement organization, New York, Springer-Verlag, 1990, p. 69-93.* 1990: ;.

61. Hill, A.V., *First and last experiments in muscle mechanics*. 1970: Cambridge [Eng.], University Press, 1970.

62. Fung, Y.C., *Structure and Stress-Strain Relationship of Soft Tissues.* American Zoologist, 1984. **24**(1): p. 13-22.

63. Magid, A. and D.J. Law, *Myofibrils Bear Most of the Resting Tension in Frog Skeletal Muscle*. 1985, The American Association for the Advancement of Science. p. 1280.

64. *MATLAB and Statistics Toolbox Release 2014b, The MathWorks, Inc.* Natick, Massachusetts, United States.

65. Dijkstra, E.W., *A note on two problems in connexion with graphs.* Numerische Mathematik, 1959. **1**(1): p. 269-271.